REPORT NO.
UCB/EERC-84/09
MAY 1984

EARTHQUAKE ENGINEERING RESEARCH CENTER

PHENOMENOLOGICAL MODELING OF STEEL BRACES UNDER CYCLIC LOADING

by

KIYOHIRO IKEDA
STEPHEN A. MAHIN
STAVROS N. DERMITZAKIS

Report to the National Science Foundation

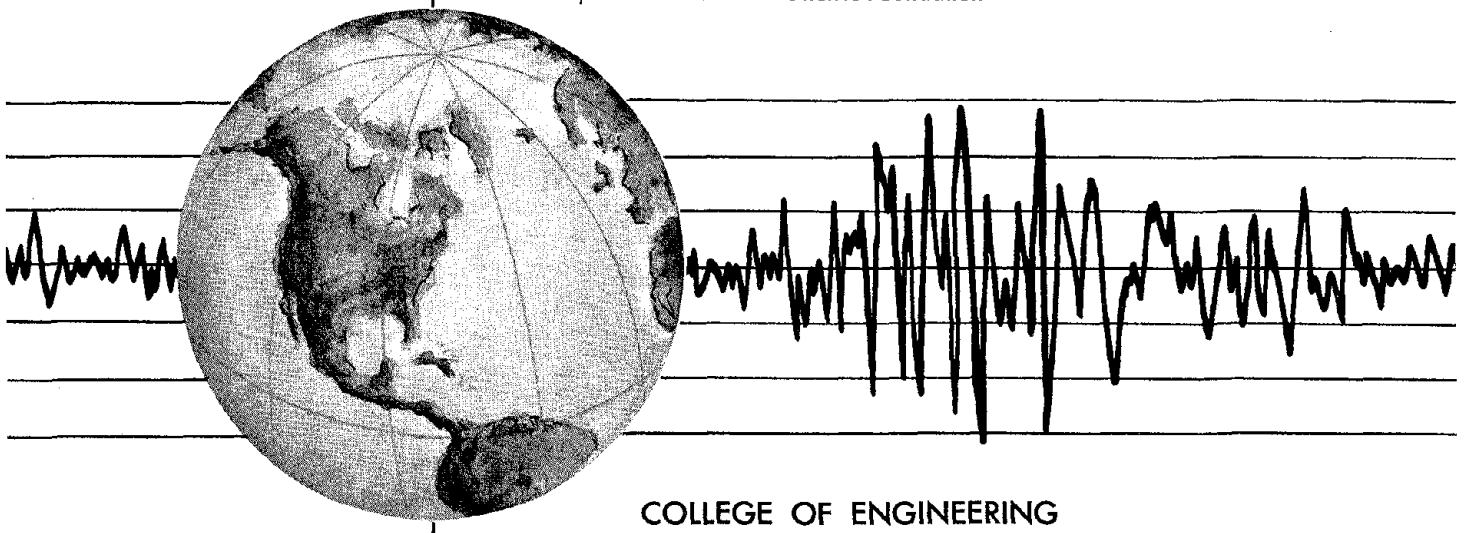

COLLEGE OF ENGINEERING

UNIVERSITY OF CALIFORNIA · Berkeley, California

For sale by the National Technical Information Service, U.S. Department of Commerce, Springfield, Virginia 22161.

See back of report for up to date listing of EERC reports.

50272-101

REPORT DOCUMENTATION PAGE	1. REPORT NO. NSF/CEE-84070	2.	3. Recipient's Accession No. PB86 132198/AS
4. Title and Subtitle: Phenomenological Modeling of Steel Braces under Cyclic Loading			5. Report Date: May 1984 6.
7. Author(s): Kiyohiro Ikeda, Stephen A. Mahin and Stavros N. Dermitzakis			8. Performing Organization Rept. No. UCB/EERC-84/09
9. Performing Organization Name and Address: Earthquake Engineering Research Center, University of California, Berkeley, 1301 South 46th Street, Richmond, Calif. 94804			10. Project/Task/Work Unit No. 11. Contract(C) or Grant(G) No. (C) (G) CEE81-07217
12. Sponsoring Organization Name and Address: National Science Foundation, 1800 G. Street, N.W., Washington, D.C. 20550			13. Type of Report & Period Covered 14.

15. Supplementary Notes

16. Abstract (Limit: 200 words)

This report introduces a refined phenomenological type analytical model for simulating the inelastic buckling behavior of steel braces. The cyclic buckling behavior of braces is simulated by pre-defined straight line segments along with simple rules regarding buckling load deterioration, plastic growth, and so on. This model achieves consistent asymptotic behavior, even for large axial brace shortenings, and extends input and output options available to the user. This element utilizes the advanced capabilities of the recently developed DRAIN-2D2 program, which performs dynamic inelastic structural analyses of two-dimensional structural systems subjected to static loads and seismic base excitations.

This research program attempts to facilitate the crucial selection of the control input parameters which define the brace hysteretic loops by the following steps. Firstly, a systematic method for selecting input parameters is proposed along with several rules governing the values of certain parameters. Secondly, input parameters for 24 different braces are presented. Thirdly, generalized parameters for commonly used types of sections are derived on the basis of these specific parameters.

A series of simple quasi-static analyses evaluate the capability of the new model and the validity of the methods for selection of input parameters. A complete user's guide for the computer program for the new model is included.

17. Document Analysis a. Descriptors

b. Identifiers/Open-Ended Terms

c. COSATI Field/Group

18. Availability Statement: Release Unlimited	19. Security Class (This Report)	21. No. of Pages: 157
	20. Security Class (This Page)	22. Price: A08

PHENOMENOLOGICAL MODELING OF STEEL BRACES UNDER CYCLIC LOADING

by

Kiyohiro Ikeda

Stephen A. Mahin

and

Stavros N. Dermitzakis

A Report to Sponsor
National Science Foundation

Report No. UCB/EERC-84/09
Earthquake Engineering Research Center
College of Engineering
University of California
Berkeley, California
May, 1984

ABSTRACT

This research report introduces a refined phenomenological type analytical model for simulating the inelastic buckling behavior of steel braces. The cyclic buckling behavior of braces is simulated by pre-defined straight line segments along with simple rules regarding buckling load deterioration, plastic growth, and so on. This model, developed on the basis of the phenomenological type approach taken by Maison *et al*, overcomes some of the limitations of earlier models. For example, consistent asymptotic behavior is achieved even for large axial brace shortenings, and extends input and output options available to the user. Furthermore, this element is able to utilize the advanced capabilities of the recently developed DRAIN-2D2 program, which performs dynamic inelastic structural analyses of two-dimensional structural systems subjected to static loads and seismic base excitations.

In phenomenological type models brace hysteretic loops are defined in terms of control input parameters. It is crucial to the successful application of these models that the input parameters be specified properly. However, due to a lack of sufficient experimental and analytical information regarding the selection these parameters, it has been difficult to select appropriate parameters. This research program attempts to facilitate this selection by the following steps. Firstly, a systematic method for selecting input parameters is proposed along with several rules governing the values of certain parameters. Secondly, input parameters for 24 different braces are presented based on available experimental results. Thirdly, generalized parameters for commonly used types of sections are derived on the basis of these specific parameters.

A series of simple quasi-static analyses were undertaken in order to evaluate the capability of the new model and the validity of the methods for the selection of input parameters proposed. A complete user's guide for the computer program developed for the new model is presented in Appendicies.

ACKNOWLEDGEMENT

This research program for this report was supported by National Science Foundation. This support is sincerely appreciated. The findings and recommendations in this report, however, are those of the authors and not necessarily those of the sponsor.

A number of people participated in this project. Professor Egor P. Popov and Dr. Benson Shing offered several important suggestions. Amir Gilani was responsible for porting the DRAIN-2D2 program to VAX computer used in these studies. Joanne Fordham and Mary Carrol Randol were helpful in proof reading the manuscript and Mary Edmunds' effort in preparing figures are greatly appreciated.

Table of Contents

LIST OF SYMBOLS

A	Cross-sectional area
$C1$	Slope of Zone 1
$C4$	Slope of Zone 4
$C5$	Slope of Zone 5
$C8$	Slope of Zone 8
E	Initial modulus of elasticity
k	Effective length factor of a member
kL/r	Effective slenderness ratio
L	Member length of a strut
P	Applied axial force
P_{cr}	Buckling load
PCR	Initial buckling load
$PCRF$	Final buckling load
P_t	Representative tensile strength
P_y	Axial yield load
$P45$	Control force defining Zones 4 and 5
$P6$	Control force defining Zone 6
$P7$	Control force defining Zone 7
$P8$	Control force defining Zone 8
r	Radius of gyration
R	Hardening ratio
$U34$	Control displacement defining Zones 3 and 4

$U45$	Control displacement defining Zones 4 and 5
$U5X$	Displacement at the intersection of zero load and Zone 5
$U6$	Control displacement defining zone 6
$U7$	Control displacement defining Zone 7
$U8$	Control displacement defining Zone 8
$U8X$	Displacement at the intersection of zero load and Zone 8
Δ	Lateral displacement of a strut
Δ_{res}	Residual lateral displacement of a strut
δ	Axial displacement of a strut
δ_{cr}	Axial displacement corresponding to buckling load
δ_{max}	Maximum axial displacement
δ_{min}	Minimum axial displacement
δ_{pl}	Plastic growth of a strut
δ_s	Axial displacement at the start of a cycle
δ_y	Axial displacement corresponding to yield load
$\sum \epsilon_p$	Absolute cumulative inelastic (plastic) strain
σ_y	Yield stress

1. INTRODUCTION

1.0 Introductory Remarks

Braced frames are often used in steel structures to provide lateral resistance and to reduce drifts under lateral loads. Where loads are well-defined and the structure is required to respond in the elastic range, conventional elastic design methods are adequate. However, in the case of earthquake response maximum loads are uncertain and it may not be economically feasible to design a structure for this extreme loading on an elastic basis. Fortunately, this may not be necessary if it is possible to take advantage of the inherent ability of steel structures to absorb and dissipate energy by means of inelastic deformations. In this manner a structure may sustain local damage, but should not collapse during a severe earthquake.

Although considerable research has been focussed on the seismic behavior of steel moment-resisting frames, comparatively few experimental results are available for steel braced systems. Eccentrically braced frames have been recently investigated. However, the braces in these systems are intended to remain "essentially" elastic and energy dissipation is achieved by yielding of the framing elements. In conventional concentrically braced frames, it is far more common to rely on inelastic deformations in the braces as the primary source of earthquake energy dissipation. The seismic response of such systems is difficult to predict due to the complexity of the cyclic inelastic behavior of the individual braces. As can be seen in Fig. 1.1, experimental hysteretic loops for braces are considerably more complex than for steel flexural members. Braces tend to exhibit both a significant deterioration of compressive strength during each cycle once the buckling load is reached, and a reduced effective "elastic" stiffness and buckling load on each subsequent inelastic cycle. Thus, the stiffness and compressive strength of bracing elements may degrade during inelastic deformations associated with severe earthquakes. In addition, for certain types of braced frames, the difference in the tension and compression capacities of braces can result in significant redistributions of internal forces not accounted for in the original "elastic" design. These factors may necessitate special design considerations when designing braced frames located in regions of high seismic risk.

To illustrate the importance of this on conventional design, it is useful to consider the simple example structure shown in Fig. 1.2. For simplicity, in this example, all members are assumed pin-ended and only a symmetrically distributed lateral load is applied. The beams and columns are, for the time being, considered infinitely rigid and strong. The axial force - axial displacement relation assumed for the diagonal braces is shown in Fig. 1.3. The sign convention adopted herein and throughout the remainder of this report is that tensile forces and elongations are positive. The tensile strength of the braces is assumed to be P_y. The slenderness ratio of the member is selected such that the buckling load is $-P_y/2$ and with increased compressive deformation the compressive strength decreases to $-P_y/4$ at point C in the figure. This assumed post-buckling behavior of the diagonal brace idealizes experimental results (see Fig. 1.1 for an example). This model includes two different phases of post-buckling behavior. First the axial load of the brace remains constant (between Pts. A and B), next its value decreases continuously (between Pts. B and C).

The conventional working stress design of the X-braced frame (see Fig. 1.2 (a)) would limit the lateral load, P, to that which would develop the allowable buckling force in the braces (i.e., $0.5P_y$/Factor of Safety). At this load level, by symmetry, the X braces would carry equal but opposite forces along each diagonal, and the beam would carry no axial load (and therefore could be designed as a small element). The column load magnitude is P.

Due to overloads inelastic behavior would be initiated when the compression diagonal buckles. Using the assumed post-buckling behavior of the diagonal braces, one can compute the redistribution of the internal forces, shown in Fig. 1.2 (a) to (d), as it occurs during overloads. As the external load increases from the working load range, the compressed brace buckles and the tensile brace is still elastic. This is shown for the onset of buckling in Fig. 1.2 (b) as Stage 1. In this stage there is still no axial load on the beam. In Stage 2 (Fig. 1.2 (c)), the compressed brace remains buckled and the tensile one yields. The unbalance in these brace forces causes a compression force in the beam. In Stage 3, the compressed brace passes into a post-buckling state (Pt. C in Fig. 1.3), and the tensile brace continues to yield, resulting in

further compression on the beam.

All three stages should be considered in the design of beam and columns. However, if the frame were designed on an elastic basis alone, the beam would have no net axial load, resulting in a very small cross-section, and the columns would be designed to resist a load of $\pm\sqrt{2}P_y/4$. With this design the frame can carry an external load up to $\sqrt{2}P_y/4$. However, if the external loads are increased, the beam is immediately overstressed and the structure becomes unstable as shown in Fig. 1.4. Moreover, the column axial loads also increase, raising the possibility of column buckling or tensile yielding or, failures of column splices or tie downs.

If the beam was designed for Stage 2 (Fig. 1.2 (c)), as might be done to account for the differences in code specified tension and compression brace capacities, the behavior is somewhat improved. The beam and columns are given more compressive strength so that they are able to resist the increased external load. Increased member strength results in increased frame strength (Fig. 1.4), but the ductility is limited.

Lastly, the beam and columns might be designed to have enough strength and ductility to carry the loads caused by the expected deterioration of the strength of the buckled brace at point C (Stage 3). This design results in increased ductility of the entire structure.

To develop the strength and ductility potential of the structure corresponding to the braces selected, the beam must be designed to have adequate compressive strength. This is necessary to avoid premature buckling of the beam. The columns must also be appropriately sized accounting for the redistribution of forces.

The K-braced frame (Structure 2 in Fig. 1.2) is also greatly influenced by the redistribution of internal forces. Because of the symmetrical construction, in the elastic stage, the K-braces carry equal but opposite forces along each brace and the beam carries no bending moment. However, after the compressed brace buckled the K-braces carry unequal loads, causing bending moment in the beam. In this situation, a conventional elastic design might result in a premature collapse of the structure after the brace buckled.

Thus, to design efficient seismic-resistant structures one need to account for redistribution of internal forces due to buckling and yielding. To do this it is necessary to predict brace behavior and perform analyses of the seismic behavior of braced systems. Such analytical predictions should be based on sound theory and verified on the basis of experimental research results.

1.1 Review of Experimental Research

Many experiments have been undertaken on inelastic behavior of axially loaded steel braces. However, most of these experiment dealt with members subject to monotonically increasing compression. Only a few experiments have been performed on the cyclic inelastic behavior of steel braces [1, 3 to 12].

Wakabayashi and his colleague have performed numerous experiments on the inelastic buckling of steel braces [3-8]. Wakabayashi *et al* tested more than 30 small-scale specimens [3,4,5]. All of these had the same square solid cross section 0.59×0.59 in. (15×15 mm) but had various effective slenderness ratios (ranging from 40.46 to 164.64). In addition, they tested steel braces restrained against rotation at both ends [6]. Twenty-one specimens having square solid cross section and eight specimens having H-shaped cross section were investigated. They had relatively short member lengths, 7.6 to 36.5 in. (193 to 928 mm).

Sherman [9] tested axially loaded struts and beam-column tubes, modeling offshore construction. However, materials were tested in the as-received condition. Jain *et al* [10] have performed experiments on 18 specimens made from 1×1 in. (25.4×25.4 mm) hollow cold-rolled steel tubes. Various effective slenderness ratios were used (from 30 to 140).

Zayas, Mahin and Popov tested four tubular steel braces, representative of one-sixth scale offshore construction [11]. They investigated the effects of material properties, of diameter to wall thickness ratios and of effective length (25 and 54).

Black, Wenger and Popov investigated the hysteretic behavior of 24 axially loaded steel struts, having a variety of cross-sectional shapes and slenderness ratios frequently encountered

in practice [1]. These specimens consisted of wide flanges, rectangular tubes, pipes, etc. Various loading histories were applied. Gugerli and Goel [12] tested nine specimens of realistic size: five of them were wide-flanges and four of them were tubes.

Several experiments [7,8,11] have been conducted on steel braced frames under cyclic loading having braces which buckle during compression. Wakabayashi *et al* tested simple braced frames under repeated horizontal loading in References 7 and 8. They consisted of single bracings and double bracings of realistic size. Wide flanges, tubes, angles, flat bars and round bars were used as brace members. Zayas, Mahin and Popov [11] tested large-scale three story braced frames under cyclic horizontal loading at the top. The lower two stories were made by X-braced frames and the top one by a K-braced frame.

1.2 Review of Analytical Models

1.2.0 General

Several models have been developed to represent the inelastic buckling behavior of steel braces. These models can be divided into three different types: finite element, physical theory brace, and phenomenological models. Finite element models generally subdivide a brace longitudinally into a series of elements which are subdivided into a number of fibers. However, the necessary computations are so costly that the method cannot be economically applied to practical analyses of large structures. Therefore, these methods will not be considered any further.

Physical theory brace models incorporate simplified theoretical formulations based on physical considerations that permit the cyclic inelastic behavior to be computed. The geometrical representation of a brace is considerably simpler than that used for a finite element model.

Phenomenological models are based on simplified hysteretic rules that only mimic observed axial force - axial displacement relationships. Currently, this type of model provides the most common approach to the analyses of large-scale braced structures. This research report follows the phenomenological type of approach.

1.2.1 Review of Phenomenological Models

Phenomenological models have been developed by Nilforoushan [13], Singh [14], Marshall [15], Roeder [16], Jain [17], and Maison [18]. The analytical hysteresis loops employed in these models are shown in Figs 1.5 through 1.10. Since the basic characteristics of these models are shown in these figures, a detailed explanation of each model is omitted herein and only the general properties of these models are compared.

The models generally possess one local degree of freedom: axial deformation. The axial force and stiffness of a strut are defined using simplified rules, defined in terms of input parameters. The values of these parameters need to be specified appropriately so as to obtain an accurate analytical result.

Properties of phenomenological models depend mostly on the number of linear segments employed to define the hysteretic loops. Historically, phenomenological models have been improved by adding new segments or removing some segments. The fewer the number of segments, the simpler and more computationally efficient a model tends to become. The more segments, the more complex the behavior that can be replicated. Table 1.1 lists the number of segments used in these models. In order to understand how the segments of these models are defined, it is useful to discuss the physical behavior during cycles. Figure 1.11 shows a cycle of a hysteresis loop physically divided into different zones. This is not the only possible explanation of physical behavior under cycling, but for convenience it is used herein for discussion. The Singh, the Marshall, and the Jain models ignore the difference between the "elastic post-buckling zone in tension" and "elastic post-buckling zone in compression," and simulate these two zones by one segment. The Marshall and the Jain models omit the "buckling zone." The Roeder and the Maison models assigned two segments to each of the "plastic zone in compression" and "plastic zone in tension," having large curvatures, to obtain a better simulation.

Several important phenomena, observed during inelastic cycling, must be adequately incorporated in a model. These include the deterioration of the buckling load, plastic growth in the brace length and local buckling. Deterioration of the buckling load is illustrated in Fig. 1.1.

The definition of plastic column growth, caused by plastic lengthening of a strut after one cycle of loading, is shown in Fig. 1.10. Local buckling usually results in the rapid deterioration of both tensile and compressive brace capacities. Whether these models take these various features into account is summarized in Table 1.1. The feature of deteriorating buckling load during cycles is included in the Jain, the Roeder and the Maison models. These three models incorporate two characteristic buckling loads to express limits on the deterioration. The Jain model uses one limit to define the buckling load for the first cycle and the other for the buckling load for all subsequent cycles (Fig. 1.9). The Roeder and Maison models use one for the maximum buckling load and the other for the minimum one. The actual values of buckling loads deteriorate between these two loads based on a simple rule.

Plastic growth is accounted for in the Jain and the Maison models. Local buckling is included only in the Marshall model, which defines brace failure due to local buckling based on an empirical formula.

Analytical results by these models were compared in a previous report [19] by applying them to the same strut data (see Fig. 1.12 (a) to (e)). In this comparison, the Maison model performed best. It is a revised version of the Roeder model; the main behavioral difference between these two models is that the Maison model included the effect of plastic growth. The Maison model has been implemented in the ANSR-I program [20] as an element called ANSR-I Element No. 4 [19].

It should be remembered, however, that phenomenological models are based on simplified rules that only mimic observed behavior and are not based on theoretical considerations. Refined phenomenological models will not necessarily result in more accurate results unless appropriate experimental or analytical data exist to properly define the input parameters.

1.3 **Objective**

As we have seen, the deterioration of brace capacity under inelastic cycling may result in significant redistributions of internal forces not usually accounted for in conventional design as

well as in considerable degradations of structural stiffness and strength. Consequently, it is highly desirable to perform realistic analyses of braced frames to assess their probable seismic performance. However, the complex cyclic inelastic behavior of braces makes prediction of the seismic behavior of braced frames difficult. The phenomenological and physical theory analytical models show the most promise for computer analysis of large-scale structure systems. Currently, the most accepted approach is based on phenomenological representations. However, the limitation of this approach is the lack of implementation on commonly available computer programs and the difficulty in selecting parameters used to define cyclic behavior.

The research program reported herein explores a simulation of cyclic buckling behavior of axially loaded steel braces by a refined phenomenological model. It is implemented into the DRAIN-2D2 computer program [21] and enables the users to economically analyze braced structures. The element, a synthesis of previous phenomenological models, is able to mimic various models for braces with effective slenderness ratio varying from 40 to 120. In addition, considerable efforts have been made in the implementation of the element to provide the user significantly increased information on the inelastic behavior of the brace.

Generally, in research programs concerned with phenomenological models, an emphasis is placed on the implementation and the computational characteristics of these models; however, relatively little attention is usually paid to their use. In order to avoid potential problems related to the use of such elements, this research program provides a complete method for selecting input parameters, and presents various kinds of generalized input parameters for commonly used braces. An extensive review of experimental data has been made to assess the reliability of the model and to identify generalized input parameters. Empirical relationships are developed to assist in modeling inelastic brace behavior.

It appears that physical theory models hold great promise for future implementation in computer analyses. These models are not investigated in this report; however, they are now under study and will be the subject of a subsequent report.

1.4 Scope

To achieve the aforementioned objectives, the following studies were performed. Chapter 2 investigates the cyclic behavior of braces by examining test data. The emphasis is placed on identifying the behavioral characteristics to be incorporated in the new model.

Chapter 3 introduces the refined phenomenological element. This element, whose prototype is the Maison model [18], includes new features which increase its capabilities. The new features, including an "event-to-event" solution strategy and "Zone 10," are discussed in detail.

Chapter 4 describes a systematic method for selecting input parameters. Several rules in selecting them are presented based on observations regarding the inelastic behavior of braces. Chapter 5 contains analytical results computed using the element. A simple analysis with the element is compared with corresponding test data to demonstrate the capability of the element. In addition, behavioral characteristics of the element are studied.

Chapter 6 presents generalized input parameters for individual sections selected on the basis of the interrelationships between optimal parameters for individual struts. These parameters are made available in response to the current shortage of data about input parameters. The validity of the generalized input parameters is assessed by comparing analytical results obtained using these parameters with corresponding test data.

Chapter 7 offers conclusions regarding the practicability and reliability of the refined phenomenological model. Behavioral characteristics which must be carefully modeled are identified in order to simplify the element. Limitations of phenomenological models are examined and the need for future work is presented so as to improve modeling of braced frames.

Appendix A presents a complete comparison of the analytical hysteresis loops obtained using the refined model with the corresponding test data. Appendix B constitutes a user's guide for the computer implementation of the refined phenomenological model.

2. REVIEW OF SOME EXPERIMENTAL DATA ON BRACE BEHAVIOR

2.0 Introductory Remarks

Prior to introducing the analytical model, it is important to study actual behavioral characteristics of steel braces in order to identify important features to be simulated by the model. For this purpose, the data from an experimental program by Black, Wenger and Popov [1], in which 24 struts were individually tested, are studied herein. The struts were subjected to cyclic quasi-statically applied axial loads simulating earthquake loading effects. These data included an axial force - axial displacement curve and an axial force - lateral displacement curve for each strut (see Fig. 2.1 for an example). The struts consisted of: nine wide-flanges, four double-angles, one double-channel, two tees, and five circular and three square tubes. Eighteen of these struts were designed to be pinned at both ends, while six of them were pinned at one end and fixed at the other. A common effective slenderness ratio of 80 was used for specimens within each structural shape category to allow for a direct comparison of results due to the variations in shapes. In addition, an effective slenderness ratio of 40, close to the range of plastic action, and one of 120, close to the range of elastic buckling, were assigned to both wide-flange and double-angle sections. Black, Wenger and Popov concluded that the effective slenderness ratio of a member appears to be the single most important parameter in describing its hysteretic behavior.

2.1 Deterioration of Buckling Loads

It is generally accepted that strut buckling loads tend to deteriorate from cycle to cycle (see Fig. 2.1 (a)). Two main causes of the deterioration have been identified as the "residual camber of the strut" and "material nonlinearities" [1]. The residual camber is represented by the amount of residual lateral displacement at the center of the strut. It was demonstrated in Reference 1 that residual lateral displacements were inversely proportional to buckling loads. Figure 2.1 (b) shows that significant residual cambers developed in Strut 19 corresponding to the drop in its buckling capacity.

Material nonlinearities can be observed in the stress-strain diagram from a coupon test shown in Fig. 2.2. This figure indicates a considerable hysteretic degradation of tangent moduli, usually denoted as the Baushinger effect. This results in a deterioration of buckling loads with cycling. An example of this is shown for Strut 12 in Fig. 2.3. This data does not indicate a significant increase of residual lateral displacements under cycling. There was still, however, a rapid deterioration of buckling loads. This can be associated with a reduction of tangent moduli of elasticity during cycles of large inelastic deformations, especially in the tension phase.

In addition to these main causes of buckling load deterioration, it is important to note the indirect influence of maximum tensile loads on buckling loads. An axial force - lateral displacement curve shown in Fig. 2.1 (b) indicates that the residual lateral displacement tends to become smaller during tension and larger during compression. In other words, the strut is straightened by tensile loads and is bent by compressive loads. The larger the residual lateral displacement of each cycle remaining at the beginning of the compression phase, the smaller the subsequent buckling load; therefore, the more a strut is straightened during tension, the larger the buckling load during the following compression cycle. For example, the axial force - axial displacement curve for this strut shows a degradation of the maximum tensile load developed from Cycles 5 through 7 (see Fig. 2.1 (a)). Because of the degradation of the maximum tensile load during the cycles, there is an increase in the residual lateral displacements as well as a decrease in the buckling load in the compression phase, as shown in Fig. 2.4.

Simple methods have been developed for predicting the effect of residual camber and the Baushinger effect on the deterioration of buckling load [22,23,24]. These methods were found to correlate well with experimental results where the residual camber and the material properties were known.

2.2 Post-Buckling Deterioration of Brace Capacity

This section investigates the post-buckling behavior of the brace capacity. After the buckling load is reached in each cycle, the load carrying capacity of a brace usually deteriorates with

increased axial brace shortening. Each phenomenological model simulates this experimental behavior by a predefined axial force - axial displacement relation, as shown in Figs. 1.5 through 1.10. However, because the starting point of each cycle in the history shifts with yielding in tension and with plastic growth, it is difficult to appropriately choose a relation simply by observing the experimental axial force - axial displacement curves. This problem can be resolved by constructing a translated axial force - axial displacement curve in which each subsequent hysteretic cycle observed for a brace is plotted such that the starting point, the point of the first compression load on a cycle, has the same origin. For example, each cycle of the hysteretic curves for Strut 19 shown in Fig. 2.1 (a) was translated and plotted in Fig. 2.1 (c). Other translated figures can be found in Fig. 2.5. The translated figures generally give deeper insight into cyclic behavior than do the original figures, and they are more useful in selecting parameters. Their use in selecting parameters will be discussed in Chapter 4.

As can be seen in these figures, the translated hysteretic curves generally form a smooth enveloping surface on the compression side. Features of cyclic behavior on the compression side are well expressed by the envelope of the translated curve. Figure 2.6 compares envelopes of translated curves on the compression side for sections with the effective slenderness ratios (kL/r) of 40, of 80, and of 120. As can be seen, the stocky member (kL/r =40) had a fuller cyclic history and the slender one (kL/r =120) had a more pinched one. Moreover, the slender member exhibited a sharper decrease of buckling loads, while the stocky member had more capacity to absorb and dissipate energy.

A rather flat region is observed near the buckling point on a translated curve for the stocky strut with a kL/r of 40. This flatter region is generally called the "buckling zone" (see Fig. 1.11). This zone, however, does not exist for struts with a kL/r of 80 or 120. Instead, there is a kink at the buckling point in these curves. These behavioral characteristics should be considered in selecting the input parameters for the new model.

2.3 Plastic Growth

Plastic lengthening of a strut after each inelastic cycle of loading (plastic growth) was noted in Reference 1. It reports that the inelastic elongations of braces which have yielded by tensile loads will not be removed when the braces buckle under compressive loads. This results in a net elongation of braces during cyclic inelastic load reversals.

Brace elongation should be described by a parameter which is able to account for the effect of a previous inelastic history. Reference 1 used the absolute cumulative plastic strain at the beginning of a loading cycle in representing this history dependent behavior. In order to understand the definition of this strain, it is useful to observe a hysteretic stress-strain diagram from a coupon test shown in Fig. 2.2. At Point d in this figure, the absolute cumulative plastic strain, $\sum \epsilon_p$, is defined as the sum of strains along the abscissa from Point a to b, from b to c, and then from c to d.

Plastic growth versus absolute cumulative plastic strain relationships for Struts 10, 12, 14 and 16 are plotted in Fig. 2.7. This figure exhibits a positive linear correlation between these two variables, and a least-square (linear) approximation for the data for each strut is shown. The slope of the approximation line, called the "growth factor," is an important parameter for modeling plastic growth. The Jain [17] and the Maison [18] models employ the growth factor in defining plastic growth.

2.4 Summary

This chapter is concerned with the experimental hysteretic behavior of steel braces. A summary of this chapter is presented below.

An experimental program for 24 cyclically loaded struts tested by Black, Wenger, and Popov [1] was reviewed. These struts consisted of various types of sections, while the effective slenderness ratio was either 40, 80, or 120.

Causes of the deterioration of buckling loads were identified. It was shown that either an increase of residual lateral displacements, a degradation of tangent moduli, or a decrease of maximum tensile loads would result in the deterioration of buckling loads.

The post-buckling deterioration of brace capacities was studied. An emphasis was placed on identifying the influence of slenderness ratios on the deterioration. The strut with a kL/r of 40 showed a fuller enveloping surface of the translated axial force - axial displacement curve and the strut with a kL/r of 120 showed a more pinched one. The buckling zone (Fig. 1.11) existed in the enveloping surface of the translated curve of struts with a kL/r of 40 but not in the surface of struts with a kL/r of 80 or 120. Plastic growth had a positive linear correlation with absolute cumulative plastic strain. Growth factor values were determined based on this correlation.

3. THE REFINED PHENOMENOLOGICAL MODEL

3.0 General

This section introduces a refined phenomenological model. This model, developed on the basis of the phenomenological type approach taken by Maison [18], is extended to overcome some of its limitations. This new element mimics hysteretic axial force - axial displacement relationships by the use of a series of predefined linear lines as shown in Fig. 3.1.

A complete description of the properties and mechanisms of the refined model can be found in Appendix B. The user's manual for the element is also included in this appendix. Considerable efforts have been devoted to avoiding inconsistent analytical results caused by poor selection of parameters. At the beginning of each analysis, input parameters are thoroughly checked and warnings concerning potential causes of misbehavior in the element are issued.

The refined phenomenological model has been developed as an inelastic truss element for the DRAIN-2D2 program [21]. This refined model utilizes the new programming capabilities of DRAIN-2D2, which more reliably models dynamic inelastic responses of structures. Detailed information on the assumptions and operating characteristics of this program can be found in Reference 21. The basic characteristics of this program are briefly described below.

The DRAIN-2D2 program is a practical and efficient computer program for the inelastic behavior analysis of two-dimensional structures. The structure is idealized as a planer assemblage of discrete elements. The program contains a series of elements in its library; furthermore, new elements may be added without changing the framework of the program. Static loads may be considered in addition to horizontal and vertical components of base ground shaking. In analysis, the direct stiffness method is used with the nodal displacements as unknowns. The dynamic response is determined using step-by-step integration based on the constant average-acceleration method. Each step uses the tangent stiffness of the structure and assumes linear structural behavior during that step. Solutions of the equations of motion in the program

can be attained either by automatic or constant time stepping strategies. Equilibrium errors (unbalanced forces) resulting from the discrepancies between this linear assumption and actual inelastic member behavior are eliminated by the application of corrective loads in the subsequent time step. These unbalanced forces, however, can become so large that they cause spurious results. The user can reduce the time step duration in such cases. Alternatively, the optional automatic event-to-event solution strategy implemented in the DRAIN-2D2 program greatly reduces unbalanced forces, thus reducing numerical errors. If this option is specified, the tangent stiffness matrix of the structure is reassembled when the stiffness of an element changes within a step. The use of this option can lessen the unbalanced forces, reducing cumulative errors and increasing the stability of analyses.

3.1 New Features of the Refined Model

3.1.0 General

The new model is nearly identical in its features to that developed by Maison [18] and reported in Reference 19. The various zones and control parameters are shown in Figs. 3.1 and 3.2. Only these new features significantly influencing its capabilities will be discussed below.

3.1.1 Event-to-Event Solution Strategy

The new model is capable of providing an "event-to-event" tracing of the axial force - axial displacement loops (see Fig. 3.3). The exact deformation value at which the element enters new zones is detected and the new stiffness is computed, thus nullifying unbalanced forces induced by the change in stiffness between different zones. The event-to-event solution strategy is performed at the expense of more execution time associated with the reassembly and re-triangularization of stiffness matrix of the structure. In case small effects due to unbalanced loads are anticipated in the response history, the user of the new element may also opt for the step-by-step method.

3.1.2 Implementation of a New Zone

In actual cyclic behavior, after the buckling load is reached, a brace will gradually lose its compressive strength as its shortening proceeds. The Maison element, the prototype of the new model, fails to mimic this behavior properly when a steep slope is attributed to Zone 5. To be precise, the brace shortening exceeding U5X will cause an unreasonable (tensile) analytical value, as shown in Fig. 3.4, where U5X expresses the value of displacement at the intersection of zero load and Zone 5. A new zone, Zone 10, has been incorporated in the new model in order to resolve this problem as shown in Fig. 3.5. If a strut is shortened further than U5X, Zone 5 exits to Zone 10. After the displacement history is reversed, and when axial displacement reaches U5X, Zone 5 enters Zone 7. As a result, the refined model guarantees consistent analytical results, even if a steep slope is specified for Zone 5.

3.2 Comparison with the Maison Model

As previously mentioned, the Maison model is superior to other phenomenological models in its ability to mimic complex hysteretic loops. In this section, the refined phenomenological element is compared with the Maison element in order to demonstrate the superiority of the refined model. Figure 3.6 compares analytical hysteresis loops obtained using the refined model and using the Maison element for the case where Zone 5 intersects with zero load. This comparison shows that the refined model provides consistent analytical results, while the Maison element provides completely spurious analytical results. It is clear that the refined model is superior to the Maison model in this regard.

4. METHOD FOR SELECTION OF INPUT PARAMETERS

4.0 General

In the refined phenomenological model, the analytical axial force - axial displacement relationship of a strut is defined by the use of a series of empirical input parameters (see Fig. 3.2). It is crucial to the successful application of the model that the values of these parameters be specified properly. In this chapter, a systematic method is proposed for the selection of the input parameters. This method makes the selection easier, although it requires the availability of an appropriate analytical or experimental axial force - axial displacement relationship for each strut analyzed. During the discussion on this method, it may be helpful to repeatedly refer to Fig. 3.2 which shows the definitions and orientations of the various input parameters.

Prior to discussing this method, it is important to note that the values of parameters must be carefully selected, as inappropriate values sometimes result in unrealistic analytical brace behavior. For example, a negative yield load would clearly lead to an absurd analytical result. The parameters values must generally fall in their certain allowable ranges, as summarized in Table 4.1.

4.1 Material Properties

This section offers a method for selecting parameters associated with the material properties of a brace, including: the yield stress and modulus of elasticity. In practice, the actual yield stress is not known with certainty. It may differ considerably from actual or measured values. However, it is advisable to use measured values when they are available as they generally reflect the actual properties influencing strut behavior.

The value of modulus of elasticity is used to define the tangent stiffness of Zone 1, which expresses both the elastic zones in "tension" and in "compression," as shown in Fig. 3.1. However, actual brace tangent stiffnesses for the elastic zone in tension are usually considerably larger than those in compression, as noted in the experimental hysteresis loops (see Fig. 2.1 for

an example). It is therefore difficult to select the values of the initial modulus of elasticity such that both zones can be perfectly simulated. Since this value does not have a big influence on energy dissipation of the resulting analytical hysteresis loops, but is required to match the initial dynamic characteristics of the structure, it is sufficient in most analyses to use the initial modulus of elasticity measured by coupon or other tests. It was not believed to be necessary at this time to introduce a new zone accounting for the reduced stiffness of the elastic zone in compression.

4.2 Initial Buckling Loads

It is suggested that initial buckling loads be evaluated according to the method presented in Reference 1 and summarized in Table 4.2. This method utilizes Eq.1.5-1 of the ASIC specifications [23], without the factor of safety, for basic calculations. For subsequent comparisons, refined computations were made for Struts 1, 2, 10, and 11 to account for the effect of excessive initial camber, and for Struts 5, 7, 17, 22, and 24 by considering the influence of material nonlinearities. The steel for tubes and especially for pipes tends to exhibit a poorly defined yield point, which limits the reliability of computations based on the initial elastic modulus. The effect of material nonlinearities was included by employing the tangent modulus in the generalized Euler formula. The Westergaad and Osgood formula, based on Von Karman's concept for inelastic buckling of eccentrically loaded struts [24], was used to include the effect of excessive initial camber. Again, it is important to be aware of the many factors influencing buckling loads and to account for them in selecting input parameters.

4.3 Growth Factor, Growth Limit, and Hardening Ratio

An empirical method for evaluating growth factors was introduced in Section 2.3 (see Fig. 2.7). As can be seen from this figure, there are strong linear correlations between the growth factor and cumulative absolute plastic strain. For this reason, this empirical method is expected to be able to evaluate growth factors reasonably well. It is advisable, however, to evaluate the

values of the growth factor by preliminary trial and error analyses for better correlation with experimental results.

A "growth limit" is used to define the maximum value of the axial elongation of a strut. This represents tensile rupture of the brace. No attempt is made to account for load history effects. Too small of a growth limit may erroneously stop the execution of a computer analysis when strut elongations exceed these limits.

Hardening ratios, used in defining the slope of the tensile yielding portion of a brace's hysteretic loops, should be determined by observing experimental axial force - axial displacement curves and by evaluating the slopes of strain hardening plateaus.

4.4 Parameters for Defining Post-Buckling Stage

The parameters, PCRF, U34, U45, P45 and C5, are used for two completely different purposes: (1) to define a linear approximation of the strut's post-buckling behavior and (2) to define the deterioration of buckling loads for subsequent cycles (see Fig. 4.1). As can be seen in Fig. 4.2, the first purpose is achieved by selecting straight line segments which best fit the enveloping surface of a shifted axial force - axial displacement curve. The second purpose is necessitated by the simplified deterioration rule used (see Fig. 4.1 and Appendix B), and is achieved as follows. Firstly, the values of experimental buckling load are plotted as a function of $(\delta_{min}-\delta_s)$, where δ_{min} denotes the minimum axial displacement at each cycle and δ_s indicates the axial displacement at the start of each cycle. Secondly, parameters, PCRF, U34, and U45, are selected such that analytical buckling loads can best fit experimental ones. It is not difficult to select optimal parameters to achieve only one of these two purposes. However, in order to achieve both purposes, some compromises may be required in selecting some parameters.

The selection of U34 values necessitates some additional care. It was demonstrated in Section 2.2 that the enveloping surface of a translated axial force - axial displacement curve exhibits a kink at the buckling point for struts with a kL/r of 80 or of 120. In analysis, this kink is expressed by setting the $U34/|\delta_{cr}|$ value close to -1. For struts with a kL/r of 40, $U34/|\delta_{cr}|$

should be specified as less than -1 to include the buckling zone.

4.5 Parameters for Defining Reversed Post-Buckling Stage

4.5.0 General

The parameters, U6, P6, U7, P7, U8, P8, and C8, define linear approximations of the reversed (reloading) post-buckling stage of the cyclic inelastic behavior (Zones 6, 7, 8, and 9). This section offers a method for the selection of these parameters.

4.5.1 Control Points (U6,P6) and (U7,P7)

Two control points (U6,P6) and (U7,P7), together with displacement history reversal points, are used to define Zones 6 and 7 (see Fig. 4.3). It is convenient to define each control point with the use of a translated axial force - axial displacement curve, plotting the tangent line of Zone 6 (or Zone 7) for each experimental cycle and then finding the focus of these lines. Figure 4.4 (a) shows an example of Point (U6,P6) perfectly defined as a focal point. However, in many cases, such an ideal focus does not exist, as shown in Fig. 4.4 (b). In this example, a small P6 (or a large U6) works well when a displacement history reverses at large brace shortenings, and a large P6 (or a small U6) works well for small ones. Unless information on the brace displacement history is known *a priori*, values of U6 and P6 must often be selected at the expense of accuracy for reversals at very small and large brace shortenings. This may require iterative analyses in cases where these parameters affect results significantly.

Note that, if the value of either U6 or U7 is too small, the analytical hysteresis loops will be unreasonable when displacement history reverses at small brace shortenings, as shown in Fig. 4.5. This problem can be settled by selecting (U6,P6) and (U7,P7) to be either in the "allowed" or the "recommended" regions indicated in Fig. 4.6. When these points fall in the "allowed" region, the tangent of Zone 6 (or 7) could possibly become very large. It would not, however, cause such unreasonable results as those shown in Fig. 4.5. When the control points fall in the recommended region, no problems should arise in the cycling behavior of Zones 6 and 7.

4.5.2 Control Point (U8,P8) and Tangent Stiffness of Zone 8, C8

The control point (U8,P8) and the tangent stiffness of Zone 8,C8,are used to define Zone 8. Originally, Zone 8 was defined to express the "plastic zone in tension" as shown in Fig. 3.1 [19]. However, this zone does not exist for all struts, as can be observed from the experimental axial force - axial displacement curves shown in Appendix A.

In the case where this zone actually exists, U8, P8, and C8 values can be used for the original purpose. In addition, care must be taken not to select excessively large values for C8. To be precise, the minimum brace axial displacement must not be less than U8X, which is the value of the axial displacement at the intersection of zero load and Zone 8. Violations of this limitation will result in unreasonable analytical results, as shown in Fig. 4.7.

In the case where the plastic zone in tension does not exist, Zone 8 can be either (1) completely eliminated (see Fig. 4.8 (b)) or (2) applied to smooth the transition from Zone 7 to Zone 9 (Fig. 4.8 (c)). In the former case, the controlling point (U8,P8) and (U7,P7) should be located at the same point and a large C8 value be specified. In the latter case, (U8,P8) should be located close to (U7,P7) and C8 should be moderately large. These three applications, which are called the original, the eliminated, and the transition applications of Zone 8 in Fig. 4.8, may be used to better simulate the reversed post-buckling stage.

4.6 Concluding Remarks

This chapter presented a systematic method for the selection of input parameters. This procedure, however, necessitates case by case observation of cyclic inelastic behavior for each strut analyzed, a requirement both restrictive and costly. Furthermore, the physical interpretation of some of the input parameters is unclear, so that selecting appropriate values of input parameters may sometimes be troublesome. In spite of these drawbacks, this procedure provides a reasonable and convenient method for selecting input parameters.

5. QUASI-STATIC ANALYSES OF INDIVIDUAL STRUTS

5.0 General

In the previous chapters, a systematic method for the selection of input parameters was established. In this chapter, sample input parameters are developed for each of the 24 struts tested by Black *et al* [1]. Simple quasi-static analyses are undertaken for these struts to verify these parameters and the new model. At the same time, behavioral characteristics of the refined phenomenological model will be assessed.

5.1 Sample Input Parameters for Individual Struts

Sample input parameters for the aforementioned 24 struts were selected following the method presented in Chapter 4. These parameters are normalized and listed in Tables 5.1 through 5.4. Note that parameters for Strut 9 were not presented because it had not undergone adequate cycles of displacement history reversals in the experiment to exhibit fully its hysteretic nature.

The values of the parameters were normalized as follows. The initial buckling load PCR and its corresponding displacement δ_{cr}, representing behavior in the post-buckling stage were used to normalize the parameters, PCRF, U34, U45, P45 and C5, defining the post-buckling stage of the hysteresis loop. The yield load P_y and its corresponding displacement δ_y, representing cycling behavior in the reversed post-buckling stage, were used to normalize the parameters ,U6, P6, U7, P7, U8, P8 and C8. A special consideration was made in normalizing the buckling load PCR. The Euler-buckling formula may be rewritten to read:

$$\frac{PCR}{P_y}\frac{\sigma_y}{\pi^2 E}=\frac{1}{(kL/r)^2} \tag{5.1}$$

where P_y is the yield load; σ_y denotes the yield stress; E is the initial modulus of elasticity. The left-hand side of this equation is used to normalize the buckling load PCR.

These sample input parameters were selected following the method presented in the previous chapter. Some detailed aspects in this selection are briefly explained below. For the initial modulus of elasticity, a commonly used value, 29000 ksi (200000 MPa), was specified for all the struts.

Three ways to define Zone 8 were proposed in Subsection 4.5.2 (see Fig. 4.8). The original application was used for Struts 2, 7, 11, 13, 16, 17, 19, and 21; the eliminated application for Struts 14, 22, and 24; the transition application was used for the remaining struts.

Table 5.5 contains the range of axial displacement for each strut imposed in the experiment. The sample input parameters selected are valid for axial displacement histories within this range. The influence of displacement histories on the optimal input parameters will be discussed later in this report.

These parameters are applicable to any brace whose effective slenderness ratio and cross section approximately match those for one of the 24 struts tested. Also, these parameters form the basis of the sample input parameters for individual sections presented in the subsequent section.

5.2 Quasi-Static Analyses of Individual Struts

Analytical and experimental hysteresis loops for the 24 individually tested struts are compared in Figs 5.1 and 5.2, and Figs. A1 through A10. The analytical results have been obtained by computing the axial forces for the axial displacement histories imposed on the test specimens. Figure 5.3 shows examples of the displacement histories used in these analyses. Because of last minute refinements in parameter values, some of the values used for parameters in these analyses differ slightly from the values presented in the previous section. The parameter values used in these analyses are indicated by the use of parentheses in Tables 5.1 to 5.4 when they are different from the sample values. The differences, however, were never so large as to significantly influence analytical results. It is therefore possible to use these comparisons for the verification of the sample input parameters.

The analytical hysteresis loops are in good accordance with experimental results, which are highly complex. It can be concluded that the sample input parameters presented above are able to provide accurate analytical results and that the refined phenomenological model is capable of simulating overall cyclic buckling behavior. In addition, the validity of the method for selecting input parameters, as presented in Chapter 4, is also demonstrated by these results.

5.3 Remarks on Analytical Behavior

5.3.0 General

Behavioral characteristics of this element are discussed in the following subsections with an aim towards identifying needs for future development.

5.3.1 Growth Factor

The quasi-static analyses were undertaken for Strut 3 using two different values of growth factors, 0.0 and 0.15, in order to monitor the effect of this parameter on the analytical results. As can be seen from Fig. 5.4, an increase in growth factors reduced cyclic tensile load capacities and tangent stiffnesses. This effect was greater in the later cycles. Thus, values of the growth factor, having large influence on analytical results, should be selected with care.

In the foregoing analyses of the 24 struts, growth factors were selected on the basis of preliminary trial and error analyses such that analytical results best simulated the corresponding test data. In practice, however, it is both costly and tedious to carry out such preliminary analyses. This problem might be resolved by employing the empirical method for the prediction of growth factors presented in Section 2.3, which utilizes growth factor versus $\sum \epsilon_p$ curves (see Fig. 2.7). Table 5.6 contains a comparison of growth factors selected in this manner with those determined based on the trial and error analyses. These two series of growth factors agree relatively well. The method presented in Section 2.3 appears to be a reasonable way to estimate growth factors especially when there is no supporting test data. Of course, more studies should be required to assess its validity.

5.3.2 Deterioration of Buckling Loads

The refined model includes an aspect of deterioration of buckling loads during inelastic cycles. A comparison of analytical and experimental buckling load capacities, shown in Fig. 5.5, shows comparatively good correlation between them. Reasons for minor discrepancies are explained below.

As previously mentioned, analytical buckling load deterioration is defined by the use of the tangent of Zone 4, C4 (see Fig. 4.1). The steeper the tangent of Zone 4, the more rapid the deterioration of buckling loads. However, it is unlikely that there is a strong direct physical interrelationship between the values of C4 and the deterioration of buckling loads. Moreover, C4 is also used for defining cyclic behavior of Zone 4. The use of C4 for these two completely different purposes not only makes the selection of its value difficult, but also causes errors in analyses.

Another source of inaccuracy in simulating the deterioration of buckling loads is the omission of the effect of residual strut camber. An example of this can be seen in the comparison of analytical and experimental results for Strut 19, shown in Fig. 5.2. As mentioned in Chapter 2.2, this strut suffered a degradation of maximum tensile loads from Cycles 5 through 7, that caused an increase of residual strut cambers, thereby reducing its buckling loads. However, this tendency is not reflected in these analyses. This is one of the common limitations of phenomenological models.

5.3.3 Straight Line Segments

Phenomenological models simulate observed axial force - axial displacement relations using a series of straight line (linear) segments. Since an actual axial force - axial displacement relation is made up of many curved lines which vary cycle after cycle, it is inherently inaccurate to mimic this behavior by a set of straight lines. In addition, the use of straight lines creates discontinuities in tangent stiffness values where the zones intersect and could result in instability in numerical methods using iteration.

There is no firm theoretical basis for phenomenological models, so that an increase in the number of segments, or other refinements may be misleading. The models rely on having either applicable experimental data or analytical results for the type of strut analyzed and the history of loading employed.

5.3.4 Tangent Stiffness

It is important to accurately simulate the variation of the tangent stiffness. Experimental results show that the tangent of the elastic zone in tension is significantly larger than that in compression. However, phenomenological models, which assign the same tangent value to both zones, fail to express this feature. It is also observed in test results that the tangent stiffness in the elastic zone degrades from one cycle to the next. Phenomenological models, which employ a constant tangent stiffness value for the elastic zone (Zone 1), fail to implement these detailed aspects regarding the variation of tangent stiffness.

5.4 Effect of Displacement Histories on Optimal Input Parameters

The dependency of input parameters on displacement history is discussed here. Firstly, we investigate whether the optimal input parameters are independent on the displacement histories used in analyses. It is interesting to note that Struts 3, 4 and 5 all have the same member and material properties (see Table 5.1), but each has experienced a different displacement history (see Fig. 5.3) and has shown a different hysteretic behavior (see Figs. 5.1 and 5.6). Because each of the struts has the same member and material properties, the resulting input parameters should be the same, if the optimal parameters were independent of displacement history. In reality, the parameters selected for these struts (as shown in Table 5.1) are not actually the same. It is apparent that the optimal parameters are dependent on displacement histories.

Secondly, the applicability of input parameters to different displacement histories is studied. For this purpose, a series of analyses were performed as follows. The parameters for Strut 3 were employed; however, the displacement histories for Struts 4 and 5 were imposed,

respectively; and the resulting hysteretic loops computed for each displacement history were compared with experimental ones. Analytical results shown in Fig. 5.6 correlate well with corresponding test results. By noting that displacement histories for these struts are basically similar, it can be concluded that parameters chosen for a displacement history are applicable to other similar displacement histories.

As we have seen, optimal input parameters are dependent on displacement histories but analytical results may not be very sensitive to the resulting variations in the parameters. The use of sample parameters in analysis is recommended where the axial displacements satisfy the recommended range of the axial displacement observed in the test for each strut (see Table 5.5). Care must be taken in applying these parameters for displacement histories which do not satisfy these ranges. Caution should also be exercised where loading histories may significantly differ from those considered herein.

5.5 Concluding Remarks

This chapter was concerned with analytical results computed using the refined phenomenological model. A summary of this chapter is presented below.

Analytical results were obtained by the use of the sample input parameters for individual struts. A comparison between these results with corresponding test results showed a good correlation. It was suggested that sample input parameters validated in this way could be used for selecting input parameters for similar struts when experimental data are not available. During the course of these analyses, it was assessed that the new element can accurately simulate overall cyclic inelastic behavior and overcome several of the limitations of previous models [18].

The optimum input parameters depend on displacement histories. The proposed sample input parameters are recommended for use when a displacement history falls within the recommended ranges listed in Table 5.5.

The growth factor is inversely proportional to both the analytical tensile load capacity and the tangent stiffness in the tension phase of loading. The method for evaluating the growth factor presented in Fig. 2.7 is expected to be able to provide reasonable estimates.

The feature to define the deterioration of buckling load used in the element lacks a firm theoretical basis and fails to express the effect of the residual camber of the strut. The model relies on having either applicable experimental data or analytical results for the type of strut analyzed and the history of loading employed.

6. GENERALIZED INPUT PARAMETERS

6.0 Introductory Remarks

As demonstrated in the previous chapter, the refined phenomenological model is capable of accurately representing cyclic inelastic behavior of steel braces. However, in order to obtain such accurate representation the users of the model need to specify appropriate input parameters of each brace analyzed. This can be troublesome, since the data currently available about input parameters are limited.

Sample input parameters for 24 different braces have been proposed in the previous chapter. However, it is unlikely that users of the refined model would often encounter these particular struts. For this reason, these sample input parameters appear to be too specific for convenient use. To counteract the shortage of available data about input parameters, sample input parameters for individual "sections" with different effective slenderness ratios are generalized in this chapter.

6.1 Generalized Input Parameters for Individual Sections

6.1.0 General

The aforementioned 24 struts are made from various sections: wide-flange, double-angle, double-channel, tee, pipe and tube sections. Among these sections, the wide flanges, tubes, and pipes were all used in sufficient numbers to develop some generalized input parameters. However, generalized input parameters are not presented for the remaining sections, because of the limited number of struts used. Instead, a representative set of generalized parameters, applicable to any type of section is devised from all of the available data.

The effective slenderness ratio is the most important parameter in describing inelastic buckling behavior of struts [1]. All data are classified according to the value of effective slenderness ratio, which equals 40, 80, or 120. As a result of this classification, generalized input parameters for the following eight categories are presented in this section. The categories

are wide flanges with a kL/r ratio of 40, of 80, and of 120; tubes with kL/r of 80; pipes of 80; and general sections of 40, of 80, and of 120. Note that parameters for either tubes or pipes with a kL/r of either 40 or 120 are not presented due to a lack of sufficient strut data.

The input parameters presented in Tables 5.1 to 5.4 are plotted in Figs. 6.1 to 6.12. Each figure contains separate plots for "wide flanges," for "tubes and pipes," and for "general sections." Note that the data for tubes and pipes, which have somewhat similar cross sections, are plotted together to monitor correlations between their data. Growth factors, PCR, PCRF, U34, and C5 are plotted using the effective slenderness ratio as the abscissas. Control points (U45,P45), (U6,P6), (U7,P7) and (U8,P8) are plotted using normalized axial displacements as abscissas and normalized axial forces as ordinates.

For the growth factor, C5, and PCRF, empirical formulae were developed to give generalized input parameters in terms of arbitrary effective slenderness ratios. Suggested generalized parameters are listed in Tables 6.1 to 6.3. More detail is provided below.

6.1.1 **Hardening Ratio and Growth Factor**

The generalized parameters for hardening ratios were obtained by simply averaging their values for individual struts for each effective slenderness ratio. Care must be taken when applying these values to analyses. The hardening ratios were selected without too much precision because their values did not have a large influence on the analytical hysteretic behavior exhibited by the struts. This is because they did not undergo a large amount of yielding in tension.

For the growth factor, two types of empirical formulae are advanced herein. One expresses the growth factor as a function of the effective slenderness ratio; another expresses it as a function of the maximum tensile load. Fig. 6.1 shows the growth factor versus effective slenderness ratio relationships, showing weak inverse proportionality. This inverse proportionality reflects the following behavioral characteristics: a stocky strut with a smaller effective slenderness ratio is closer to plastic action, thereby developing larger plastic growth. The least-square linear approximation developed for the wide flanges is

$$Growth\ Factor = -0.00103(kL/r) + 0.185 \tag{6.1}$$

and for general sections.

$$Growth\ Factor = -0.00107(kL/r) + 0.169 \tag{6.2}$$

Although there is relatively large amount of scattering in data points, these linear approximations will provide convenient and reasonable estimates of growth factors.

For tubes and pipes, it is not possible to develop such a linear approximation due to a lack of sufficient data. Instead, averages of growth factor values, 0.087 for tubes and 0.104 for pipes, are advanced as generalized values. Because growth factors for pipes have small variations, the estimate for pipes is expected to be reliable. However, the estimate for tubes may be less certain since their growth factors have bigger variations.

The correlations of plastic growths to normalized maximum elongations δ_{max}/δ_y are shown in Fig. 6.2. There is a strong direct proportionality between these two variables in the plot for wide flanges. A linear approximation

$$Growth\ Factor = 0.02\frac{\delta_{max}}{\delta_y} - 0.053 \tag{6.3}$$

may be used to refine the value of the growth factor, when information about the maximum elongation is available.

For tubes and pipes with a kL/r ratio of 80, the growth factor versus δ_{max}/δ_y relationship shows a very strong direct proportionality, except for the data point for Strut 16. Among the 24 struts considered, this strut has an uncommon small yield load, P_y; therefore, the data point for Strut 16 was omitted in evaluating the following linear approximation for tubes and pipes with a kL/r of 80,

$$Growth\ Factor = 0.014\frac{\delta_{max}}{\delta_y} + 0.031 \tag{6.4}$$

Because the data points for "wide flanges" and for "tubes and pipes" have small spreads from the linear approximations, the empirical formulae in Eqs. 6.3 and 6.4 would be expected to be reliable. The data points for general sections have a relatively large scatter, so that the formula

$$Growth\ Factor = 0.0053\frac{\delta_{max}}{\delta_y} + 0.044 \tag{6.5}$$

might be less precise. However, this equation would at least be a convenient method for estimating growth factors, without prior test data about the strut analyzed.

6.1.2 **Initial Buckling Loads and Final Buckling Loads**

The method suggested for the evaluation of initial buckling loads in Reference 1 has been presented in Section 4.2. This method enables us to make good estimates; however, it may be sometimes too complicated in practice. Plots of normalized initial buckling loads PCR/P_y, shown in Fig. 6.3, indicate that buckling loads are relatively in good accordance with the Euler buckling formula for kL/r ratios of 80 and 120. For simplicity, this formula can be used for struts with kL/r ratios ranging from 80 to 120.

Plots of the normalized final buckling load versus effective slenderness ratio relationship, shown in Fig. 6.4, do not indicate any significant correlation between them. For simplicity, it is suggested that the average of the normalized final buckling load for each effective slenderness ratio be used as an estimate.

Several other types of estimates can be attempted. However, the best results are obtained from PCRF/|PCR| versus P_t/P_y relations, shown in Fig. 6.5, where P_t is the average maximum tensile force. There are strong positive proportionalities between these two variables. These proportionalities are in good accordance with the hysteretic behavior of braces, that is, large tensile loads reduce residual lateral displacements and increase buckling capacities. Straight line approximations are presented for wide flanges,

$$\frac{PCRF}{|PCR|} = -0.48\frac{P_t}{P_y} + 0.098 \tag{6.6}$$

for tubes and pipes,

$$\frac{PCRF}{|PCR|} = -0.34\frac{P_t}{P_y} - 0.114 \tag{6.7}$$

and for general sections,

$$\frac{PCRF}{|PCR|} = -0.64\frac{P_t}{P_y} + 0.068 \tag{6.8}$$

6.1.3 **Control Displacement U34**

As previously mentioned, the normalized control displacement, $U34/|\delta_{cr}|$, must be less than or equal to -1, where -1 corresponds to the case for which the axial force - axial displacement curve does not have the "buckling zone" (see Fig. 2.6 for an example). Plots of $U34/|\delta_{cr}|$ versus kL/r relationship shown in Fig. 6.6 indicate that their values equal -1 for struts with a kL/r of 120, that they are very close to or equal to -1 for those with a kL/r of 80, and that they are less than -1 for those with a kL/r of 40. Hence, it is suggested that $U34/|\delta_{cr}| = -1$ be used for struts with a kL/r ratio greater than or equal to 80. The average of $U34/|\delta_{cr}|$ be an good estimate for struts with kL/r of 40. There is insufficient data to estimate values for other kL/r ratios.

6.1.4 **Tangent Stiffness of Zone 5, C5**

Figure 6.7 shows plots of normalized tangents of Zone 5, C5. As can be seen, its values are inversely proportional to the effective slenderness ratio. It reflects a tendency for stocky members to have upward concave hysteretic curves in the compression side, and for slender ones to have convex curves. As a result, stocky members have steeper tangents of Zone 5 than slender ones do. Linear approximations for wide flanges,

$$\frac{C5}{C1} = 0.000079 \cdot (kL/r) - 0.016 \tag{6.9}$$

and for general sections

$$\frac{C5}{C1} = 0.00008 \cdot (kL/r) - 0.018 \tag{6.10}$$

are obtained by employing the least-square method. For tubes and pipes with a kL/r of 80, it is recommended that averages of the data points be employed.

6.1.5 Control Points (U45,P45), (U6,P6) and (U7,P7)

Figures 6.8 to 6.10 show plots of control points (U45,P45), (U6,P6) and (U7,P7). These plots indicate a small amount of scattering for the cases with a kL/r of 80 and of 120. In addition, control point (U45,P45) for general sections with a kL/r of 40 show a relatively small amount of scattering. For each of these cases, the center of gravity of data points could serve as an excellent estimate (see Tables 6.1 through 6.3).

In evaluating control points (U6,P6) and (U7,P7) for general sections with a kL/r of 40, a problem arises because U6, P6, U7, and P7 values for Strut 21 are more than twice as large as those for other struts. The control points (U6,P6) and (U7,P7) for Strut 21 each are out of the range of Figs. 6.9 and 6.10. Note that Strut 21 has the smallest yield load and has shown the fullest experimental axial force - axial displacement curve (see Fig. A8). Due to such uncommon nature, the data for Strut 21 were omitted in the evaluation of generalized parameter values. It is suggested that the center of gravity for the remaining data be used as generalized values for (U6,P6) and (U7,P7), respectively.

6.1.6 Control Point (U8,P8) and Tangent Stiffness of Zone 8, C8

Fig. 6.11 contains plots of the control point (U8,P8). These plots show a small amount of scattering in the data for wide flanges and for general sections for each effective slenderness ratio, with one exception, the data for general sections with a kL/r of 80. Except for this case, it is suggested that the generalized parameter for control points (U8,P8) be the center of gravity for the data points and those for C8 be the average (see Fig. 6.12).

In discussing the wide spread data for general sections with a kL/r of 80, it must be noted that there are three different applications for zone 8: the "original", the "eliminated" and the "transition" applications, introduced in Subsection 4.5.2 (see Fig. 4.7). The values of

parameters U8, P8, and C8 depend entirely upon which application is employed. The transition application, employed for the majority of struts with a kL/r of 80, was recommended to be employed in evaluating generalized parameters. Therefore, only the data for the struts which employed the transition application were used and the parameters for (U8,P8) were chosen as the center of gravity of (U8,P8) for these struts and that for C8 as the average of C8 for them.

For tubes and pipes the determination of the generalized input parameters was problematic. Among three applications of Zone 8, each application was employed for no more than two struts; therefore, there were not sufficient data to decide generalized parameters. For convenience, generalized parameters for general sections can also be used for tubes and pipes.

6.2 Analyses using Generalized Input Parameters for Individual Sections

Tables 6.1 to 6.3 list generalized input parameters for individual types of "sections", which have been presented in the previous section. For the verification of these parameters, analyses were performed for Strut 3 (kL/r=80) and Strut 6 (kL/r=120) by using the generalized parameters for wide flanges and for general sections, respectively. The resulting analytical axial force - axial displacement curves, shown in Figs. 6.13 and 6.14, exhibit good correlation with test results. The generalized parameters seem to be valid. The generalized parameters for different sections currently provide a convenient and reasonable method for the selection of input parameters in analysis.

6.3 Concluding Remarks

This chapter advanced generalized input parameters for individual types of "sections," which provide more versatile and convenient information than those developed just for individual "braces." Of course, generalized parameters do not provide such accurate analytical results as those for specific braces. Still, they are convenient when specific parameters are not available. It must be, however, noted that the generalized parameters were determined on the basis of a limited number of strut data. In order to make the generalized input parameters more

accurate it will be necessary to undertake an even more comprehensive series of cyclic buckling tests so as to increase the data base.

The generalized parameters for sections are prepared for wide flanges with a kL/r ratio of 40, of 80, and of 120, tubes with a kL/r of 80, pipes of 80, and general sections of 40, of 80, and of 120. Although generalized parameters are advanced only for these discrete values of kL/r, judicious interpolation of these data can enable us to arrive at values for kL/r ratios ranging from 40 to 120. Caution should be employed for sections with unusual configuration and material properties, and subjected to significantly different displacement histories.

7. SUMMARY, CONCLUSIONS, AND RECOMMENDATIONS

7.1 Summary

This report outlines the development and workings of a refined phenomenological model, developed to simulate the cyclic inelastic behavior of struts in steel braced frames. Several empirical and analytical studies have been conducted to assess the behavioral characteristics of this element. In addition, attempts have been made to identify appropriate parameters to use in conjunction with this type of element.

In Chapter 1, previous research on the cyclic inelastic behavior of steel braces was reviewed. In addition, the influence of brace buckling on the performance of simple braced frames was examined, indicating the need for accurate modeling of the inelastic characteristics of braces.

The cyclic inelastic buckling behavior of braces was studied in Chapter 2 to identify the behavioral characteristics that need to be incorporated in such elements. This investigation focused on the deterioration of the buckling load, the post-buckling degradation of the brace capacity, and the progress of plastic growth with cycling. In Chapter 3, the refined model was introduced, together with an explanation of the new features, including an "event-to-event solution strategy" and "Zone 10".

A systematic method for selecting input parameters was proposed in Chapter 4. Care was taken to avoid selecting values of input parameter which could result in unrealistic analytical results. In Chapter 5, quasi-static analyses of individual struts were carried out using the element. The validity of the method for selecting input parameters, as well as of the sample input parameters themselves, was assessed on the basis of these analyses. Results of simple analyses by the refined element are compared with those obtained using the Maison element in order to demonstrate the efficiency of new features. Several behavioral characteristics of the element were discussed with an aim towards identifying future development needs.

A series of generalized input parameters for various types of struts sections were advanced in Chapter 6. An extensive study on the dependence of these input parameters on slenderness ratios and other parameters led to generalized input parameters which provide versatile information to users of this type of phenomenological element.

7.2 Conclusions

The following major conclusions were drawn from the results of this research program. The refined model is capable of simulating overall cyclic buckling behavior reasonably well for all kinds of sections with the slenderness ratio ranging from 40 to 120.

The refined model overcomes several limitations of the previous Maison element. In particular, inclusion of Zone 10 guarantees consistent analytical results even when large brace shortenings occur. Also, the output information provided for the user is considerably extended.

The method proposed for the selection of parameters proved capable of providing reasonable parameter values. This method includes rules for the prevention of unreasonable analytical results. The physical meaning and dependency of some of the input parameters is unclear, so that their selection is sometimes expected to be troublesome.

The sample and generalized input parameters presented are able to produce analytical results which reasonably simulate corresponding test data. These input parameters can be of assistance to users of the model, especially when experimental data are not available. The sample input parameters for individual types of struts provide accurate but very specific information, while the generalized parameters for individual sections provide somewhat less accurate but more convenient information. However, in order to make the data for generalized parameters more accurate, it is necessary to undertake an expanded series of cyclic buckling tests.

This study has indicated that there is relatively large uncertainty in the values that should be selected for some input parameters. However, it appears that, so long as a consistent set of parameters is chosen, the overall hysteretic response is likely to be accurately simulated. Thus,

the generalized input parameters are not expected to be sensitive to moderate changes in loading history or section type.

This work also clearly emphasizes the fact that phenomenological models do not have a firm theoretical basis so that their usefulness is somewhat limited. The models rely on having applicable experimental data or analytical results regarding the type of strut analyzed and the displacement history employed. It appears that physical theory models hold great promise for future implementation in computer analyses.

7.3 Recommendations

For practical application of phenomenological brace models, it is necessary to develop an improved method for selecting input parameters for struts where no test data exists. There are two possible ways to resolve this problem. The first is to prepare generalized input parameters for commonly used types of sections on the basis of available experimental data. In this research report, a first attempt is made at this by inspecting input parameters for 24 different braces. However, this information is limited and more experimental work is necessary to increase the accuracy and versatility of these parameters. The second method is to use physical theory or finite element analytical models to the preparation of sample parameters.

Several potential improvements in the phenomenological model were also identified. These include:

(1) Deterioration of elastic stiffness in compression with cycling.

(2) Improved methods for modeling deterioration of buckling load with cycling.

(3) Local buckling and failure algorithms.

The need for these should be assessed and appropriate means of achieving them be addressed in future research.

Since the phenomenological models only mimic observed behavior, further refinements in capabilities may result in an unwarranted sense of confidence. Results obtained may be

unreliable unless there is data available to establish the required input parameters. Because of the difficulties in establishing this data, it appears that efforts should be directed at developing improved analytical techniques based on physical theory and finite element approaches. Because of the increasing complexity of phenomenological models, it appears that physical theory models may be particularly attractive to study.

REFERENCES

1 Black, R.G., Wenger, W.A.B. and Popov, E.P., "Inelastic Buckling of Steel Strut under Cyclic Load Reversals," Report No. UCB/EERC-80/40, Earthquake Engineering Research Center, University of California, Berkeley, CA., October 1980.

2 Popov, E.P., Bertero, V.V., and Chandramouli, S., "Hysteretic Behavior of Steel Columns," Report No. UCB/EERC-75/11, Earthquake Engineering Research Center, University of California, Berkeley, CA., September 1975.

3 Wakabayashi, M., Nonaka, T., Koshiro, O. and Yamamoto, N., "An Experiment on the Behavior of a Steel Bar Under Repeated Axial Loading," Annuals, Disaster Prevention Research institute, Kyoto University, No. 14A, pp. 371-381, 1971 (in Japanese).

4 Wakabayashi, M., Nonaka, T., Nakamura, T., Morino, S. and Yoshida, N., "Experimental Studies on the Behavior of Steel Bars Under Repeated Axial Loading, Part-1," Annuals, Disaster Prevention Research Institute, Kyoto University, No. 16B, pp. 113-125, 1973 (in Japanese).

5 Shibata, M., Nakamura, T., Yoshida, N., Morino, S., Nonaka, T., and Wakabayashi, M., "Elastic-Plastic Behavior of Steel Braces Under Repeated Axial Loading," Proc. of the 5th WCEE, pp. 845-848, Rome, 1973

6 Wakabayashi, M., Matsui, C. and Mitani, I., "Cyclic Behavior of a Restrained Steel Brace Under Axial Loading," 6th World Conference on Earthquake Engineering, New Delhi, 1977, Preprint, Vol. 11, pp.189-194.

7 Wakabayashi, M., Nakamura, T. and Yoshida, N., "Experimental Studies on the Elastic-Plastic Behavior of Braced Frames Under Repeated Horizontal Loading, Part-1," Bulletin of Disaster Prevention Institute, Kyoto University, Vol. 27, Part 3, No. 251, September 1977, pp. 121-154.

8 Wakabayashi, M., Nakamura, T., and Yoshida, N., "Experimental Studies on the Elastic-Plastic Behavior of Braced Frames under Repeated Horizontal Loading, Part-2," Bulletin of Disaster Prevention Research Institute, Kyoto University, Vol. 27, Part 3, No. 264, March 1980

9 Sherman, D.R., and Erzurumlu, H., "Ultimate Capacity of Tubular Beam-Columns," Presented at the ASCE National Structural Engineering Conference, Madison, Wisconsin, August 1976.

10 Jain, A.K., Goel, S.C and Hanson, R.D., "Inelastic Response of Restrained Steel Tubes," Journal of the Structural Division, Proceeding of ASCE, Vol. 104, No. ST6, June 1978.

11 Zayas, A.Z., Mahin, S.A. and Popov, E.P., "Cyclic Inelastic Behavior of Steel Offshore Structures," Report No. UCB/EERC-80/27, Earthquake Engineering Research Center, University of California, Berkeley, CA., October 1980.

12 Gugerli, H. and Goel, S.C., "The inelastic Cyclic Behavior of Axially-Loaded Steel Members," Report No. UMEE 82R1, Department of Civil Engineering, The university of Michigan, Ann Arbor, Michigan, January 1982.

13 Nilforoushan, R, "Seismic Behavior of Multi-Story K-Braced Frame Structures," University of Michigan Research Report UMEE 73R9, Ann Arbor, November 1973.

14 Singh, P., "Seismic Behavior of Braces and Braced Steel Frames," Report No. UMEE 77R1, Department of Civil Engineering, University of Michigan, Ann Arbor, July 1977.

15 Marshall, P.W., "Design Considerations for Offshore Structures Having Nonlinear Response to Earthquakes," Preprint, ASCE Annual Convention and Exposition, Chicago, October 1978.

16 Roeder, C.W., and Popov, E.P., "Inelastic Behavior of Eccentrically Braced Frames Under Cyclic Loading," EERC Report No. 77-18, Earthquake Engineering Research Center, University of California, Berkeley, CA., August 1977.

17 Jain, A.K., and Goel, S.C., "Hysteresis Models for Steel Members Subjected to Cyclic Buckling or Cyclic End Moments and Buckling," University of Michigan Research Report UMEE 78R6, Ann Arbor, December 1978.

18 Maison, B., and Popov, E.P., "Cyclic Response Prediction for Braced Steel Frames," Journal of the Structural Division, ASCE, July 1980.

19 Zayas, A.Z., Shing, P.B., Mahin, S.A. and Popov, E.P., "Inelastic Structural Modeling of Braced Offshore Platforms for Seismic Loading," Report No. UCB/EERC-81/04, Earthquake Engineering Research Center, University of California Berkeley, CA., January 1981.

20 Mondkar, D.R., and Powell, G.H., "ANSR-I, General Purpose Program for Analysis of Nonlinear Structural Response," Report No. UCB/EERC-77-18, Earthquake Engineering Research Center, University of California, Berkeley, December 1975.

21 Golafshani, A.A., "DRAIN-2D2: A Program for Inelastic Seismic Response of Structures," Ph.D. Dissertation, University of California, Berkeley, January 1982.

22 Timoschenko, S.P. and Gere, J.M., "Theory of Elastic Stability, Second Edition," Mcgraw-Hill Book Co., New York, N.Y., 1961, p. 200.

23 "Manual of Steel Construction," 8th ed., American Institute of Steel Construction, Chicago, Ill., 1980.

24 Westergaard, H.M., and Osgood, W.R., "Strength of Steel Columns," A.S.M.E. Transactions, 1927-1928, APM-50-9

25 Riahi, A., Row, D.G., Powell, G.H., "Three Dimensional Inelastic Frame Elements for the ANSR-I Program," Report No. 77/18, Earthquake Engineering Research Center, University of California, Berkeley, August, 1978.

Table 1.1 Comparison of Phenomenological Models

Name of Model	Number of Segments	Deterioration of Buckling Loads	Plastic Growth	Local Buckling
Nirforoushan	9	No	No	No
Singh	5	No	No	No
Marshall	7	No	No	Yes
Jain	6	Yes	Yes	No
Roeder	9	Yes	No	No
Maison	9	Yes	Yes	No

Table 4.1 Allowable Ranges of the Values of Input Parameters

Required Ranges	Recommended Ranges
$0 > U13 > U34 > U45$	$U7 > \frac{P7}{C1}$
$0 > P45 > PCR$	$U8 > \frac{P8}{C1}$
$0 > PCRF > PCR$	
$C5 < 0$	
$U6 \geqslant 0$	
$P6 > 0$	
$U7 \geqslant 0$	
$P7 > 0$	
$U8 < P_y \frac{L}{EA}$	
$0 < P8 < P_y$	
$C8 > 0$	
Growth Factor $\geqslant 0$	
Hardening Ratio $\geqslant 0$	

Table 4.2 Initial Buckling Loads for 24 Struts [1]

STRUT NO.	EXPERIMENTAL σ_y (ksi)	P_{cr}^{exp}(kips)	$P_{cr}^{exp} / P_{cr}^{calc*}$		
			Based on σ_y=36ksi	Based on Exper. σ_y	Refined Estimate
1	40.4[a]	95	0.81	0.81	0.98[d]
2	42.2[b]	263	1.05	0.90	1.07[e]
3	40.2[b]	202	1.19	1.09	-
4	40.2[b]	201	1.19	1.09	-
5	40.2[b]	152	0.90	0.83	0.96[f]
6	44.7[b]	112	1.19	1.21	-
7	50.0[c]	201	1.28	0.95	-
8	40.8[b]	197	1.08	0.98	-
9	43.6[b]	292	1.43	1.17	-
10	41.6[c]	97	0.92	0.92	1.06[g]
11	35.5[c]	105	0.79	0.79	1.05[h]
12	39.5[b]	186	0.98	0.91	-
13	41.8[a]	196	1.11	0.99	-
14	47.5[c]	114	1.25	1.03	-
15	47.5[c]	110	1.21	0.99	-
16	24.0[c]	87	0.69	0.95	-
17	59.0[c]	123	1.21	0.88	0.98[f]
18	82.0[b]	272	1.54	1.00	-
19	40.2[b]	240	1.19	1.07	-
20	40.8[b]	180	0.98	0.89	-
21	24.0[c]	107	0.99	1.05	-
22	82.0[b]	239	1.35	0.88	-
23	35.7[c]	165	1.22	1.23	-
24	46.3[c]	85	1.10	0.92	1.05[f]

* $P_{cr}^{calc} = Q_s \left[1 - \frac{(K\ell/r)^2}{2C_c^2}\right] \sigma_y A$

[a] 0.2% offset in coupon test

[b] Average yield from coupon tests

[c] First yield in strut test

[d] Initial max Δ=0.094 in.

[e] Initial max Δ = 0.16 in.

[f] Tangent modulus theory

[g] Initial max Δ = 0.05 in.

[h] Initial max Δ = 0.10 in.

NOTE: 1 ksi = 6.89 MPa; 1 kip = 4.45 kN; 1 in. = 25.4 mm

Table 5.1 Sample Input Parameters for Struts 1 though 6

Strut No.	1	2	3	4	5	6
Section	W8×20	W6×25	W6×20	W6×20	W6×20	w6×16
Bound. Con.	Pinned at Both Ends					
kL/r	120	40	80	80	80	120
Length (ft)	12.50	5.10	10.07	10.07	10.07	9.67
Area ($in.^2$)	5.90	7.34	5.87	5.87	5.87	4.74
Initial Mod.	29000.	29000.	29000.	29000.	29000.	29000.
($k/in.^2$)	(32370.)	(50000.)	(31743.)	(34500.)	(26000.)	(50430.)
δ_{cr} (in.)	-0.085	-0.071	-0.132	-0.131	-0.112	-0.078
PCR (k)	-96.9	-245.8	-185.3	-184.4	-158.3	-92.6
δ_y (in.)	0.209	0.089	0.168	0.168	0.168	0.179
P_y (k)	238.0	310.0	236.0	236.0	236.0	212.0
Hard. Ratio	0.010	0.010	0.	0.010	0.010	0.010
Growth Fac.	0.026	0.210	0.150	0.150	0.085	0.070
PCR / P_y	-0.41	-0.79	-0.79	-0.78	-0.67	-0.44
PCRF / |PCR|	-0.31	-0.44 (-0.47)	-0.38	-0.40 (-0.43)	-0.37 (-0.32)	-0.37
U34 / $\|\delta_{cr}\|$	-1.00	-1.68	-1.00	-1.00	-1.20	-1.00
U45 / $\|\delta_{cr}\|$	-2.97	-5.87	-2.36	-1.83	-3.74	-3.58
P45 / |PCR|	-0.31	-0.37	-0.34	-0.25	-0.32	-0.33
C5 / C1	-0.0048	-0.0107	-0.0125 (-0.0146)	-0.0078	-0.0075	-0.0080
U6 / δ_y	0.34	0.00 (-0.34)	0.30	0.09	0.18	0.56
P6 / P_y	0.25	1.31 (1.24)	0.42	0.48	0.44	0.26
U7 / δ_y	0.06	0.00 (-0.95)	0.35	0.12	0.00 (-0.13)	0.
P7 / P_y	0.21	1.25 (0.59)	0.61	0.35	0.32 (0.31)	0.21
U8 / δ_y	-0.14	-2.49	-0.45	-0.36	0.18	-0.56
P8 / P_y	0.21	0.41	0.28	0.35	0.58	0.21
C8 / C1	0.219	0.034	0.177	0.241	0.284	0.378
Zone 3 Exists	No	Yes	No	No	No	No
Zone 8 Exists	No	Yes	No	No	No	No

( ) : Values Used in Analysis C1 : Tangent of Zone 1

Table 5.2 Sample Input Parameters for Struts 7 through 12

Strut No.	7	8	10	11	12
Section	W6×15.5	2-L6×3$\frac{1}{2}$×$\frac{3}{8}$	2-L4×3$\frac{1}{2}$×$\frac{3}{8}$	2-C8×11.5	WT5×22.5
Bound. Con.	Pinned at Both Ends				
kL/r	40	80	120	120	80
Length (ft)	4.87	9.27	12.50	9.83	8.33
Area ($in.^2$)	4.60	6.84	5.34	6.76	6.63
Initial Mod.	29000.	29000.	29000.	29000.	29000.
($k/in.^2$)	(28890.)	(32040.)	(43000.)	(67000.)	(49000.)
δ_{cr} (in.)	-0.093	-0.113	-0.089	-0.060	-0.106
PCR (k)	-211.6	-201.0	-91.5	-100.0	-204.4
δ_y (in.)	0.101	0.156	0.215	0.150	0.136
P_y (k)	230.0	279.0	222.0	250.0	262.0
Hard. Ratio	0.010	0.010	0.010	0.010	0.010
Growth Fac.	0.075	0.035	0.002	0.004	0.070
PCR / P_y	-0.92	-0.72	-0.41	-0.40	-0.78
PCRF / |PCR|	-0.33	-0.28	-0.48	-0.50	-0.22
U34 / $\|\delta_{cr}\|$	-1.83	-1.00	-1.00	-1.00	-1.00
U45 / $\|\delta_{cr}\|$	-3.99	-2.66	-3.95	-3.56	-2.456
P45 / $\|P_{cr}\|$	-0.25	-0.25	-0.39	-0.28	-0.22
C5 / C1	0.0101	-0.0087	-0.0126	-0.0048	-0.0052
U6 / δ_y	0.00 (-1.24)	0.49	0.19	0.35	0.38
P6 / P_y	0.78 (0.57)	0.30	0.25	0.18	0.55
U7 / δ_y	0. (-0.60)	0.	0. (-0.14)	0.	0.07
P7 / P_y	0.48 (0.35)	0.20	0.25 (0.20)	0.20	0.31
U8 / δ_y	-1.84	-0.48	-0.47	-1.60	0.15
P8 / P_y	0.15	0.20	0.20	0.09	0.48
C8 / C1	0.010	0.280	0.402	0.005	0.602
Zone 3 Exists	Yes	No	No	No	No
Zone 8 Exists	Yes	No	No	Yes	No

Parameters for Strut 9 were not presented, because it had not undergone enough cycles of loading to determine them.

( ) : Values Used in Analysis C1 : Tangent of Zone 1

Table 5.3 Sample Input Parameters for Struts 13 through 18

Strut No.	13	14	15	16	17	18
Section	WT8×22.5	Pipe4 Std.	Pipe4 Std.	Pipe4 X-S	TS4×4×.25	TS4×4×½
Bound. Con.	Pinned at Both Ends					
kL/r	80	80	80	80	80	80
Length (ft)	10.47	10.07	10.07	9.87	10.00	9.07
Area ($in.^2$)	6.63	3.17	3.17	4.41	3.59	6.36
Initial Mod. ($k/in.^2$)	29000. (30000.)	29000. (33390.)	29000. (30880.)	29000. (67140.)	29000. (29570.)	29000. (39740.)
δ_{cr} (in.)	-0.129	-0.146	-0.146	-0.085	-0.145	-0.161
PCR (k)	-198.0	110.7	-111.1	-91.6	-125.5	-272.0
δ_y(in.)	0.181	0.198	0.198	0.098	0.244	0.308
P_y (k)	277.0	151.0	151.0	106.0	212.0	522.0
Hard. Ratio	0.010	0.025	0.010	0.010	0.010	0.010
Growth Fac.	0.060	0.125	0.110	0.075	0.150	0.080
PCR / P_y	-0.71	-0.73	-0.74	-0.86	-0.59	-0.52
PCRF / |PCR|	-0.36	-0.48	-0.40	-0.40	-0.52	-0.33
U34 / $\|\delta_{cr}\|$	-1.00	-1.00	-1.00	-1.00	-1.00	-1.00
U45 / $\|\delta_{cr}\|$	2.50	-1.51	-2.05	-3.82	-2.90	-3.43
P45 / |PCR|	-0.29	-0.45	-0.34	-0.33	-0.39	-0.33
C5 / C1	-0.0077	-0.0156	-0.0120 (-0.0141)	-0.0051	-0.0184	-0.0106
U6 / δ_y	0.15	0.	0.13	0.0 (-0.97)	0.35	0.06
P6 / P_y	0.45	0.42	0.45	0.76 (0.67)	0.40	0.26
U7 / δ_y	0.00 (-0.26)	0.28	0.00 (-0.08)	0.00 (-0.20)	0.36	0.00 (-0.10)
P7 / P_y	0.32 (0.29)	0.53	0.40 (0.34)	0.67 (0.57)	0.48	0.30 (0.29)
U8 / δ_y	-1.14	0.29	0.55	-2.68	-2.58	0.24
P8 / P_y	0.19	0.53	0.69	0.38	0.12	0.42
C8 / C1	0.014	Large Val.	0.329	0.014	0.012	0.515
Zone 3 Exists	Yes	No	No	No	No	No
Zone 8 Exists	Yes	No	No	Yes	Yes	No

( ) : Values Used in Analysis C1 : Tangent of Zone 1

Table 5.4 Sample Input Parameters for Struts 19 through 24

Strut No.	19	20	21	22	23	24
Section	W6×20	2-L6×3$\frac{1}{2}$×$\frac{3}{8}$	Pipe4 X-S	TS4×4×½	W5×16	Pipe3 Std.
Bound. Con.	Pinned at One End and Fixed at the Other End					
kL/r	40	80	40	80	80	80
Length (ft)	7.19	13.24	7.19	12.95	12.00	12.76
Area ($in.^2$)	5.87	6.84	4.41	6.36	4.68	2.68
Initial Mod.	29000.	29000.	29000.	29000.	29000.	29000.
($k/in.^2$)	(31230.)	(38000.)	(22000.)	(31830.)	(28000.)	(27380.)
δ_{cr} (in.)	-0.114	-0.162	-0.069	-0.229	-0.142	-0.160
PCR (k)	-224.3	-202.2	-101.9	-271.6	-134.1	-81.0
δ_y (in.)	0.120	0.223	0.072	0.440	0.177	0.244
P_y (k)	236.0	279.0	106.0	522.0	167.0	124.0
Hard. Ratio	0.025	0.010	0.050	0.005	0.010	0.010
Growth Fac.	0.120	0.053	0.040	0.030	0.080	0.105
PCR / P_y	-0.95	-0.72	-0.96	-0.52	-0.80	-0.65
PCRF / |PCR|	-0.30	-0.27	-0.46	-0.28	-0.29	-0.42 (-0.47)
U34 / $\lvert\delta_{cr}\rvert$	-1.70 (-1.29)	-1.00	-2.00 (-4.55)	-1.00	-1.03	-1.07
U45 / $\lvert\delta_{cr}\rvert$	-8.09	-1.11	-4.00 (-20.36)	-3.32	-2.39	-2.19
P45 / |PCR|	-0.30	-0.27	-0.44 (-0.40)	-0.40	-0.28	-0.42 (-0.47)
C5 / C1	-0.0175 (-0.0253)	-0.0192	-0.0175 (-0.0216)	-0.0219	-0.0117	-0.0200 (-0.0246)
U6 / δ_y	0.	0.38	1.05	0.11	0.59	0.29
P6 / P_y	2.03	0.29	7.36	0.26	0.60	0.60
U7 / δ_y	0. (-0.54)	0.	2.59	0.18	0.34	0.08
P7 / P_y	1.11 (1.04)	0.23	3.96	0.40	0.43	0.42
U8 / δ_y	-1.78	-0.22	-1.45	0.18	0.06	0.08
P8 / P_y	0.49	0.23	0.92	0.40	0.43	0.42
C8 / C1	0.066	0.392	0.039	Large Val.	0.180	Large Val.
Zone 3 Exists	Yes	No	Yes	No	No	No
Zone 8 Exists	Yes	No	Yes	No	No	No

( ) : Values Used in Analysis C1 : Tangent of Zone 1

Table 5.5 Range of Displacement

Strut No.	Max. Compression		Max Elongation	
	Value (in.)	$\delta/\lvert\delta_{cr}\rvert$	Value (in.)	δ/δ_y
1	-2.7	-31.8	1.0	4.8
2	-1.3	-18.3	1.0	11.2
3	-0.8	-6.1	1.6	9.5
4	-2.1	-16.0	1.7	10.1
5	-2.3	-20.5	1.6	9.5
6	-2.2	-28.2	1.1	6.1
7	-1.2	-12.9	0.7	6.9
8	-1.8	-15.9	1.2	7.7
9				
10	-2.3	-25.8	0.9	4.2
11	-2.3	-38.3	1.2	8.0
12	-2.1	-19.8	1.5	11.0
13	-2.3	-17.8	1.4	7.7
14	-1.3	-8.9	1.2	6.1
15	-2.4	-16.4	1.4	7.1
16	-2.0	-23.5	1.6	16.3
17	-1.4	-9.7	1.9	7.8
18	-2.3	-14.3	0.8	2.6
19	-0.7	-6.1	0.7	5.8
20	-1.0	-6.2	0.8	3.6
21	-0.7	-10.1	0.7	9.7
22	-2.0	-8.7	0.3	0.7
23	-1.4	-9.9	1.2	6.8
24	-1.2	-7.5	1.2	4.9

Table 5.6 Comparison of Growth Factors Evaluated using Two Different Methods

Strut No.	Method Used	
	Fig. 2.7	Trial-and-Error Analysis for Best Fit
10	0.029	0.002
12	0.037	0.070
14	0.101	0.125
16	0.060	0.075

TABLE 6.1 Generalized Input Parameters for Wide-Flange Sections

	Methods Used	Slenderness Ratio (kL/r)		
		40	80	120
Hard. Ratio	Average	0.015	0.075	0.01
Growth Factor	Least-Square	- 0.00103 (kL/r) + 0.185 0.02 δ_{max}/δ_y - 0.053		
PCR	Euler Formula		Eq. (5.1)	
PCRF/|PCR|	Average Least-Square	-0.35 $-0.48\frac{P_t}{P_y} + 0.098$		
U34/$\|\delta_{cr}\|$	Average	-1.74	-1.0	-1.0
C5 /C1	Least-Square	0.000079 (kL/r) - 0.016		
$(\frac{U45}{\|\delta_{cr}\|}, \frac{P45}{\|PCR\|})$	Center of Gravity	(-5.98,-0.31)	(-2.58,-0.3)	(-3.28,-0.32)
$(\frac{U6}{\delta_y}, \frac{P6}{P_y})$	Center of Gravity	(0.,1.37)	(0.29,0.49)	(0.45,0.26)
$(\frac{U7}{\delta_y}, \frac{P7}{P_y})$	Center of Gravity	(0.0,0.95)	(0.20,0.44)	(0.03,0.21)
$(\frac{U8}{\delta_y}, \frac{P8}{P_y})$	Center of Gravity	(-2.04,0.28)	(-0.14,0.41)	(-0.35,0.21)
C8 / C1	Average	0.037	0.22	0.30
Zone 8 Exists		Yes	No	No
Zone 3 Exists		Yes	No	No

TABLE 6.2 Generalized Input Parameters for Tube and Pipe Sections

	Methods Used	Types of Sections	
		Tubes (kL/r = 80)	Pipes (kL/r = 80)
Hard. Ratio	Average	0.014	0.008
Growth Factor	Average	0.087	0.104
	Least-Square	0.014 δ_{max}/δ_y + 0.0131	
PCR	Euler Formula	Eq. (5.1)	
PCRF/|PCR|	Average	-0.38	-0.43
	Least-Square	- 0.34 $\frac{P_t}{P_y}$ - 0.114	
U34/$\|\delta_{cr}\|$	Average	-1.0	-1.0
C5 / C1	Average	-0.017	-0.013
$(\frac{U45}{\|\delta_{cr}\|}, \frac{P45}{\|PCR\|})$	Center of Gravity	(-3.22,-0.37)	(-2.39,-0.39)
$(\frac{U6}{\delta_y}, \frac{P6}{P_y})$	Center of Gravity	(0.17,0.31)	(0.11,0.56)
$(\frac{U7}{\delta_y}, \frac{P7}{P_y})$	Center of Gravity	(0.18,0.39)	(0.09,0.51)
$(\frac{U8}{\delta_y}, \frac{P8}{P_y})$	Center of Gravity	(0.018,0.42)	(0.018,0.42)
C8 / C1	Average	0.22	0.22
Zone 8 Exists		No	No
Zone 3 Exists		No	No

TABLE 6.3 Generalized Input Parameters for General Sections

	Methods Used	Slenderness Ratio (kL/r)		
		40	80	120
Hard. Ratio	Average	0.024	0.01	0.01
Growth Factor	Least-Square	- 0.00107 (kL/r) + 0.169 0.0053 δ_{max}/δ_y + 0.044		
PCR	Euler Formula		Eq. (5.1)	
PCRF/|PCR|	Average Least-Square	-0.44 $-0.64\frac{P_t}{P_y} + 0.068$		
U34/$\|\delta_{cr}\|$	average	-1.8	-1.0	-1.0
C5 / C1	Least-Square	0.000080 (kL/r) - 0.018		
$(\frac{U45}{\|\delta_{cr}\|}, \frac{P45}{\|PCR\|})$	Center of Gravity	(-5.49,-0.33)	(-2.55,-0.33)	(-3.52,-0.33)
$(\frac{U6}{\delta_y}, \frac{P6}{P_y})$	Center of Gravity	(0.,1.37)	(0.20,0.45)	(0.36,0.24)
$(\frac{U7}{\delta_y}, \frac{P7}{P_y})$	Center of Gravity	(0.0,0.95)	(0.12,0.40)	(0.015,0.22)
$(\frac{U8}{\delta_y}, \frac{P8}{P_y})$	Center of Gravity	(-1.89,0.49)	(0.018,0.42)	(-0.69,0.18)
C8 / C1	Average	0.037	0.33	0.33
Zone 8 Exists		Yes	No	No
Zone 3 Exists		Yes	No	No

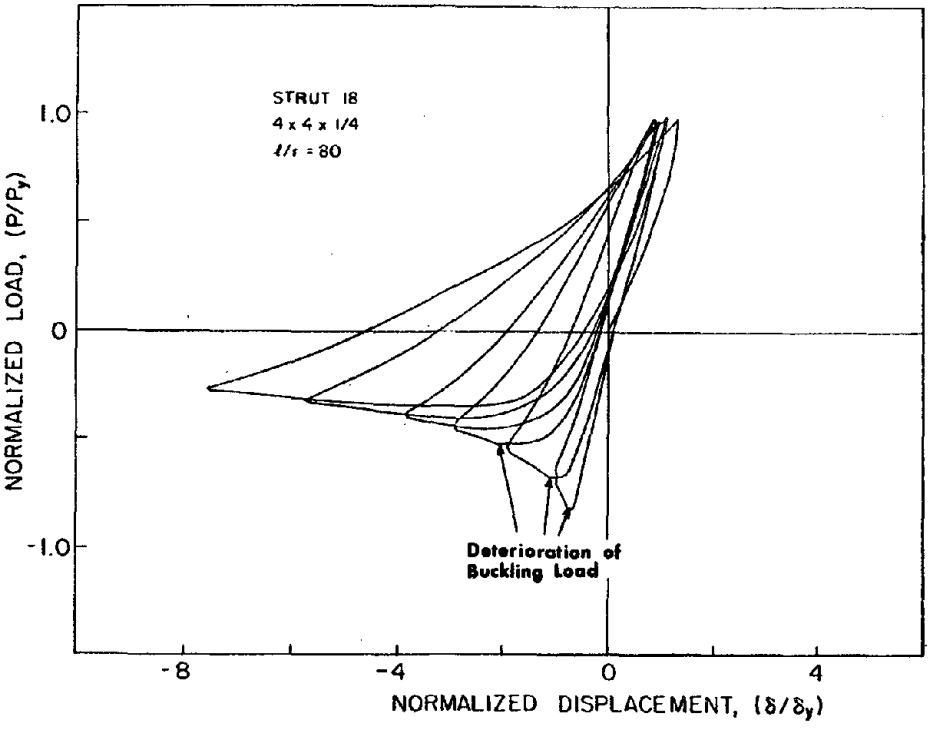

(a) Hysteresis Loop for a Brace [1]

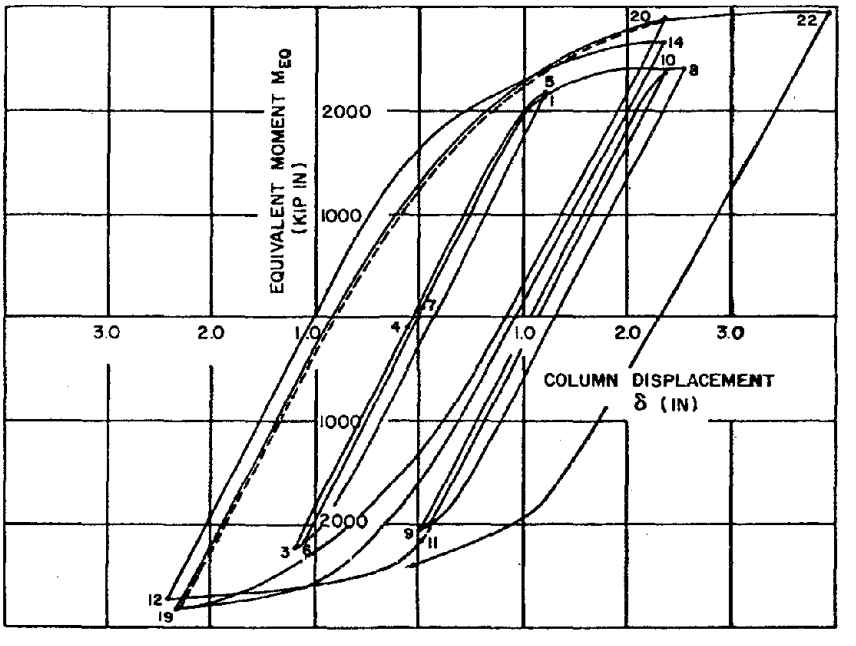

(b) Hysteresis Loop for a Column [2]

Fig. 1.1 Comparison of Hysteresis Loops for a Brace and for a Column

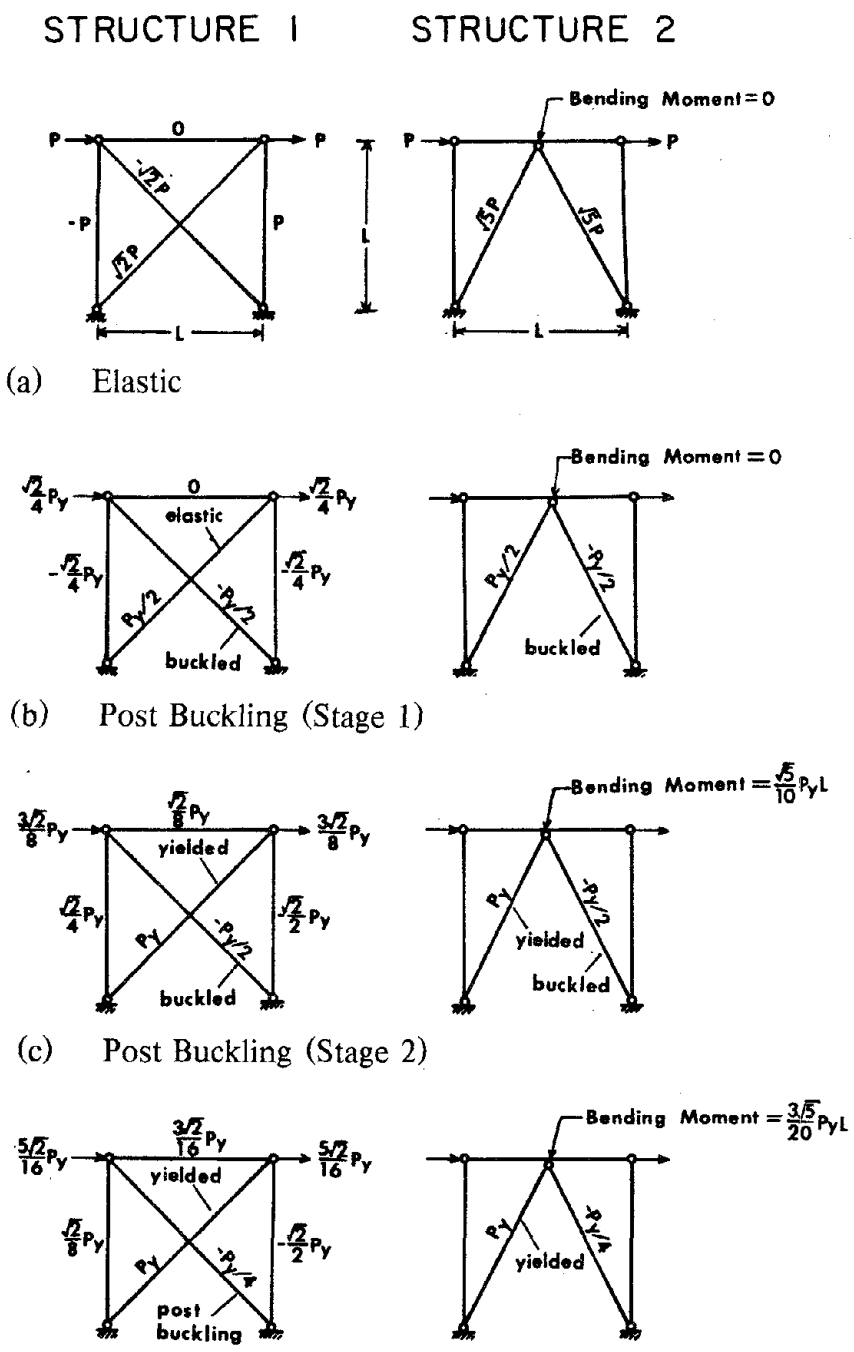

Fig. 1.2 Process of Redistribution of Internal Forces

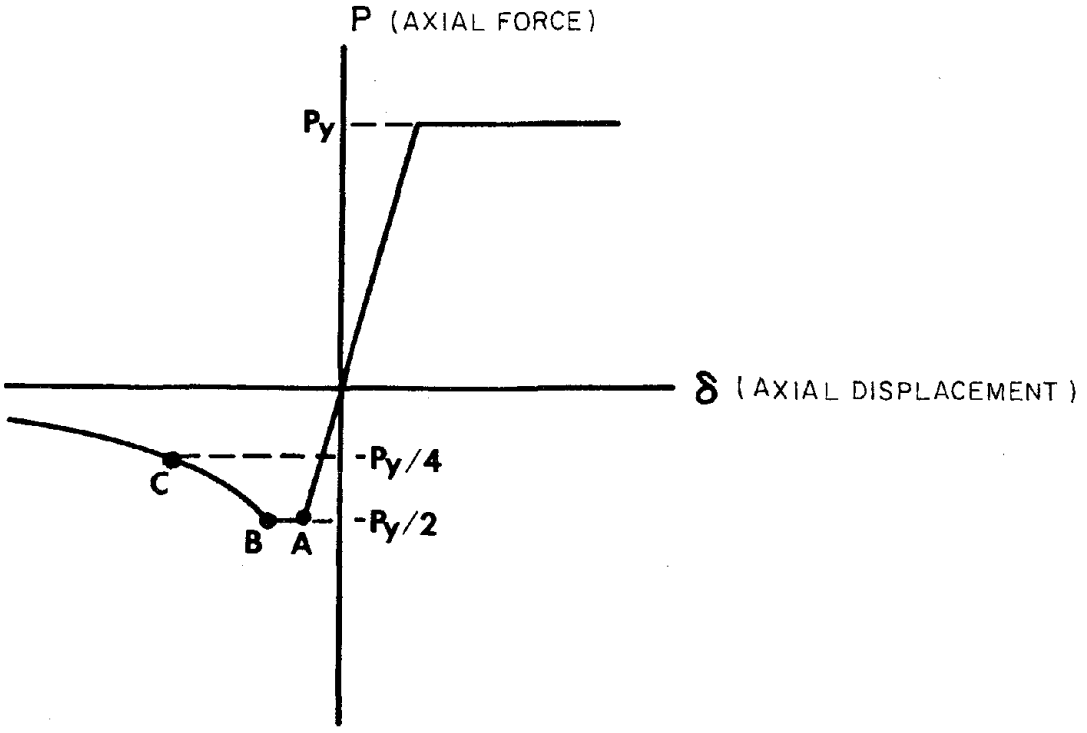

Fig. 1.3 Axial Force Versus Axial Displacement Relationship for Diagonal Braces

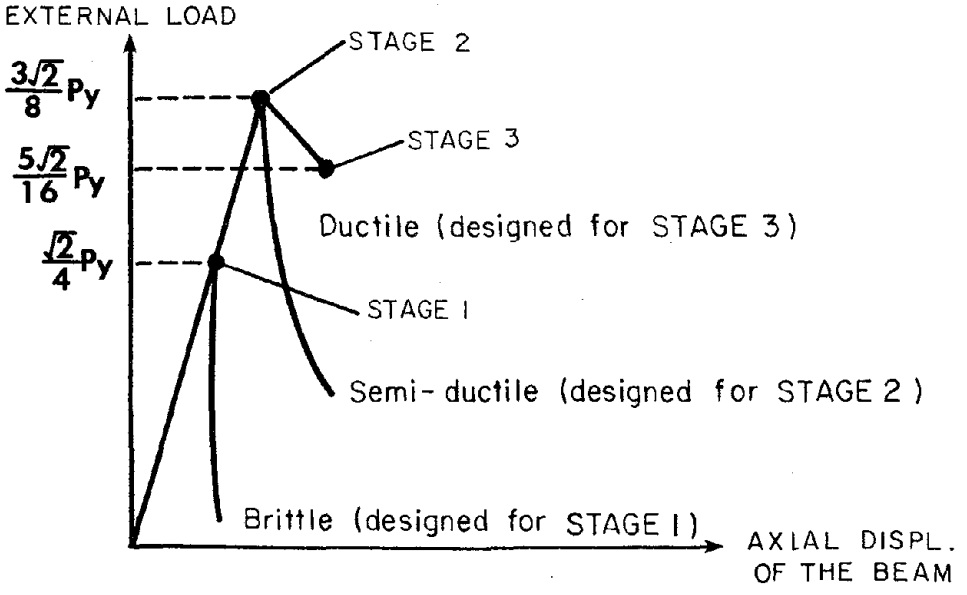

Fig. 1.4 Resistant Strength of the Structure

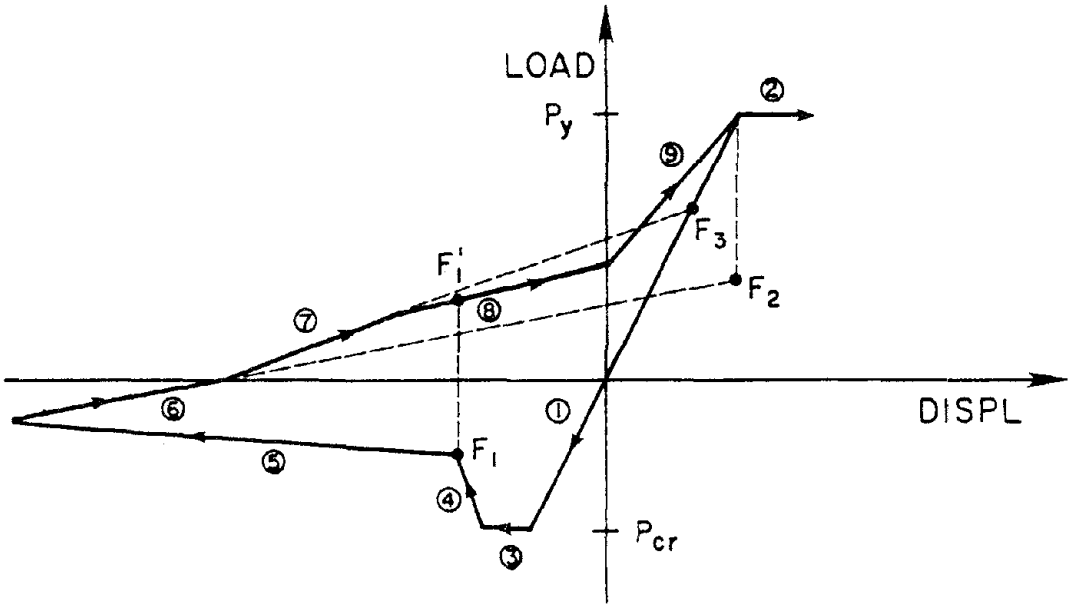

Fig. 1.5 Nilforoushan Model [13]

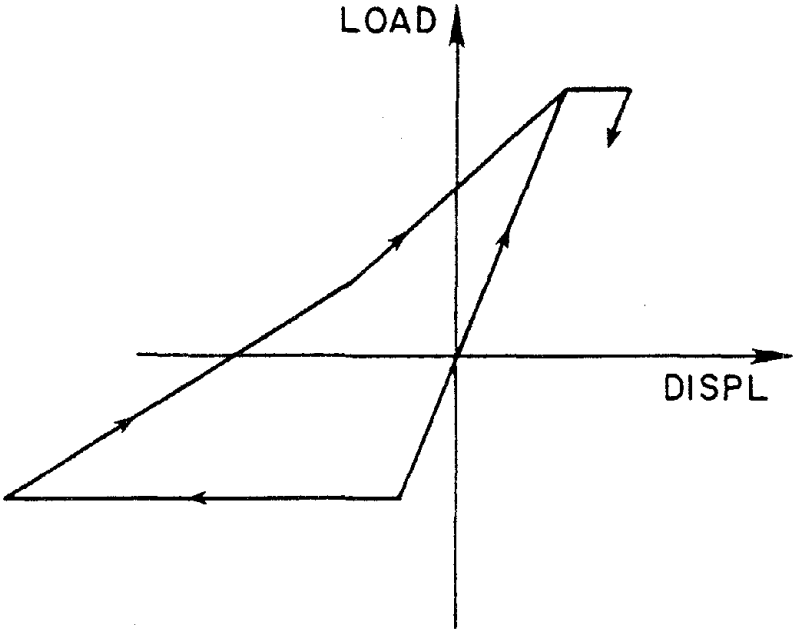

Fig. 1.6 Singh Model [14]

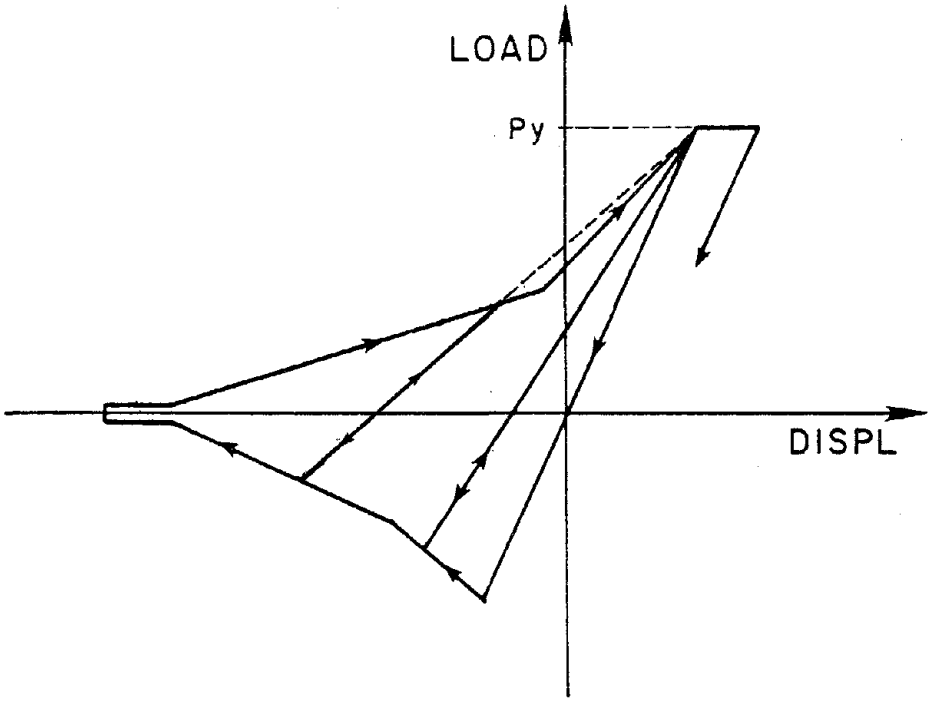

Fig. 1.7 Marshall Model [15]

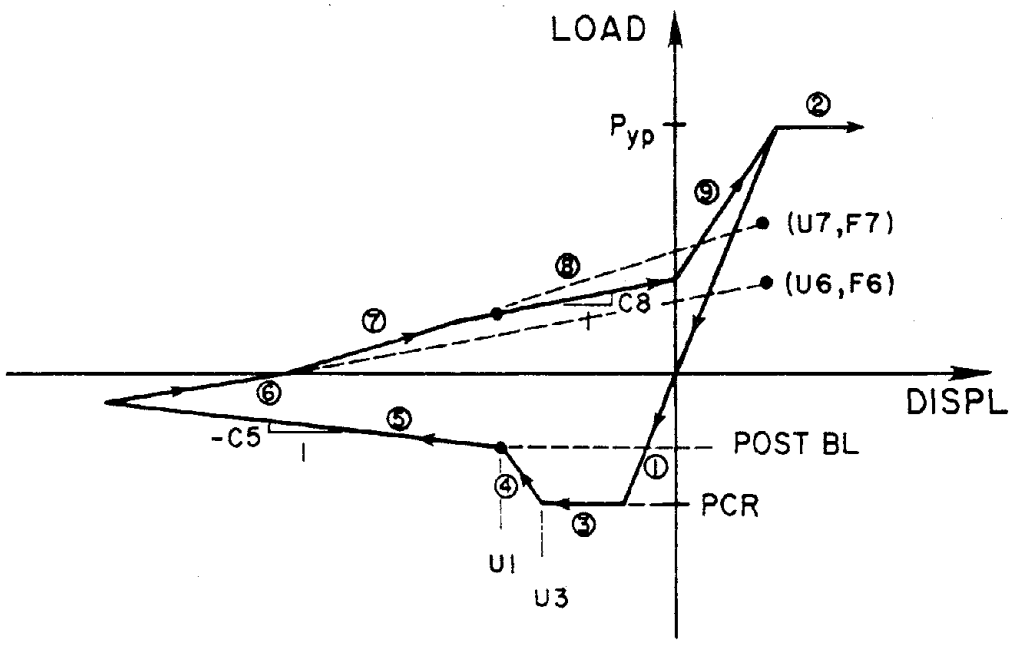

Fig. 1.8 Roeder Model [16]

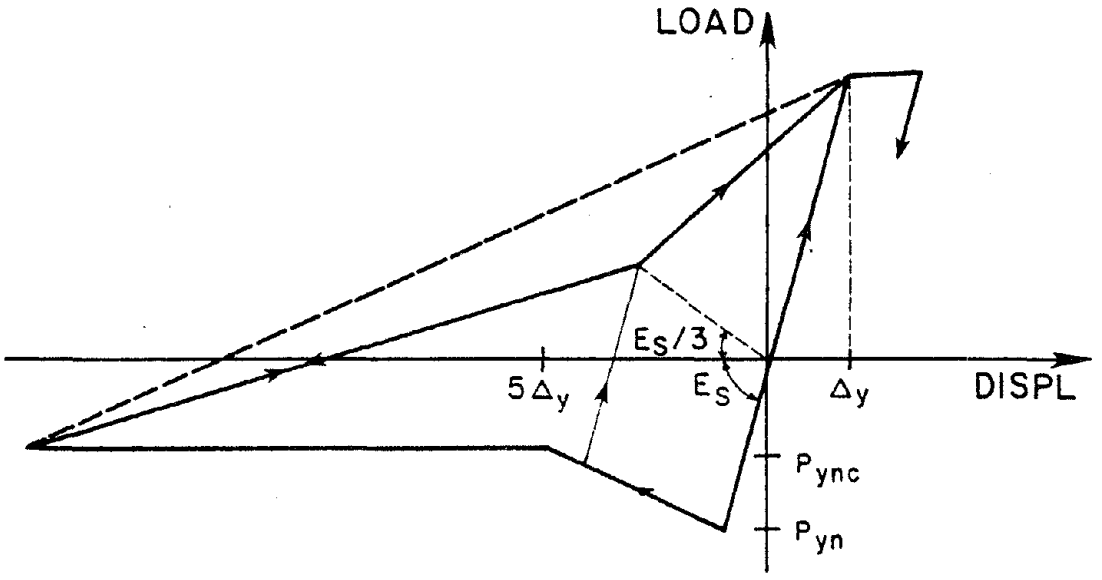

Fig. 1.9 Jain Model [17]

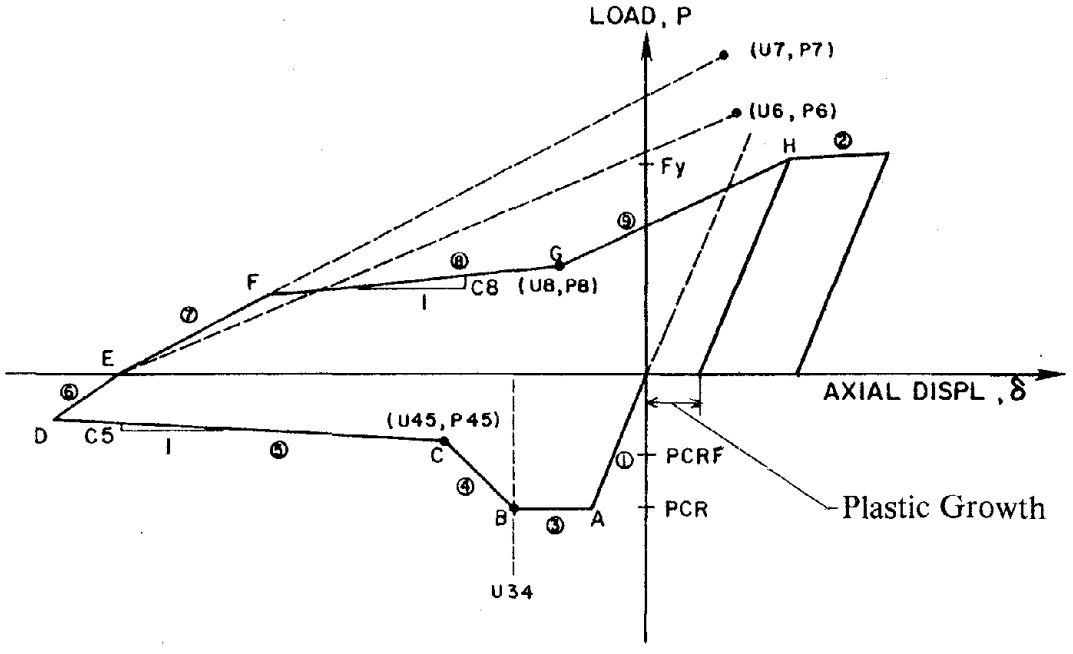

Fig. 1.10 Maison Model [18]

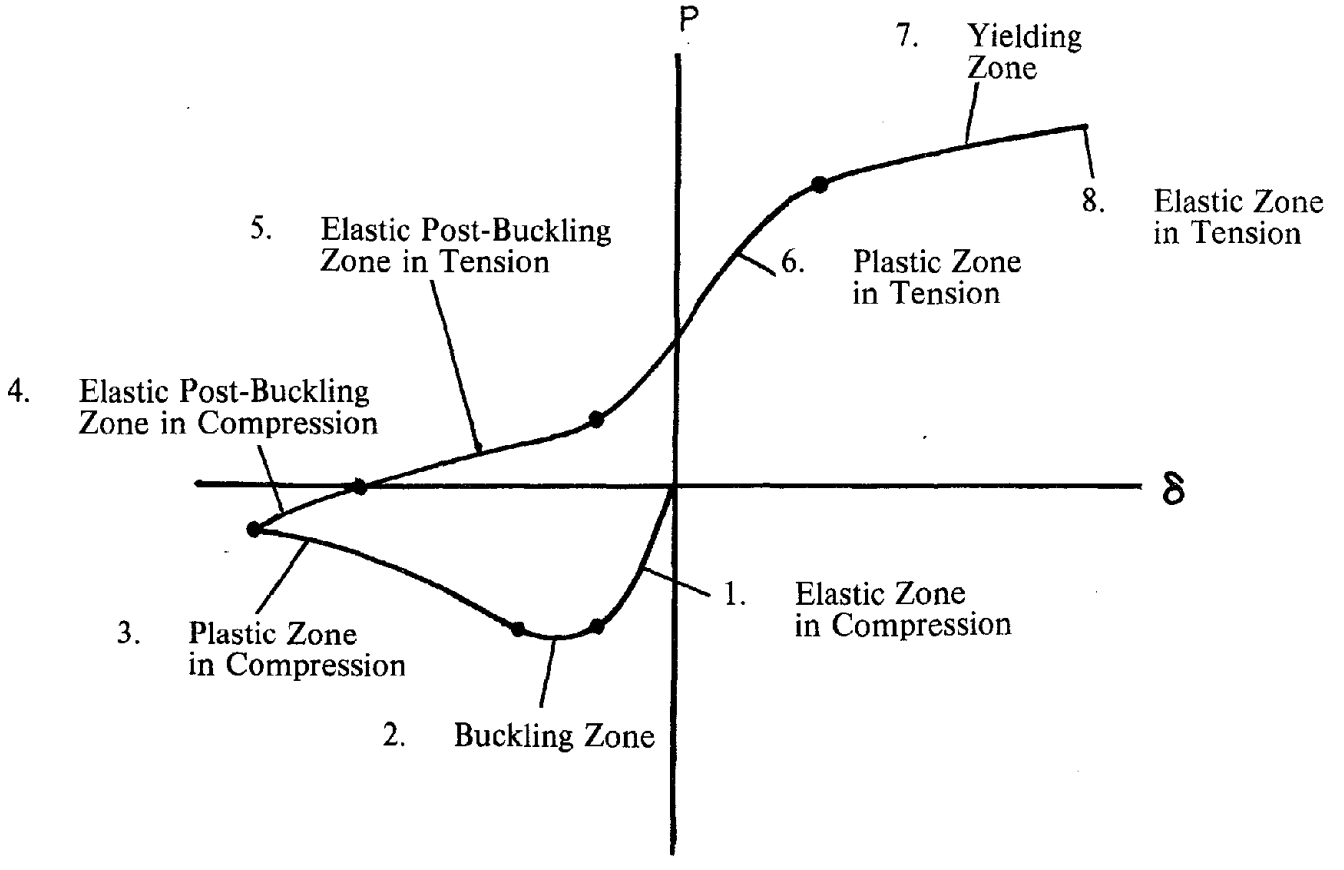

Fig. 1.11 Physical Meaning of Brace Hysteretic Loop

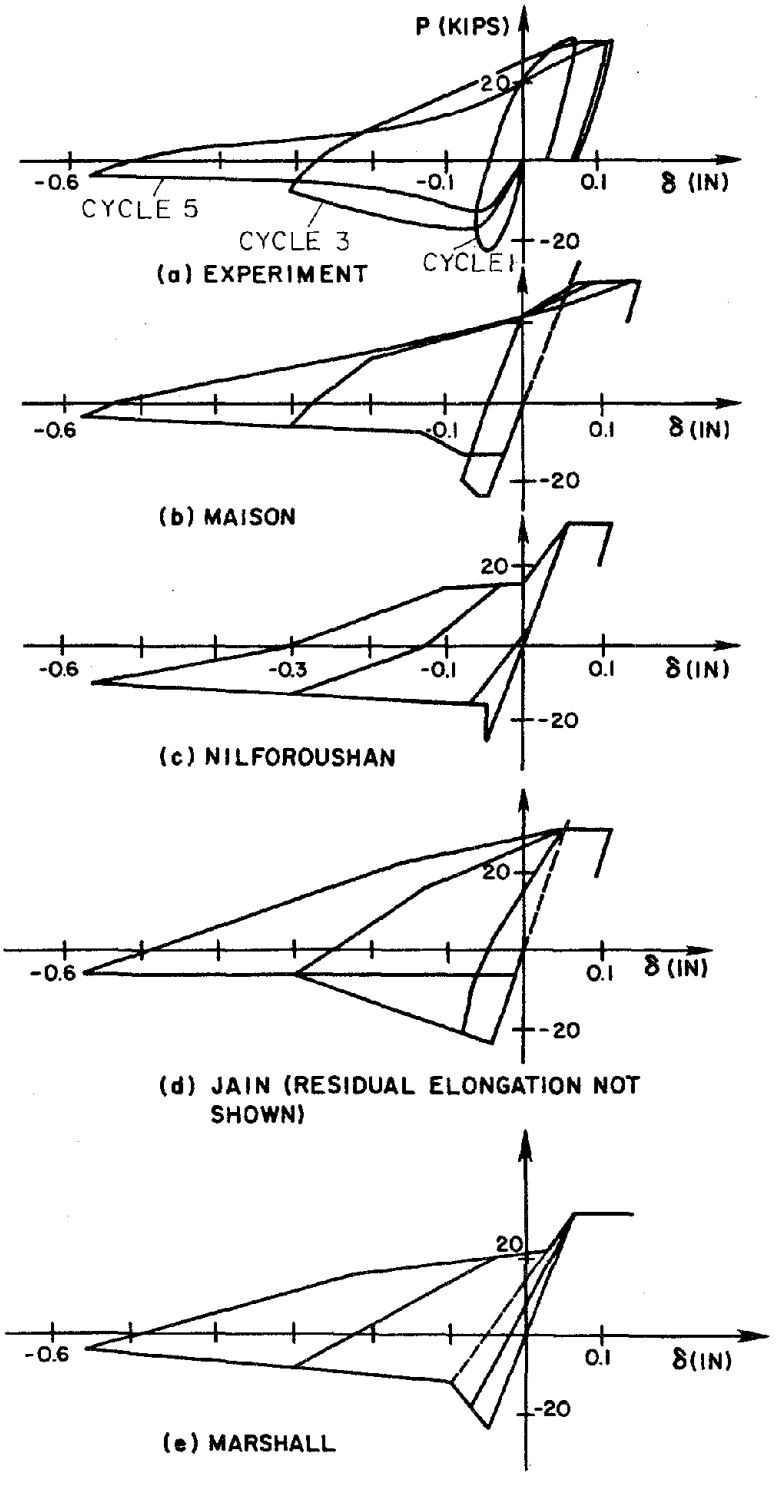

Fig. 1.12 Comparison of Different Phenomenological Models [19] (kL/r = 54; D/t = 48) (1 kip = 4.45 kN; 1 in. = 25.4 mm)

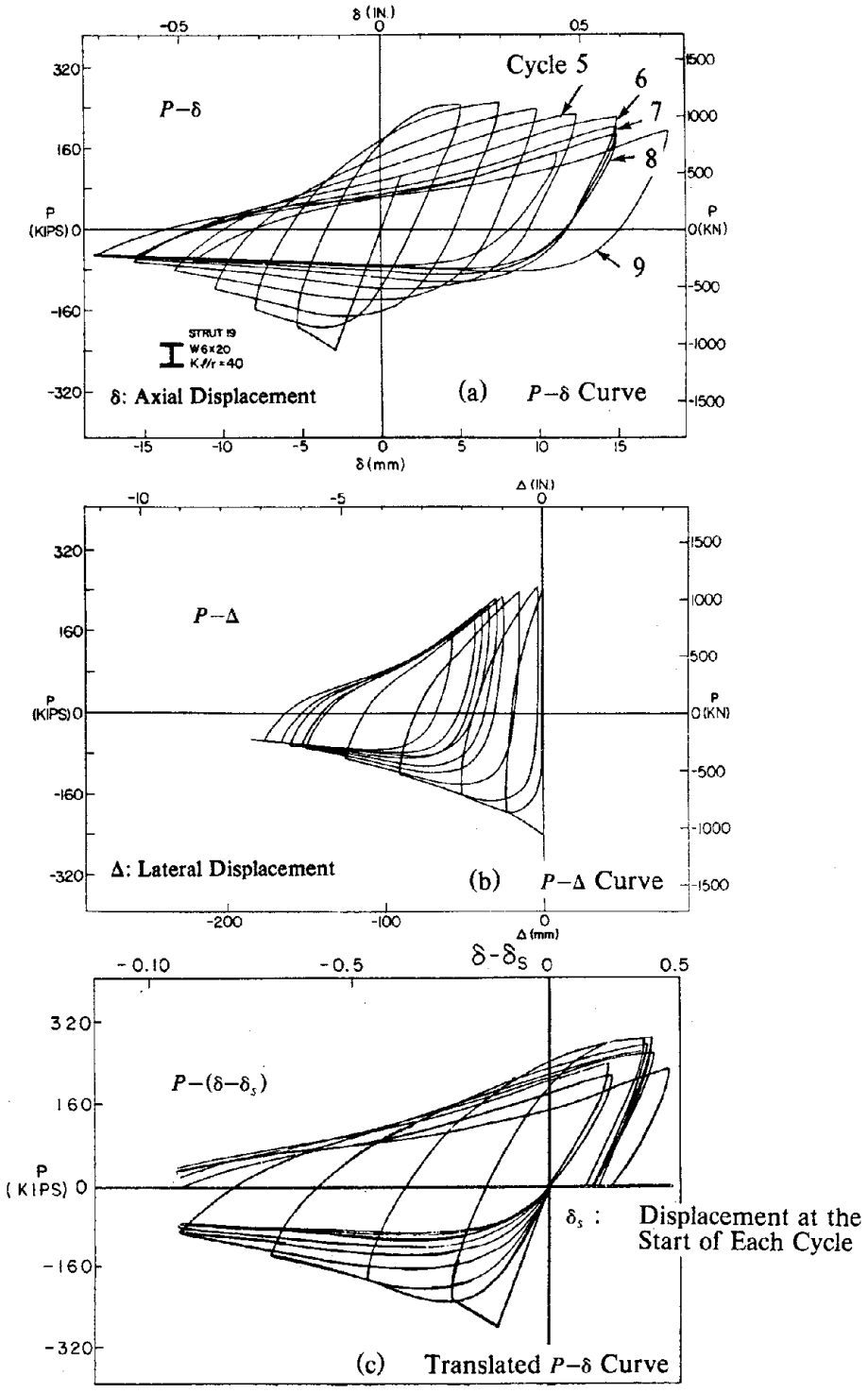

Fig. 2.1 Hysteretic Behavior of a Steel Brace
(1 kip = 4.45 kN; 1 in. = 25.4 mm)

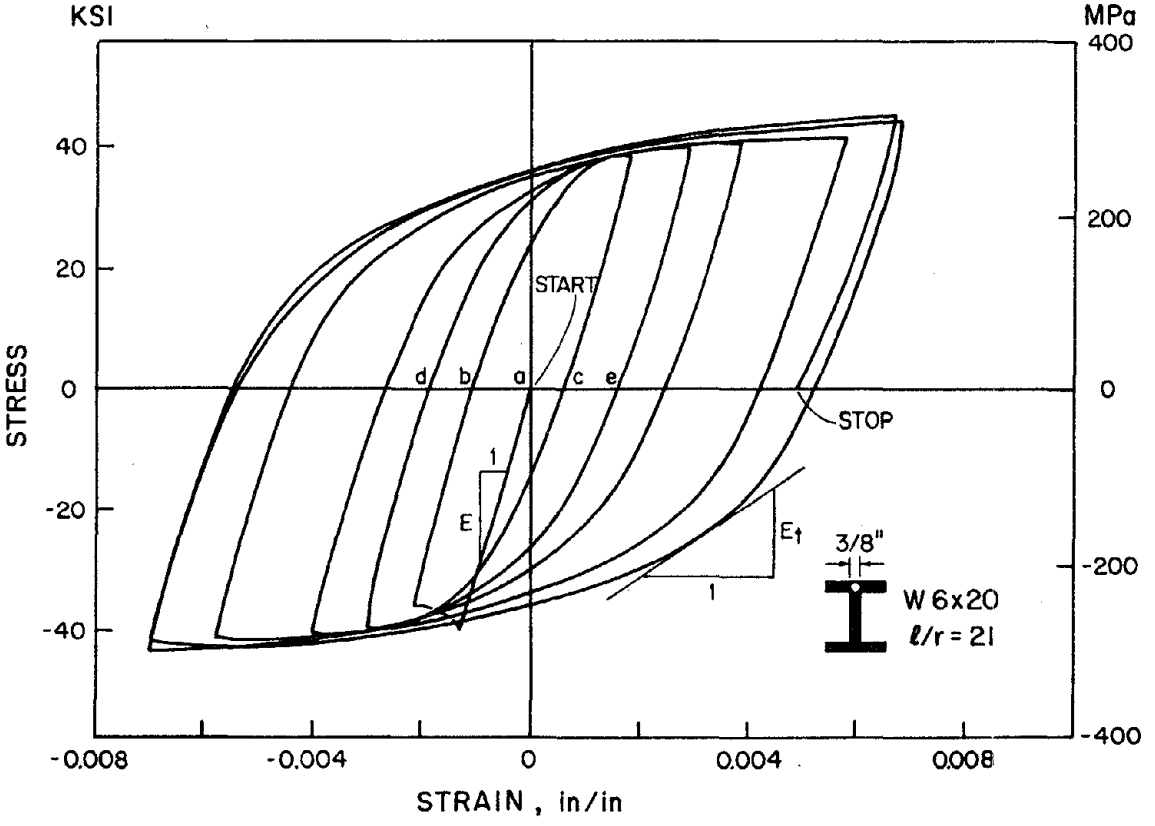

Fig. 2.2 Hysteretic Curves From a Cyclic Coupon Test [1]

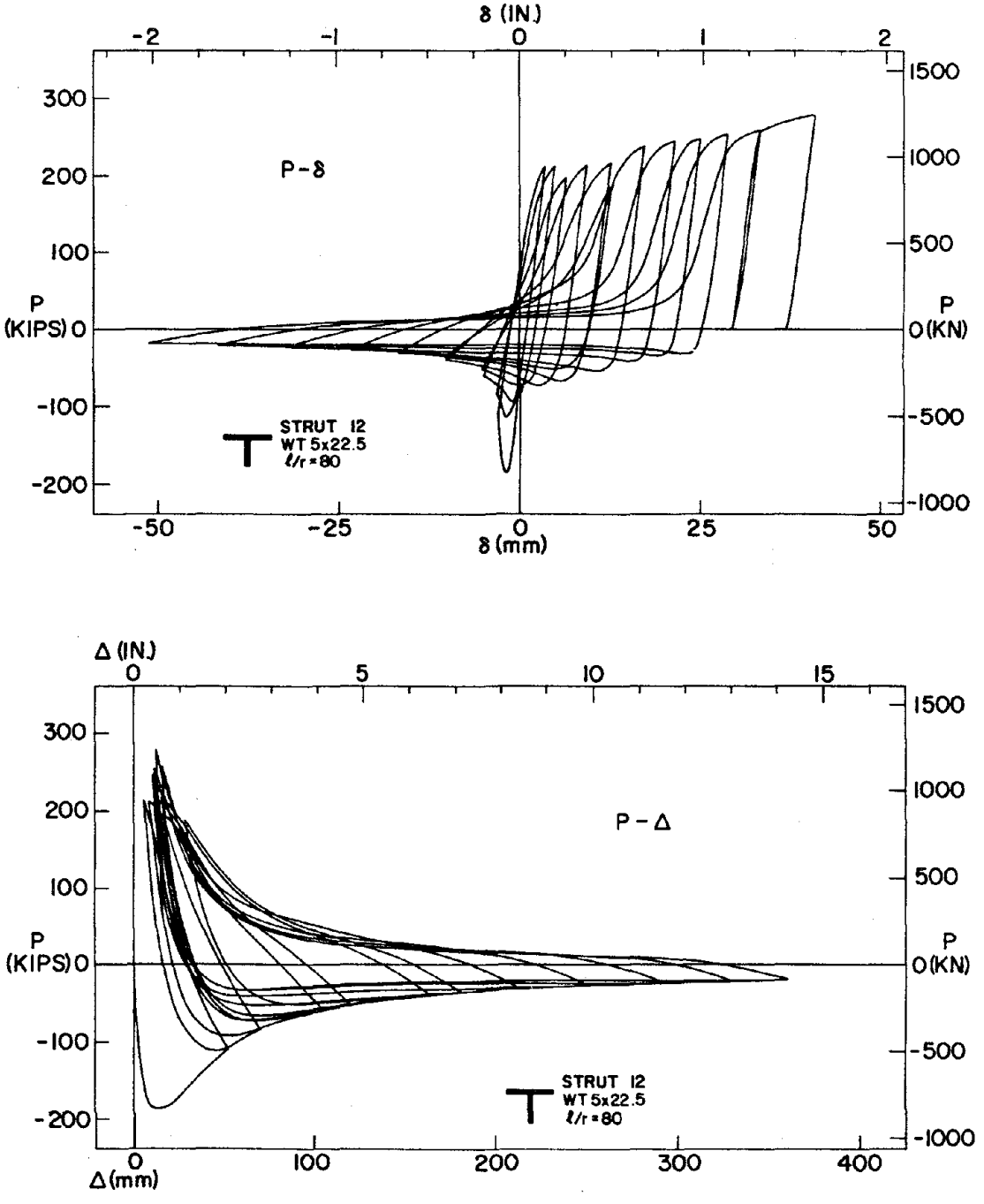

Fig. 2.3 P–δ and P–Δ Curves for Strut 12 [1]

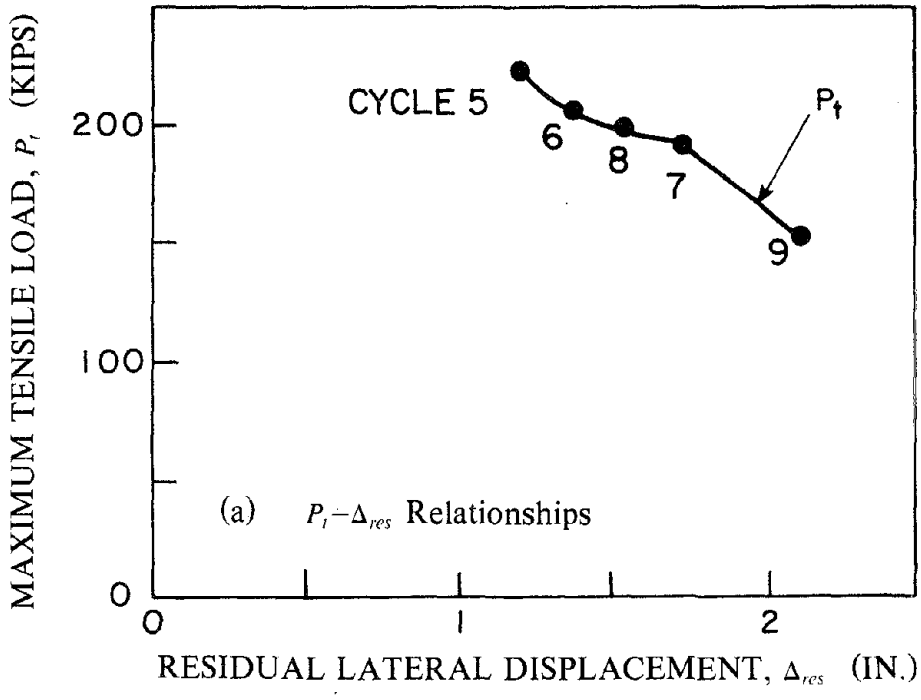

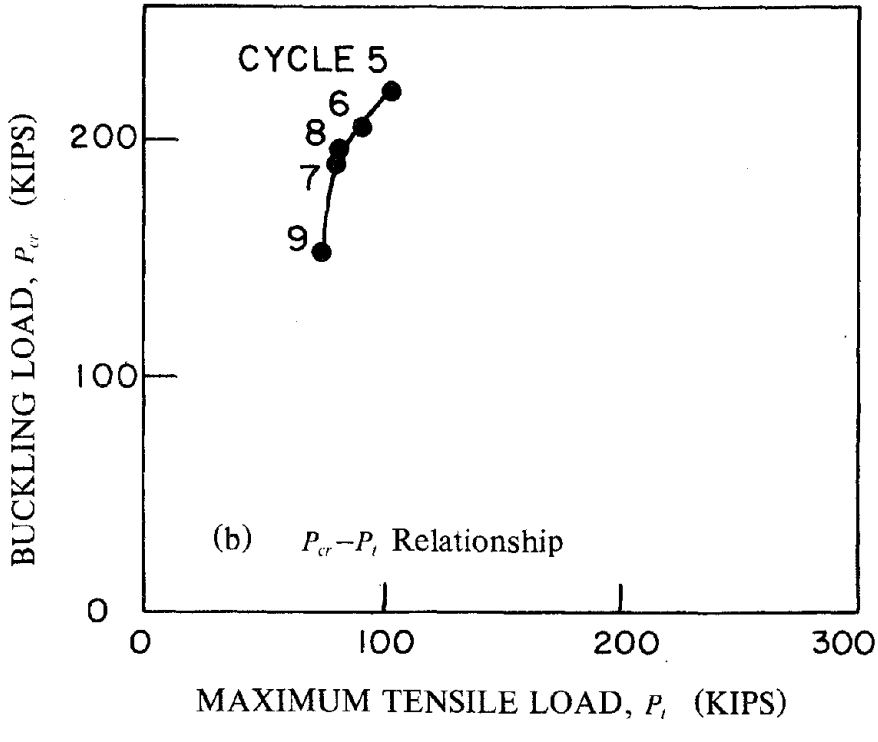

Fig. 2.4 Influence of Lateral Displacements and of Maximum Tensile Loads (1 kip = 4.45 kN; 1 in. = 25.4 mm)

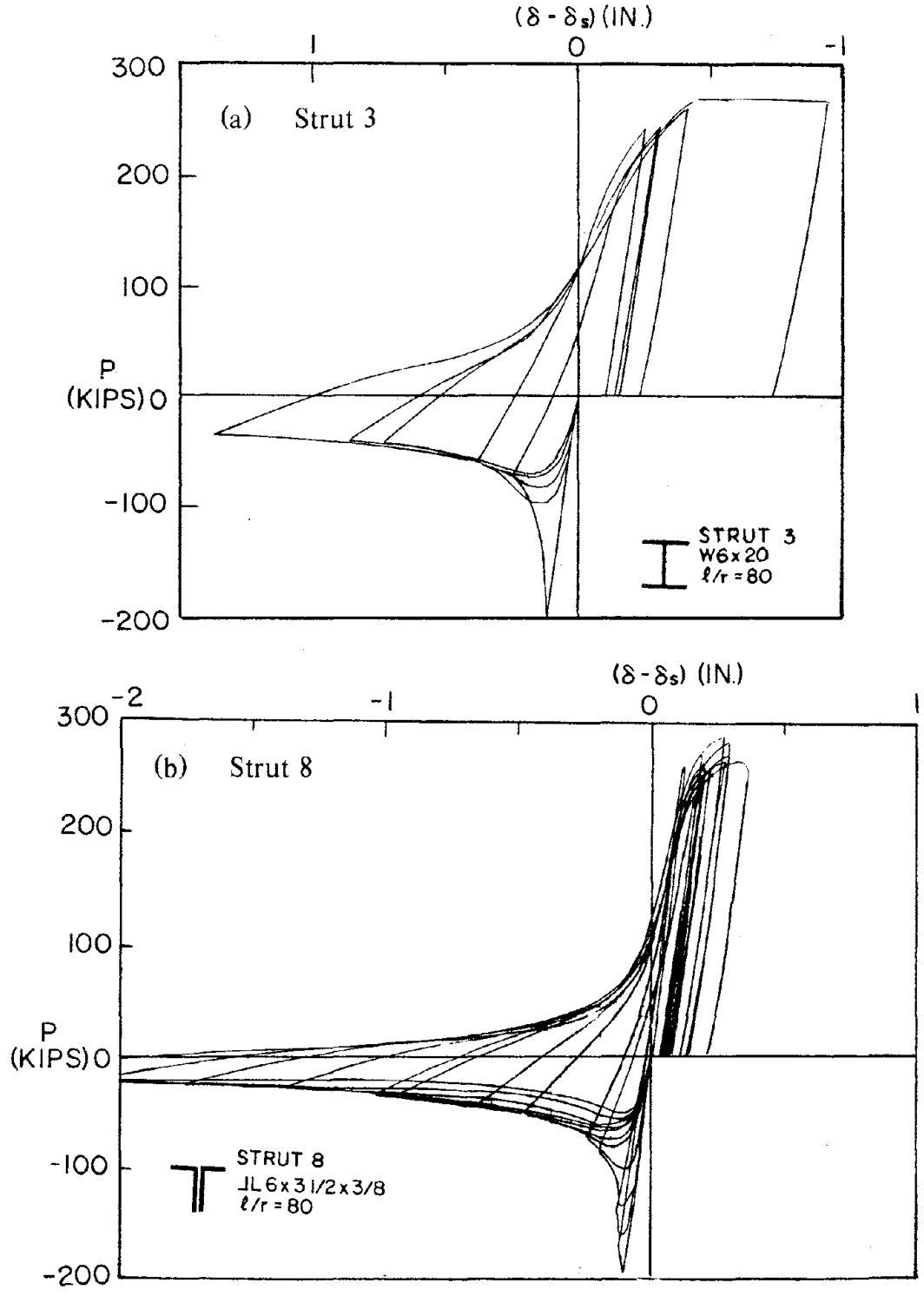

Fig. 2.5 Translated P–δ Curves
(1 kip = 4.45 kN; 1 in. = 25.4 mm)

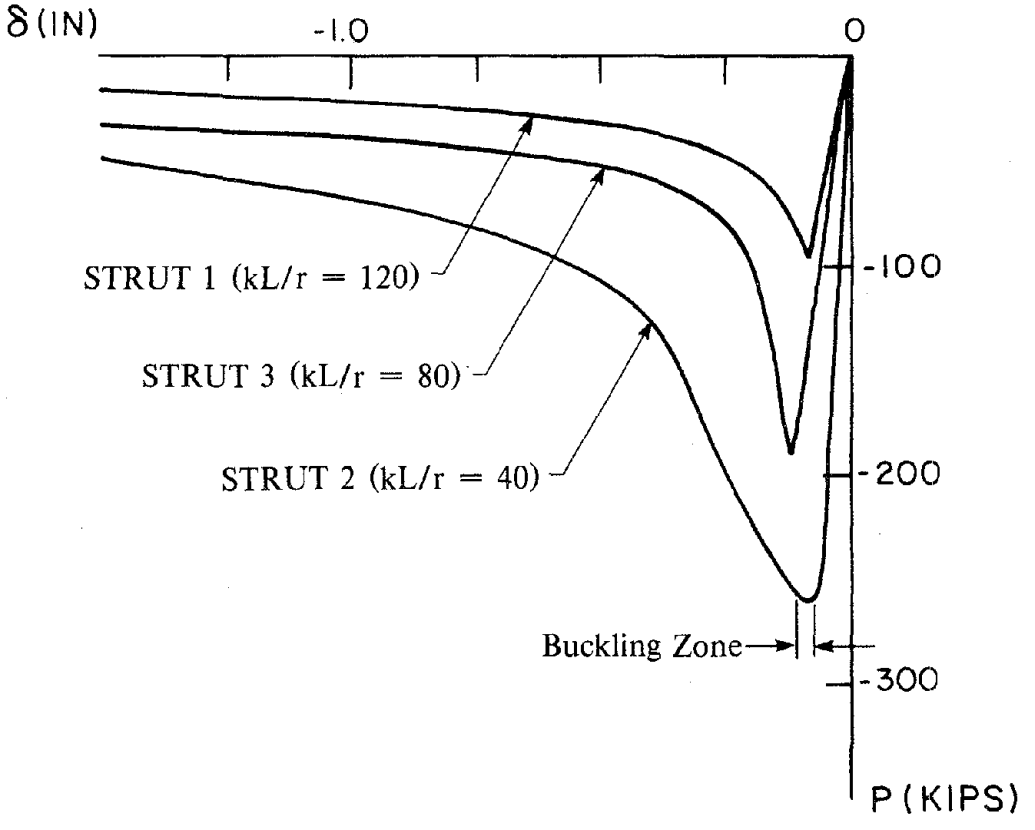

Fig. 2.6 Comparison of Envelopes of Translated Axial Force - Axial Displacement Curves for Struts with Various kL/r (1 kip = 4.45 kN; 1 in. = 25.4 mm)

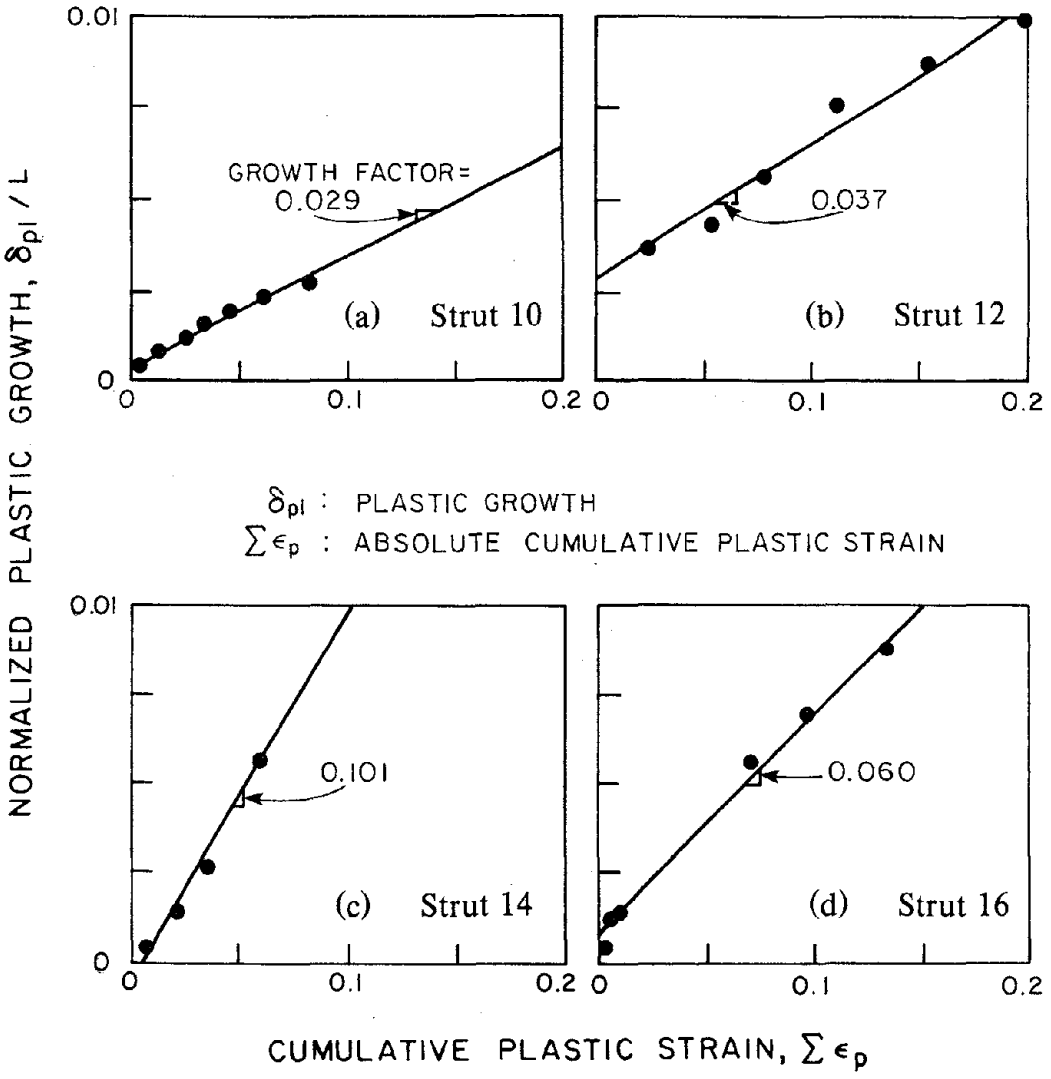

Fig. 2.7 Absolute Cumulative Plastic Strain versus Plastic Growth Relationships

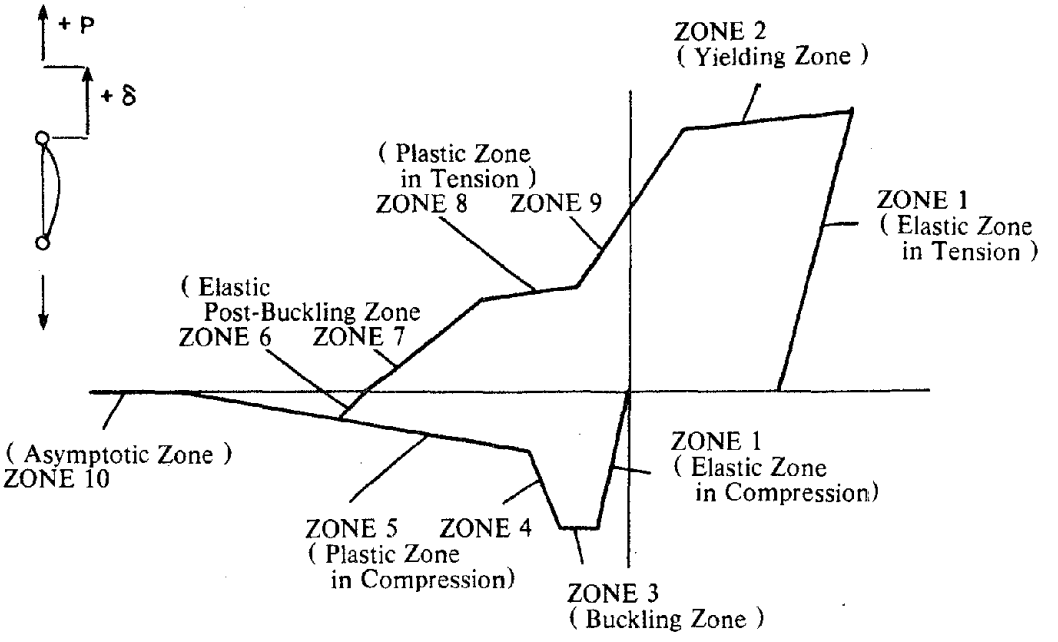

Fig. 3.1 Physical Explanation of Zones Used in the Refined Phenomenological Model

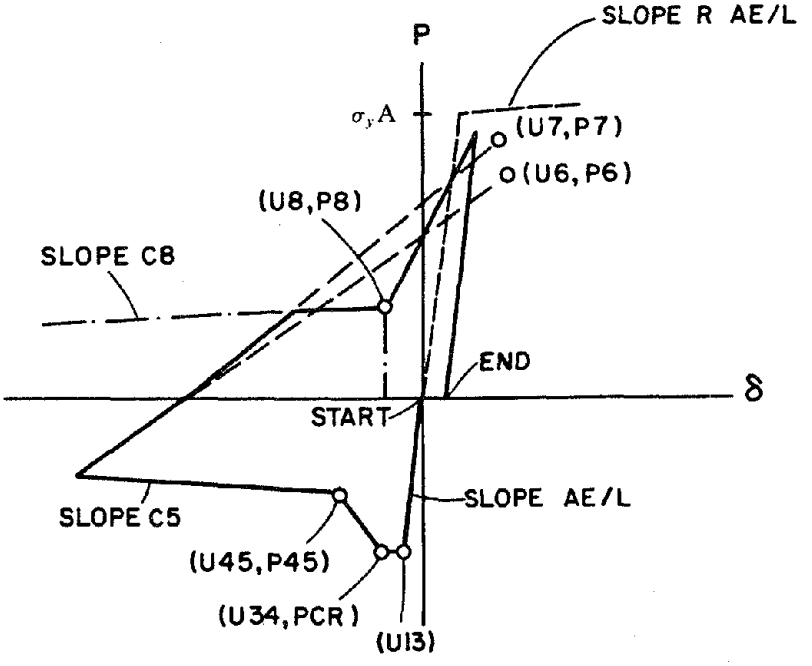

Fig. 3.2 Input Parameters [19]

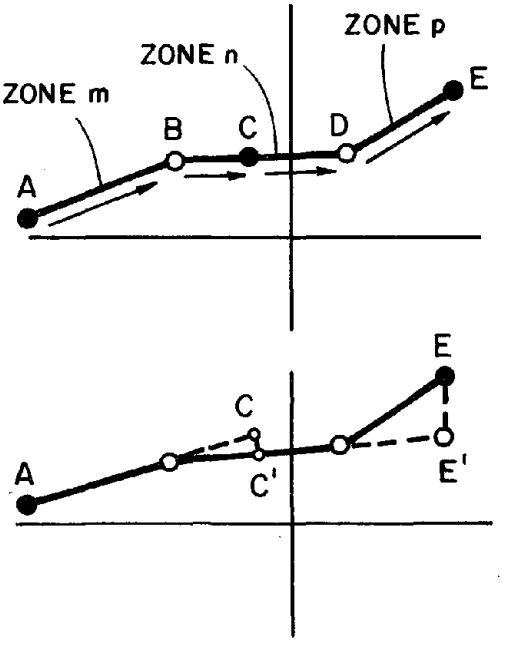

Fig. 3.3 Event-to-Event Solution Strategy

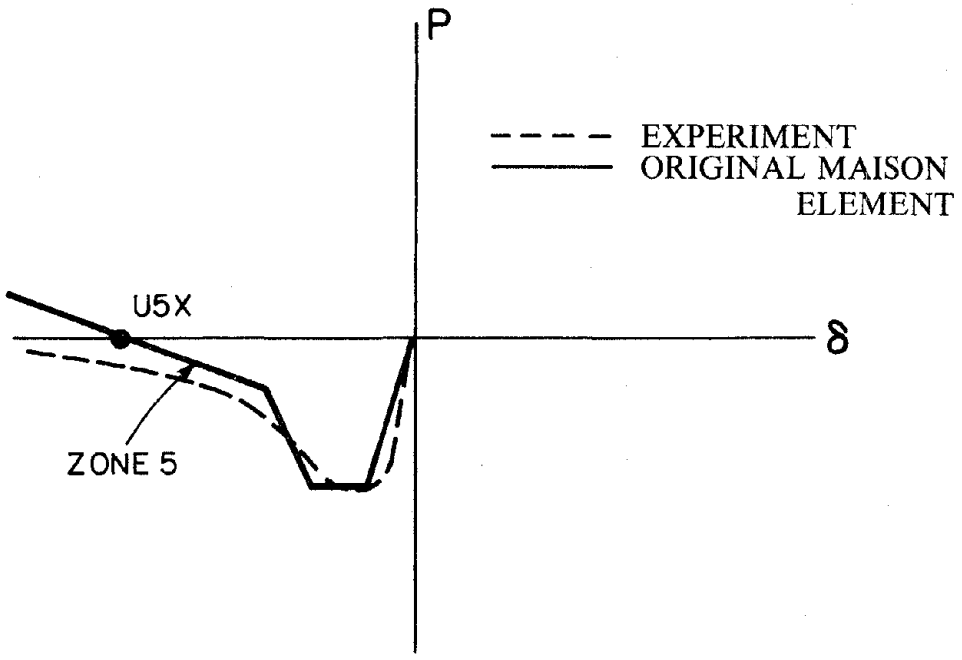

Fig. 3.4 Erroneous Analytical Post-Buckling Behavior

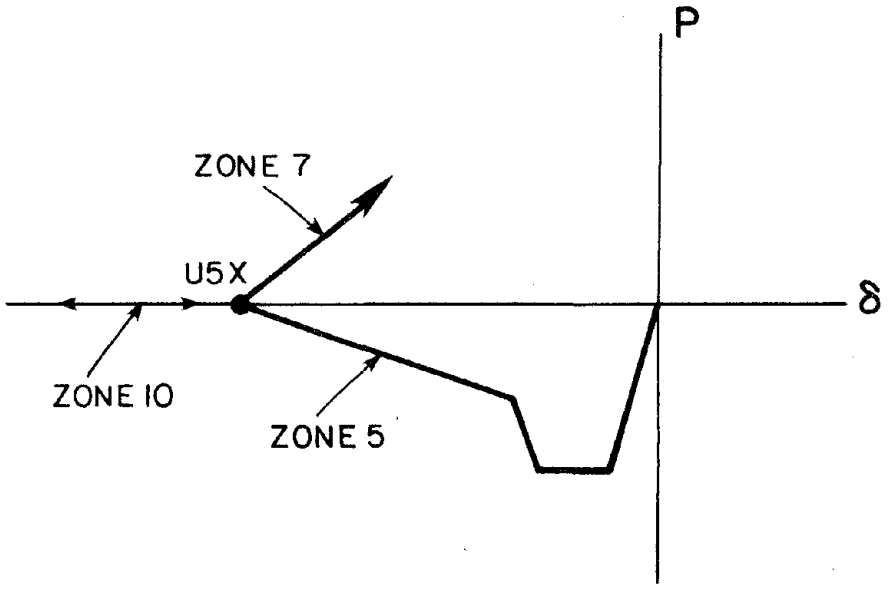

Fig. 3.5 Improved Representation of Post-Buckling Behavior Employed in the Refined Model

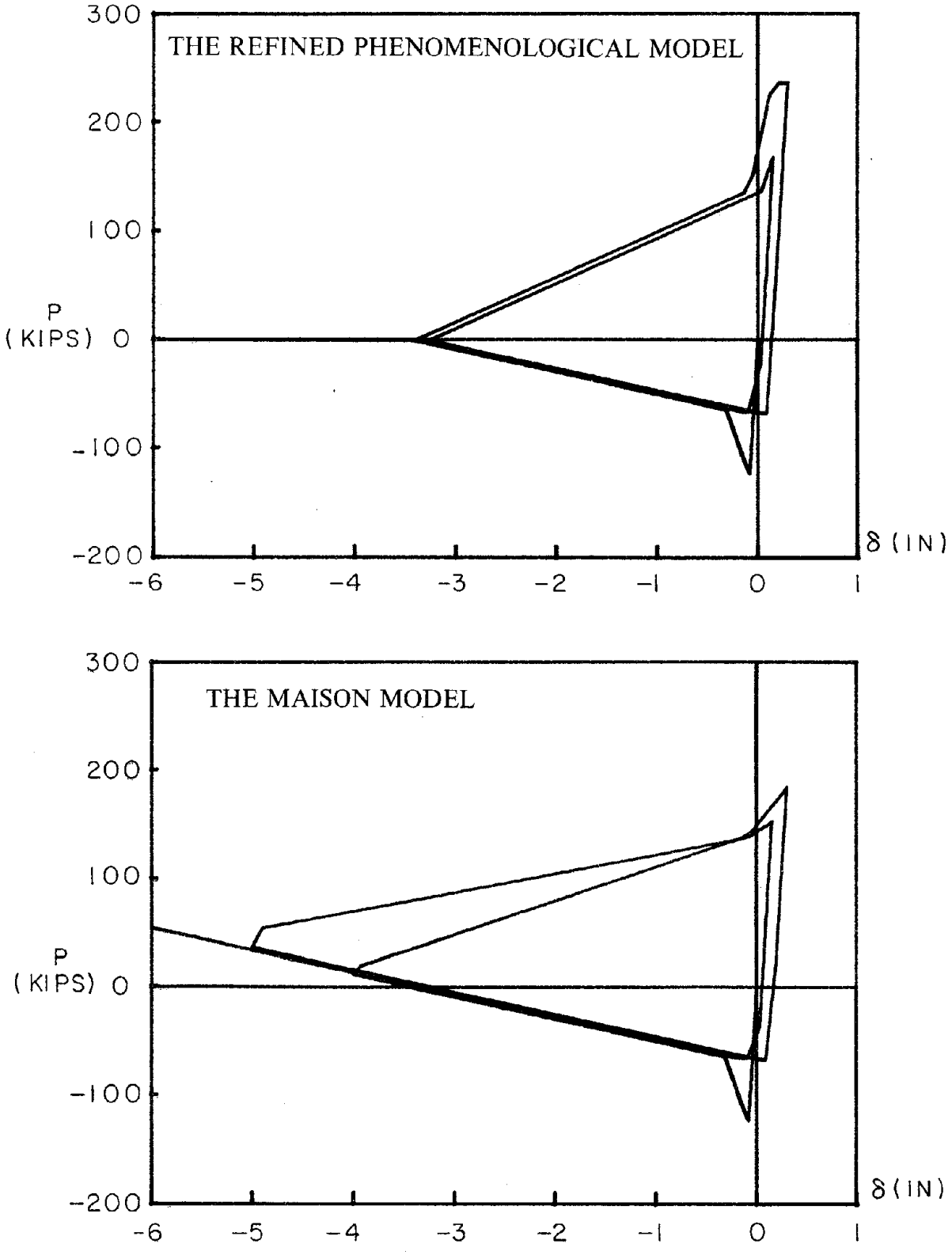

Fig. 3.6 Comparison of the Refined Model and the Maison Model (1 kip = 4.45kN; 1 in. = 25.4 mm)

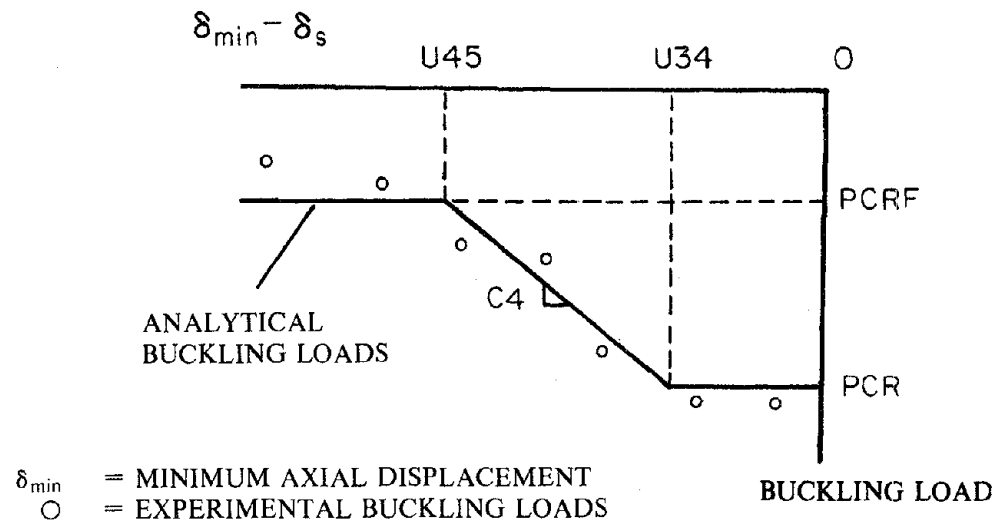

Fig. 4.1 Definition of Deterioration of Buckling Loads

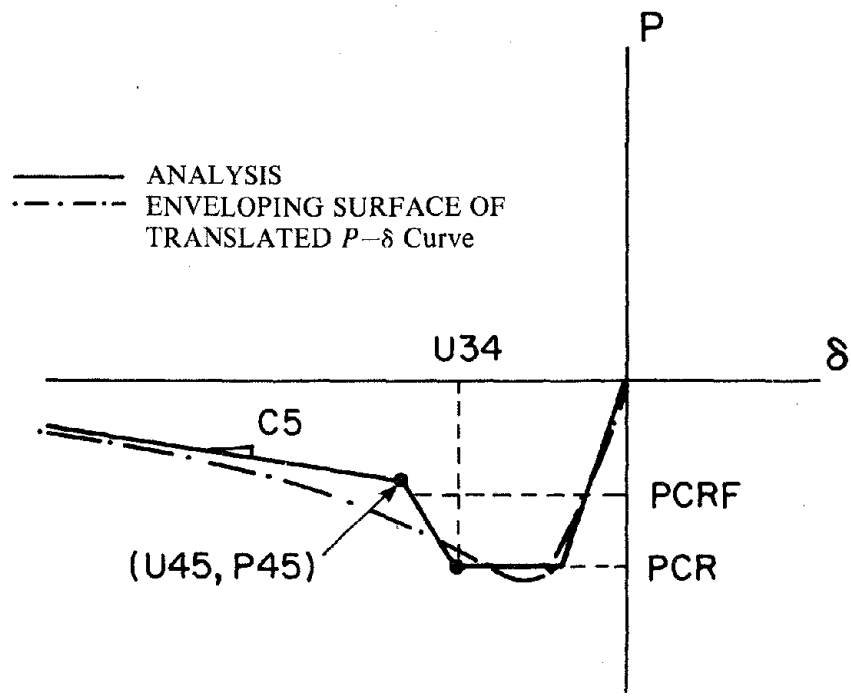

Fig. 4.2 Method for Selecting Input Parameters in the Post-Buckling Phase

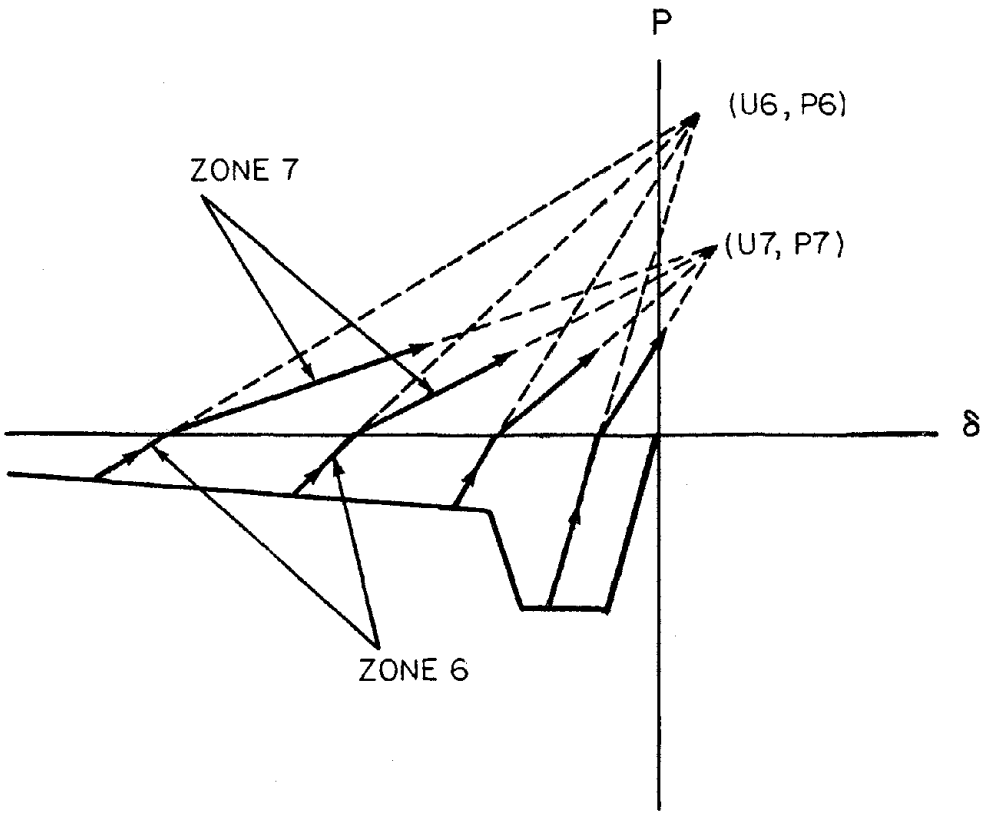

Fig. 4.3 Definition of Zones 6 and 7

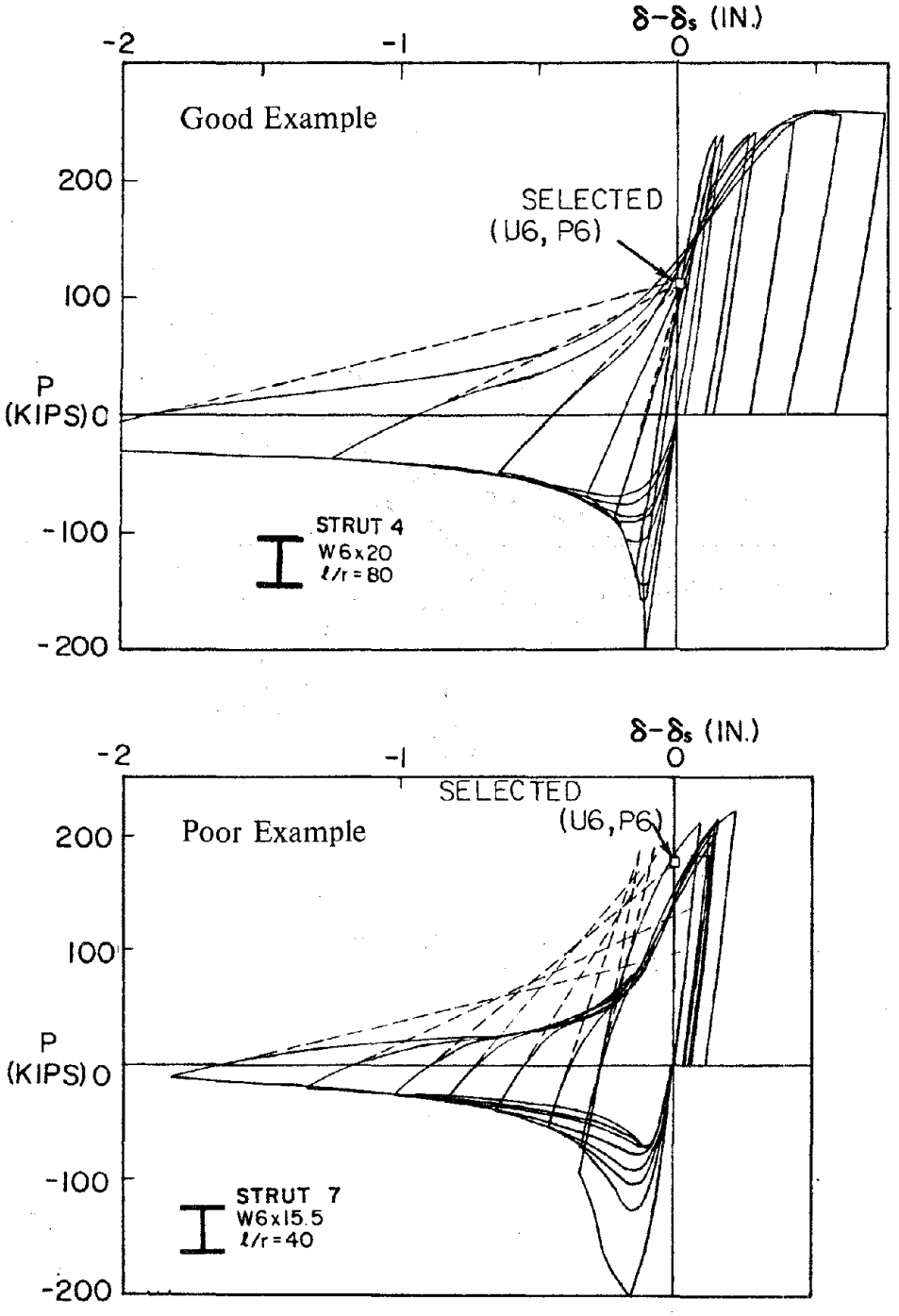

Fig. 4.4 Selection of (U6,P6) Using Translated $P-\delta$ Curve

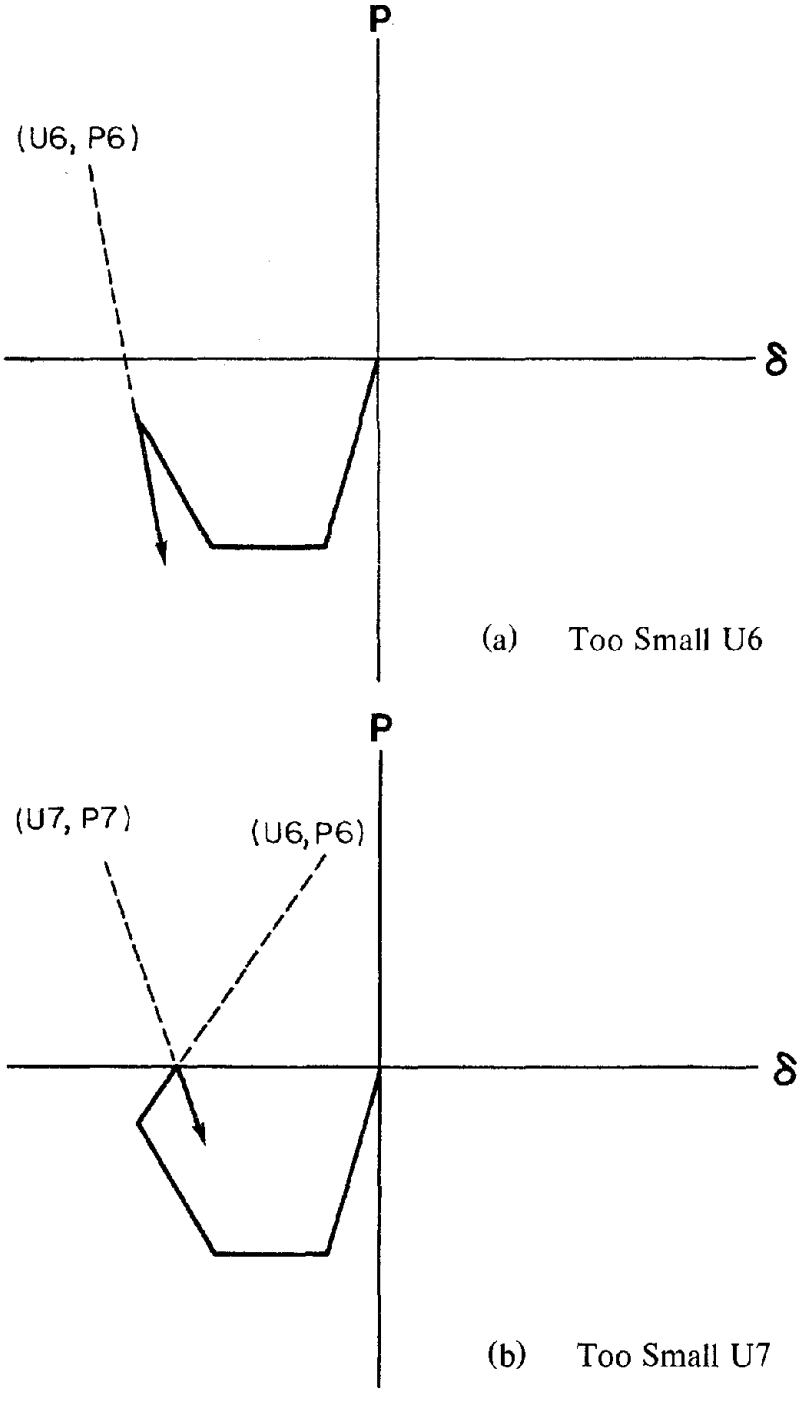

Fig. 4.5 Spurious Analytical Results Caused by Specifying Too Small U6 or U7

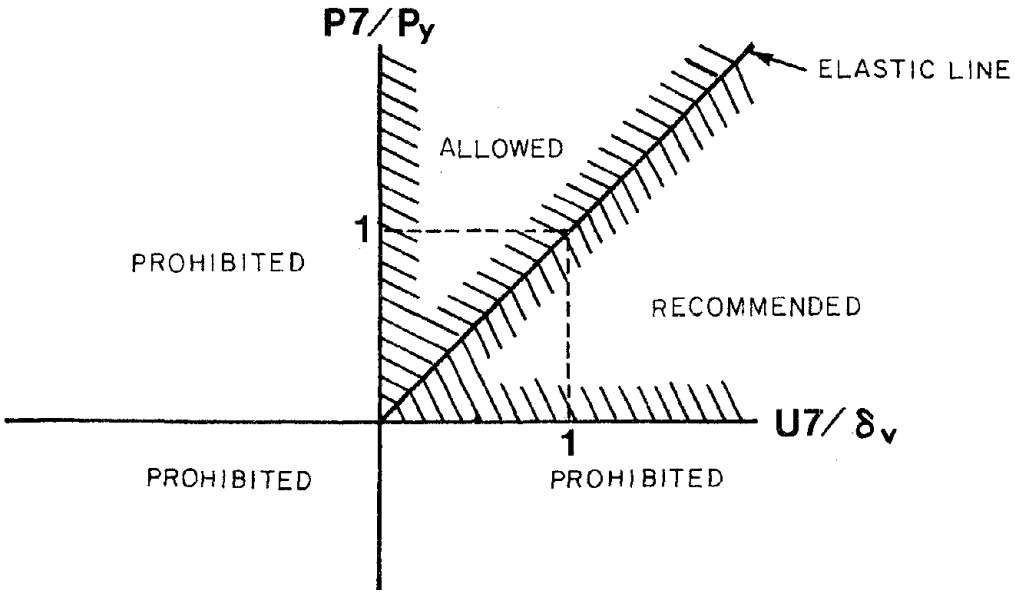

Fig. 4.6 Rules in Selecting Points (U6,P6) and (U7,P7)

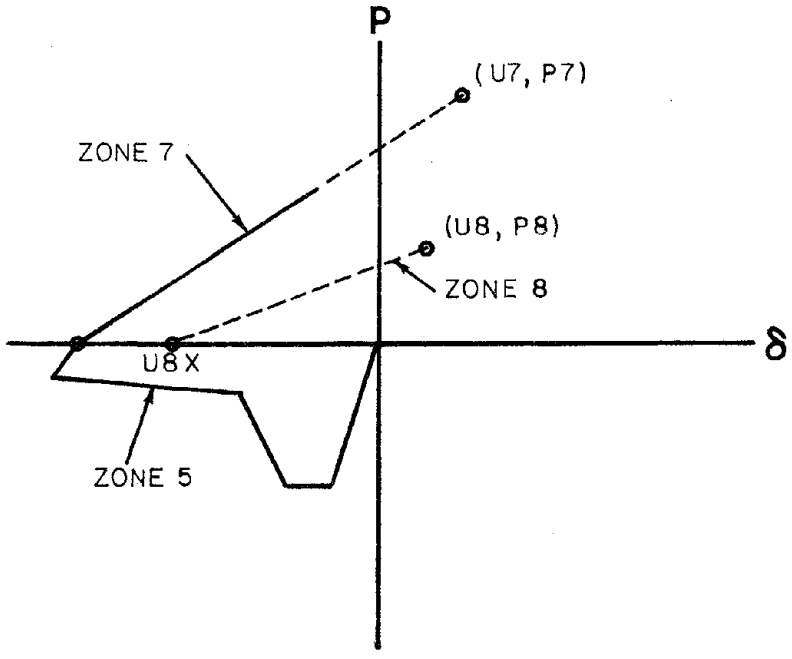

Fig. 4.7 Unreasonable Analytical Results
Caused by Specifying Too Small U8

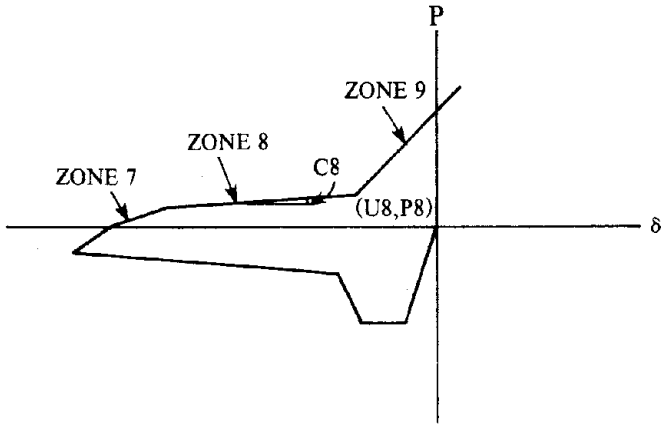

(a) Original Application of Plastic Zone in Tension

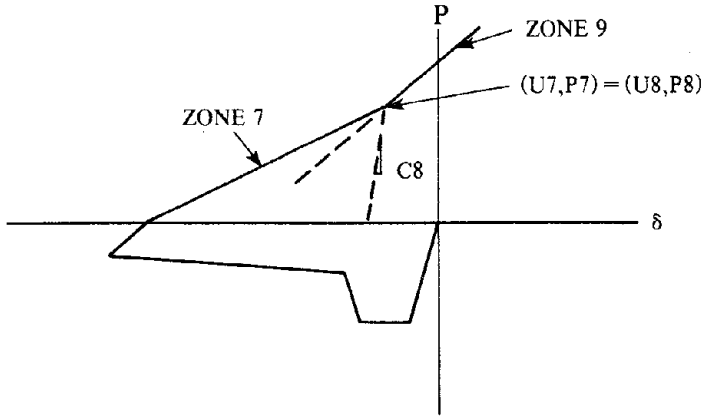

(b) Eliminated Application of Zone 8

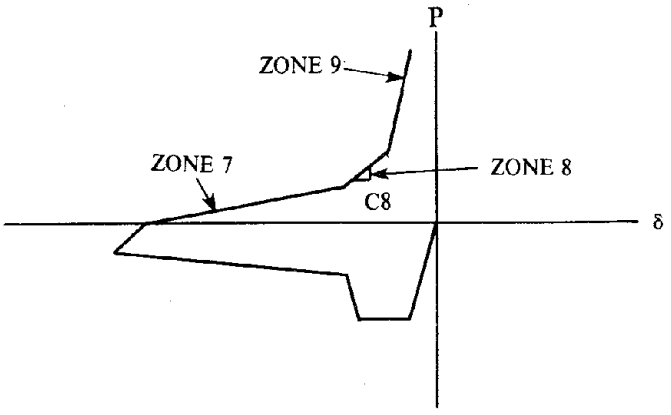

(c) Use of Zone 8 as Transition Region

Fig. 4.8 Three Different Applications of Zone 8

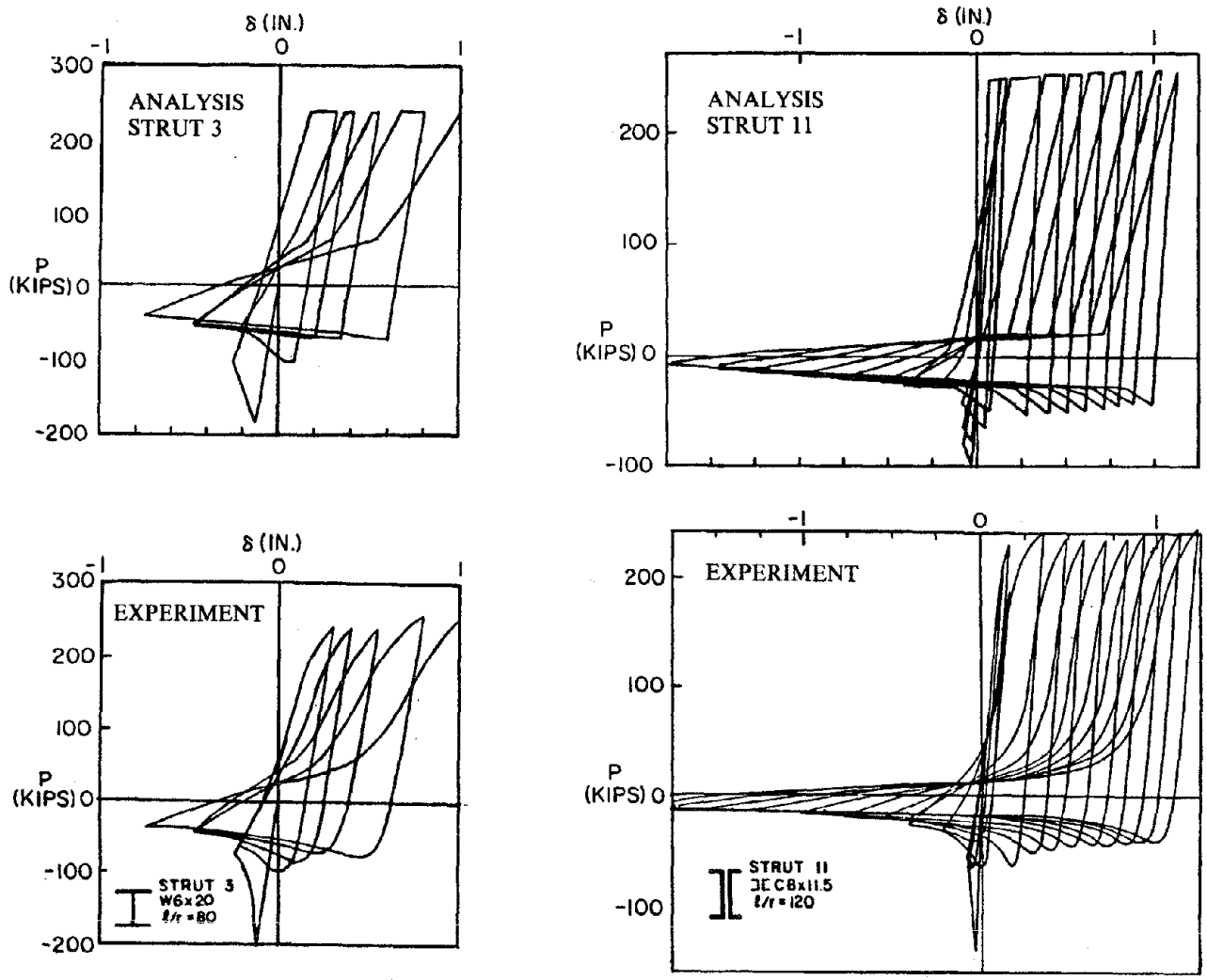

Fig. 5.1 Comparison of Analytical and Experimental Hysteresis Loops for Struts 3 and 11 (1 kip = 4.45 kN; 1 in. = 25.4 mm)

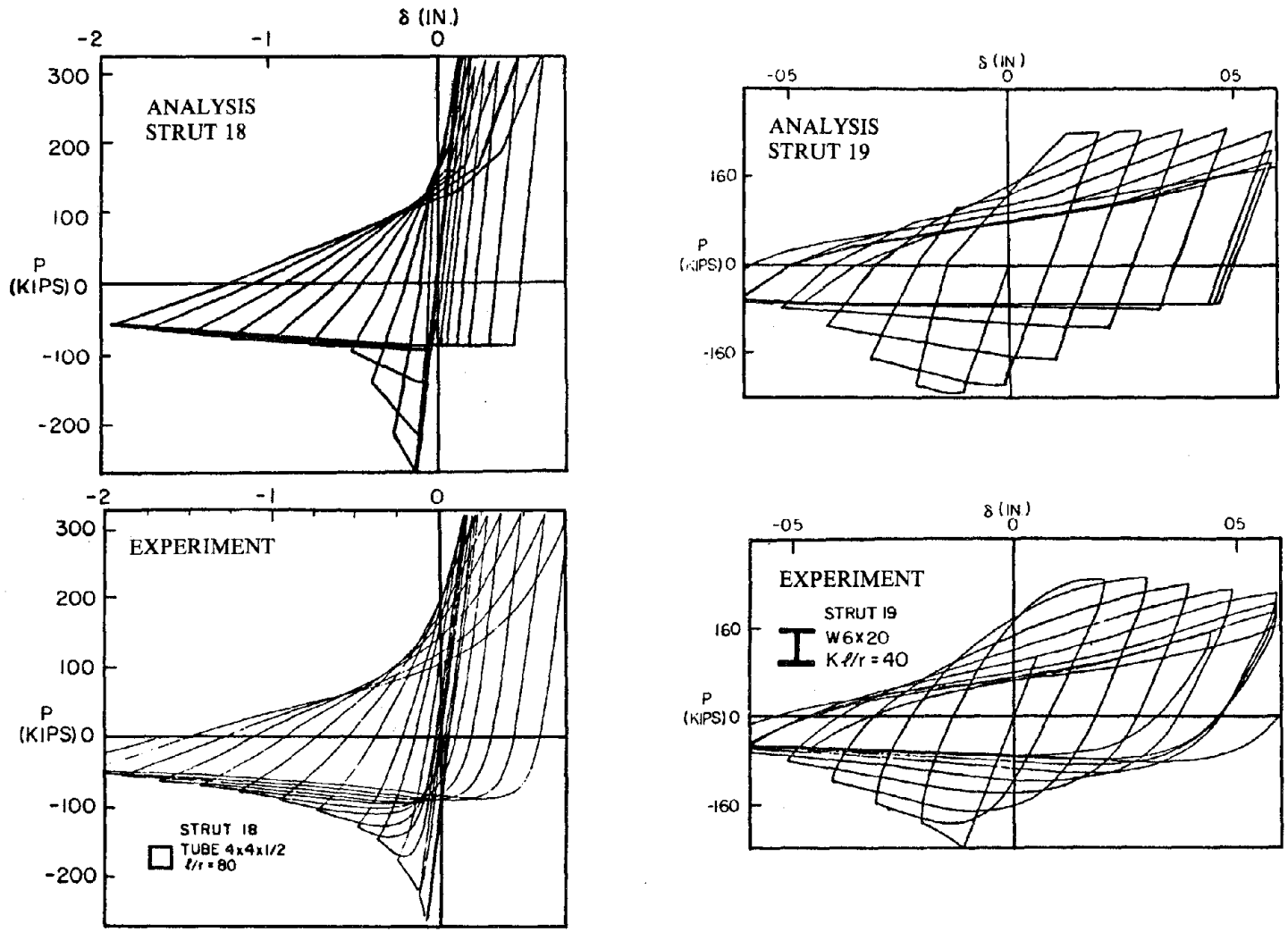

Fig. 5.2 Comparison of Analytical and Experimental Hysteresis Loops for Struts 18 and 19 (1 kip = 4.45 kN; 1 in. = 25.4 mm)

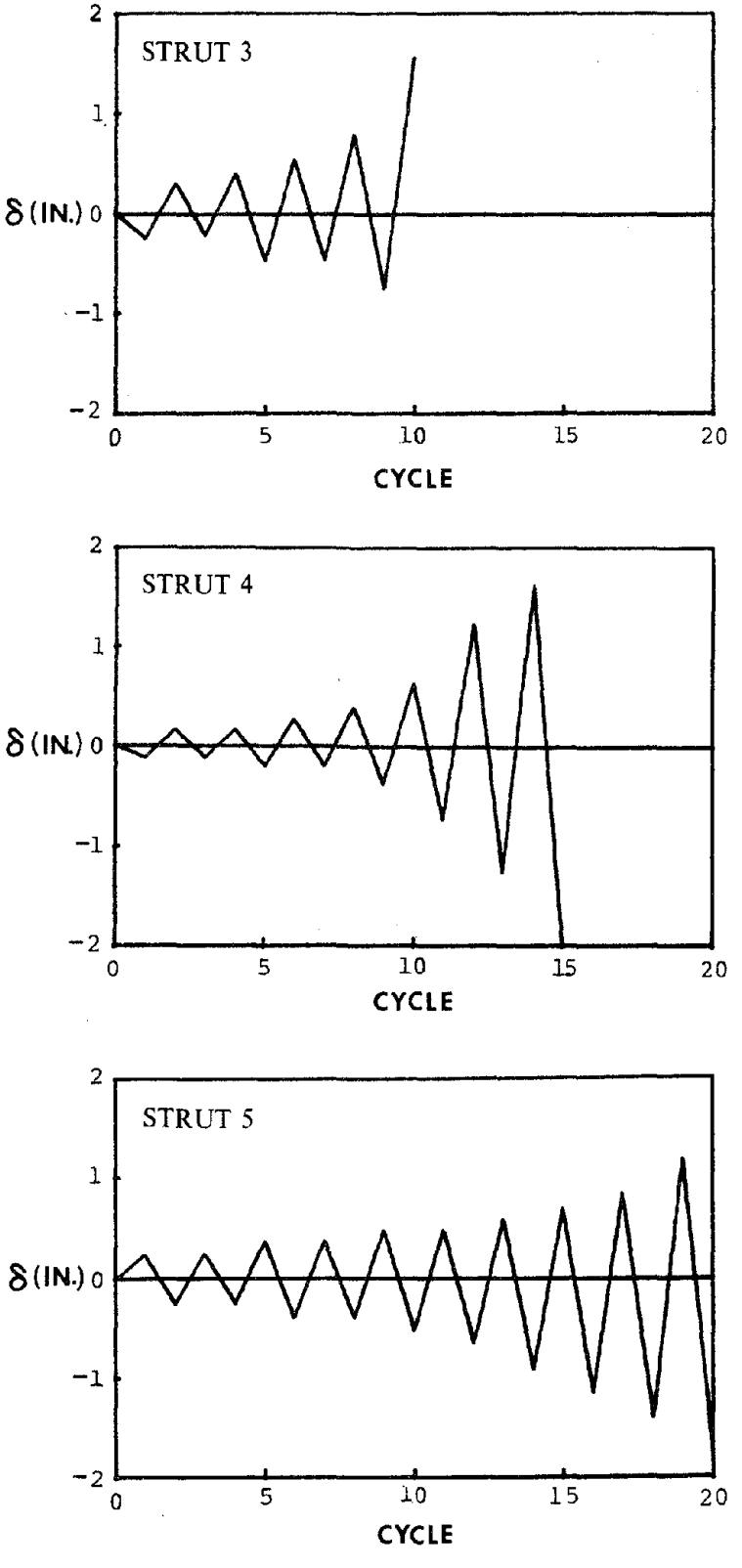

Fig. 5.3 Displacement Histories for Struts 3, 4, and 5 (1 in. = 25.4 mm)

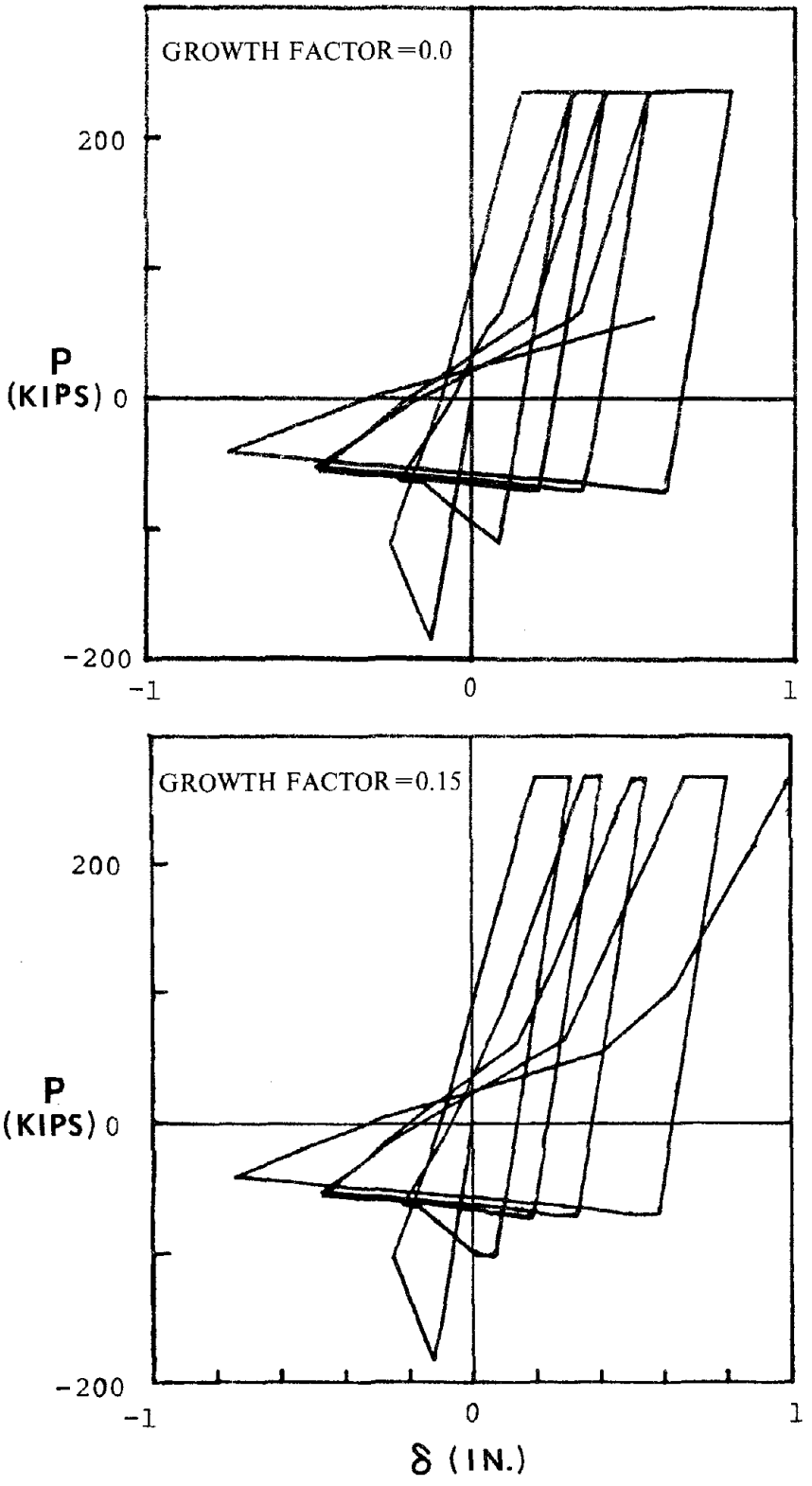

Fig. 5.4 Effect of Growth Factors on Analytical Results (Strut 3, kL/r = 80) (1 kip = 4.45 kN; 1 in. = 25.4 mm)

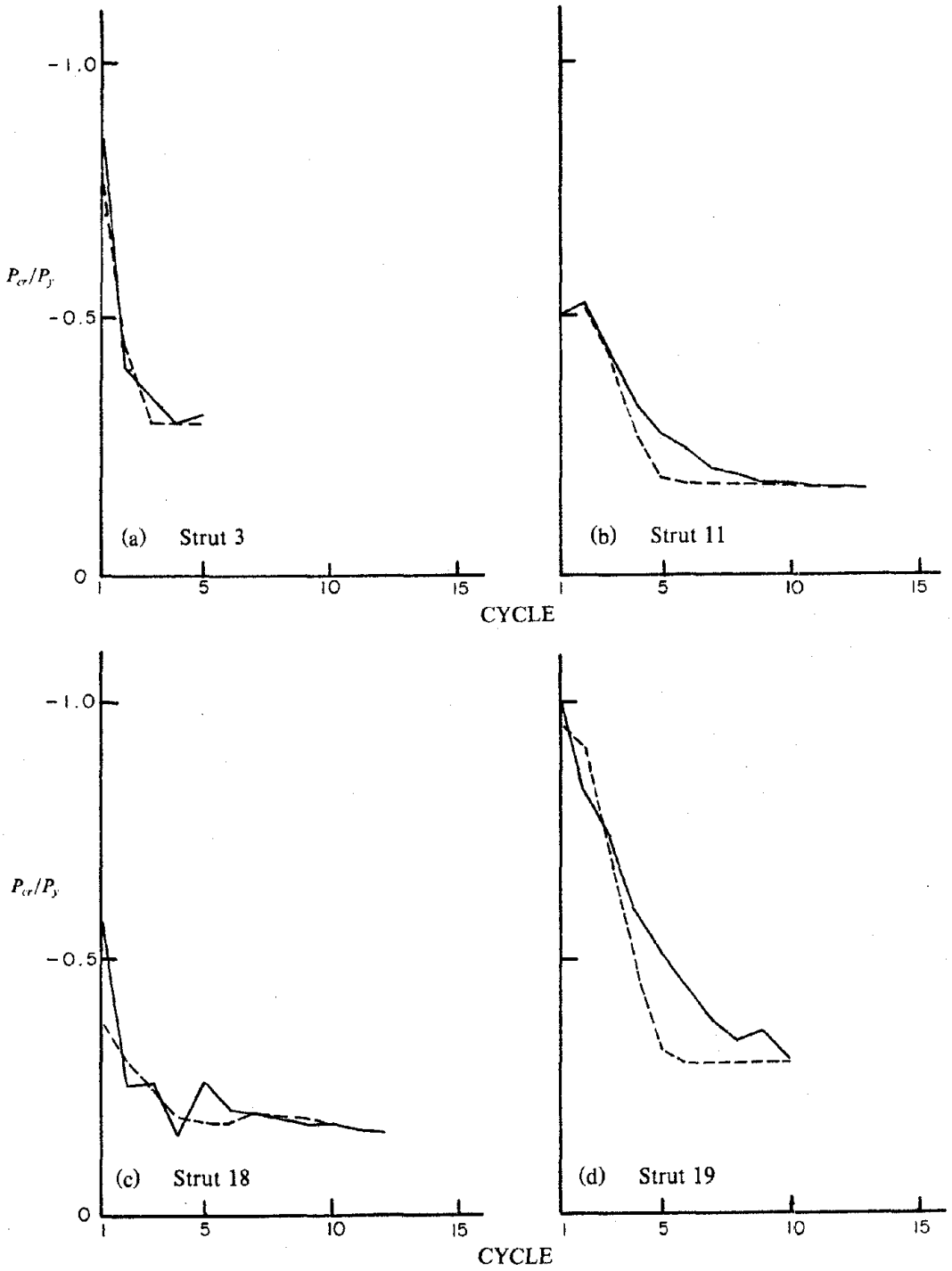

Fig. 5.5 Deterioration of Buckling Load

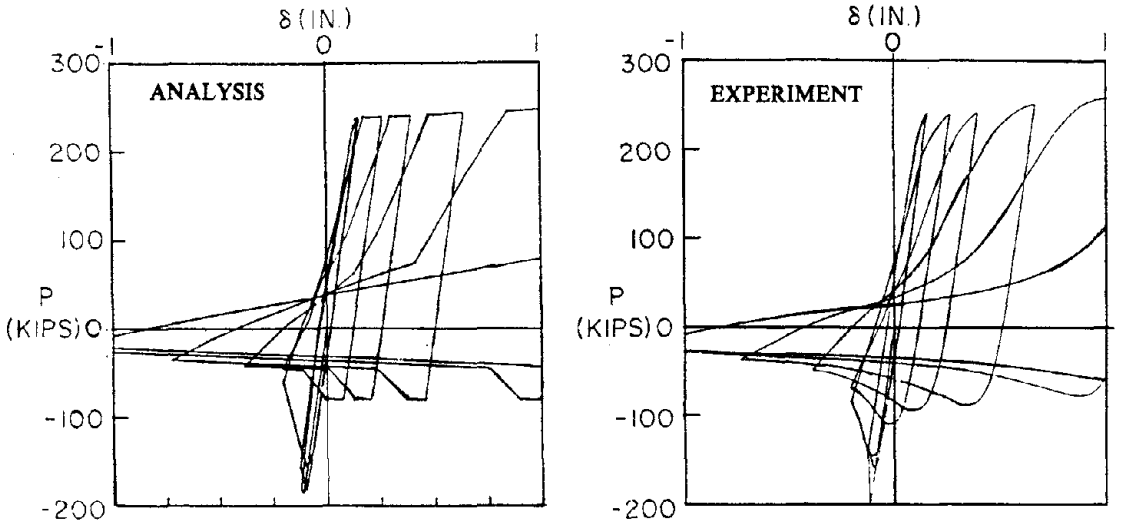

(a) Strut 4 Parameters for Strut 3
Displacement History for Strut 4

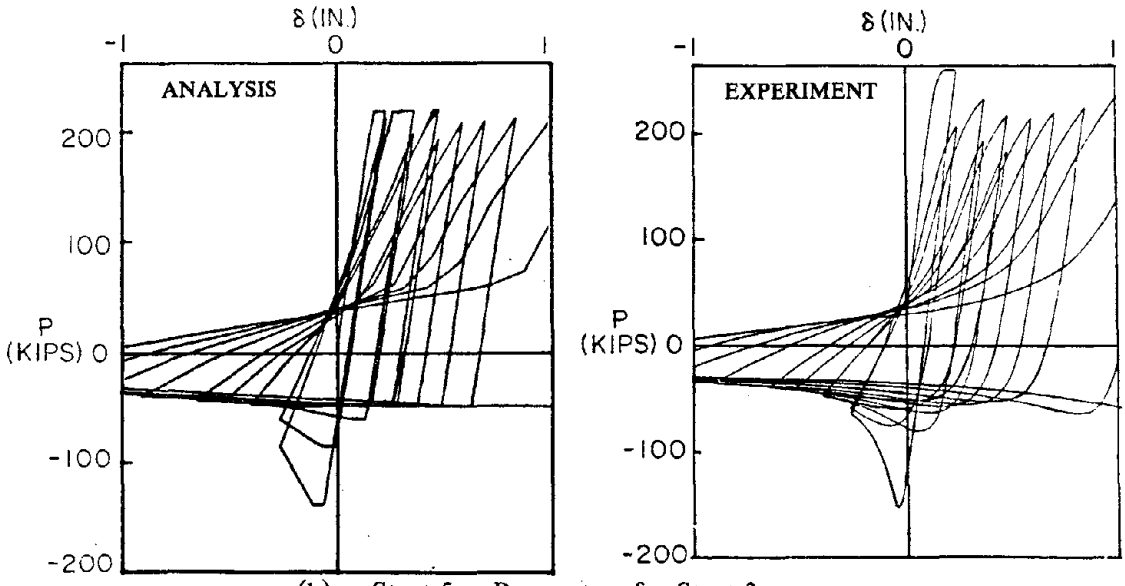

(b) Strut 5 Parameters for Strut 3
Displacement History for Strut 5

Fig. 5.6 Use of the Parameters for Strut 3 for Other Displacement Histories (1 kip = 4.45 kN; 1 in. = 25.4 mm)

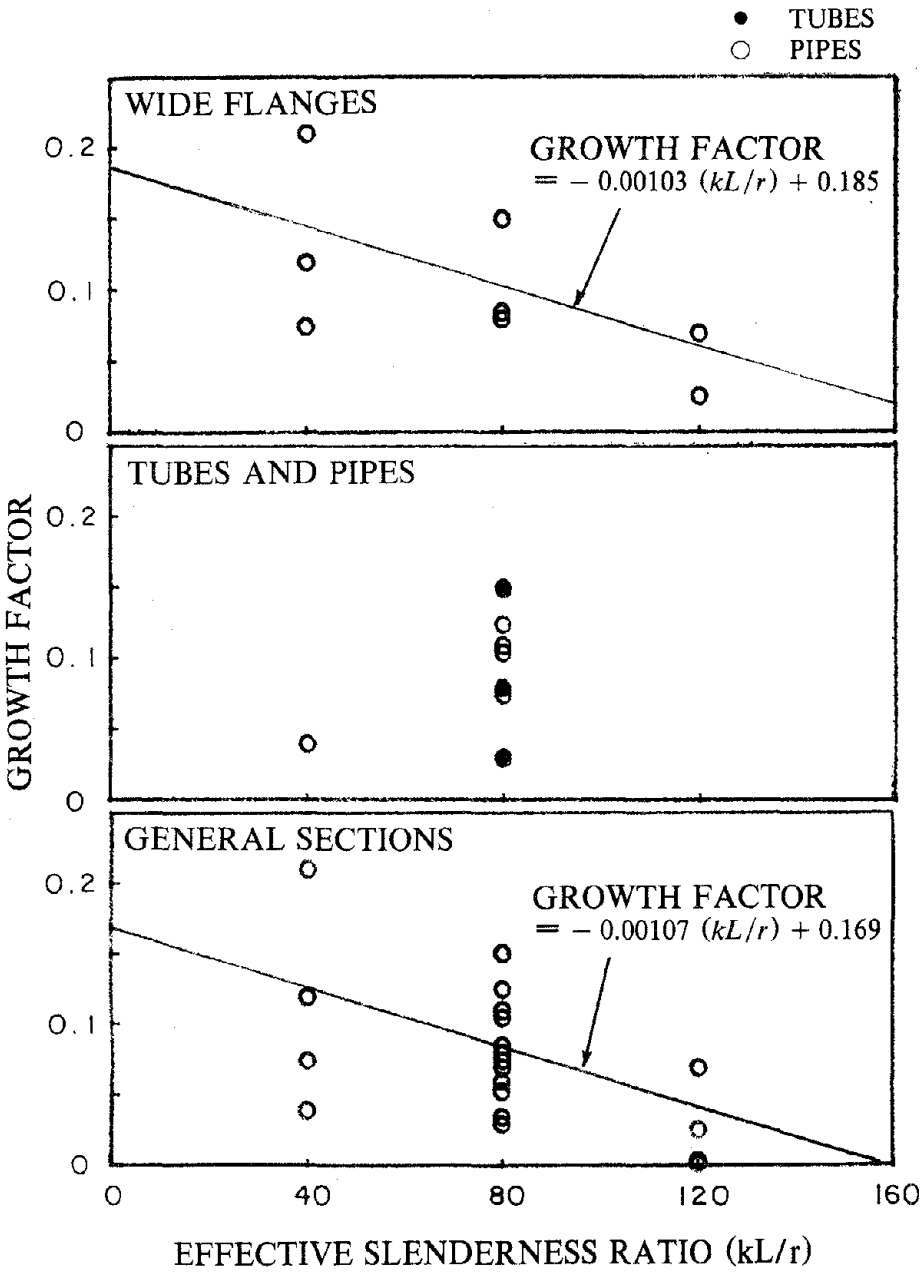

Fig. 6.1 Growth Factor versus Effective Slenderness Ratio Relationships

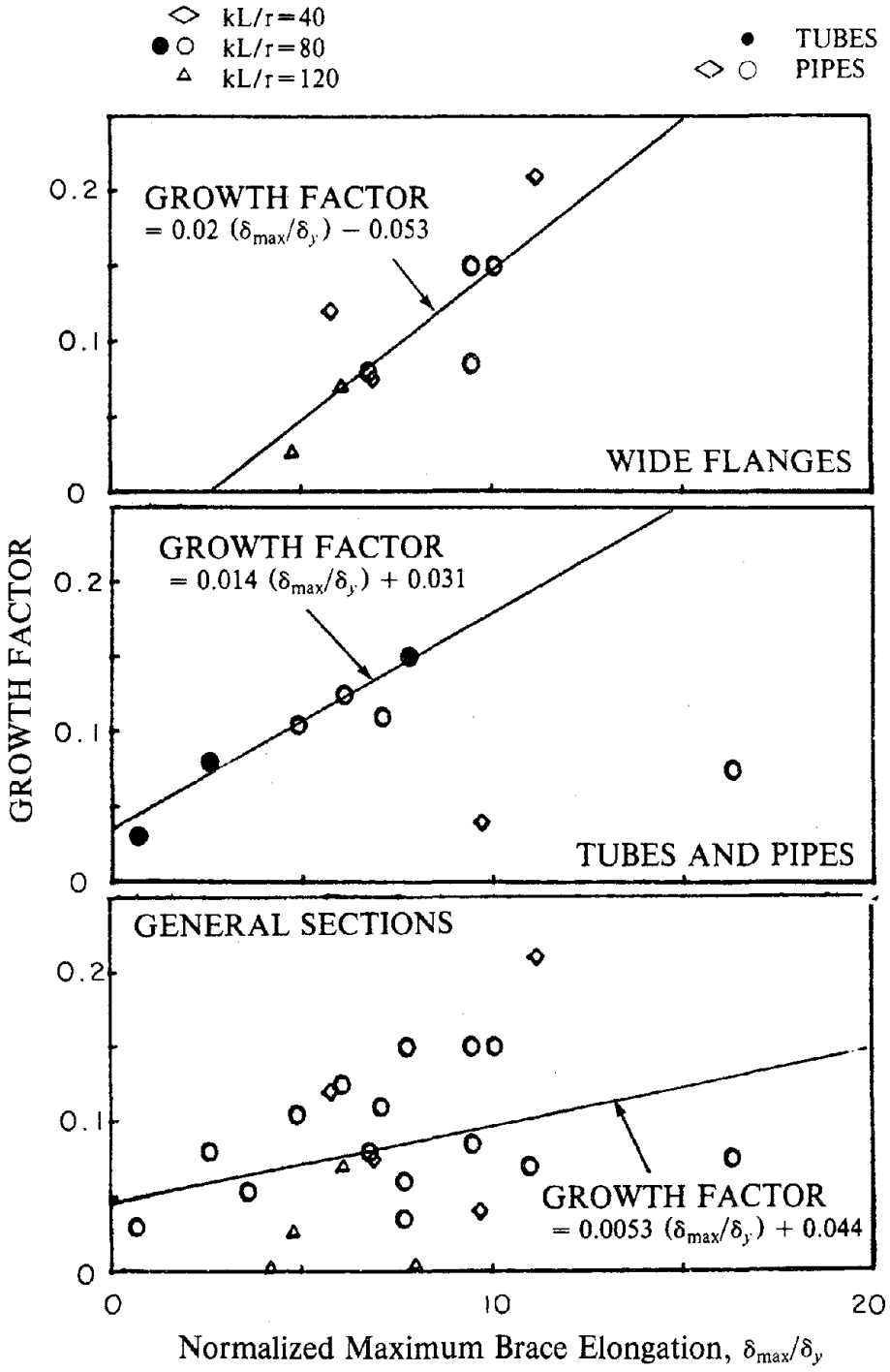

Fig. 6.2 Growth Factor versus δ_{max}/δ_y Relationships

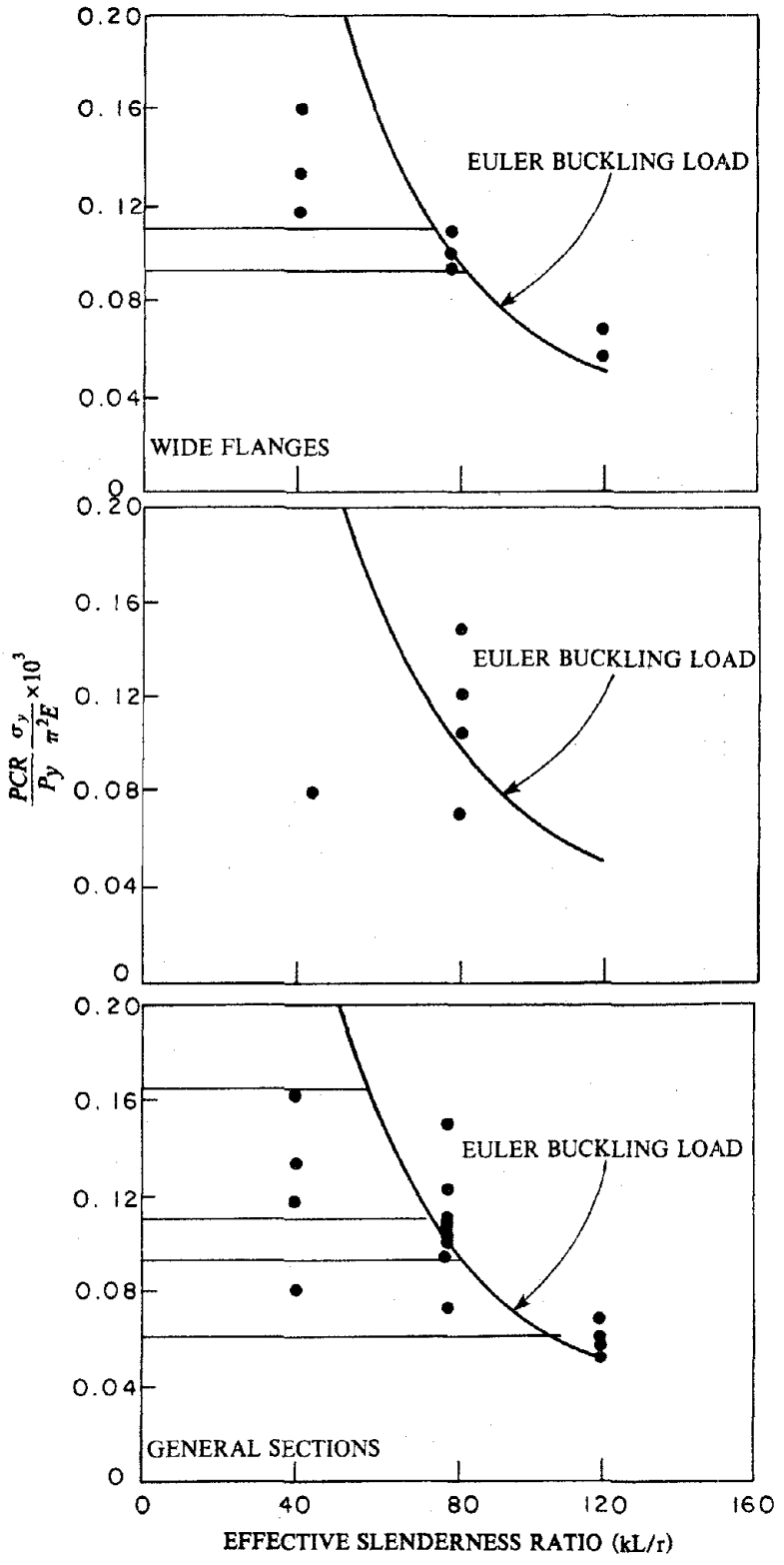

Fig. 6.3 PCR versus kL/r

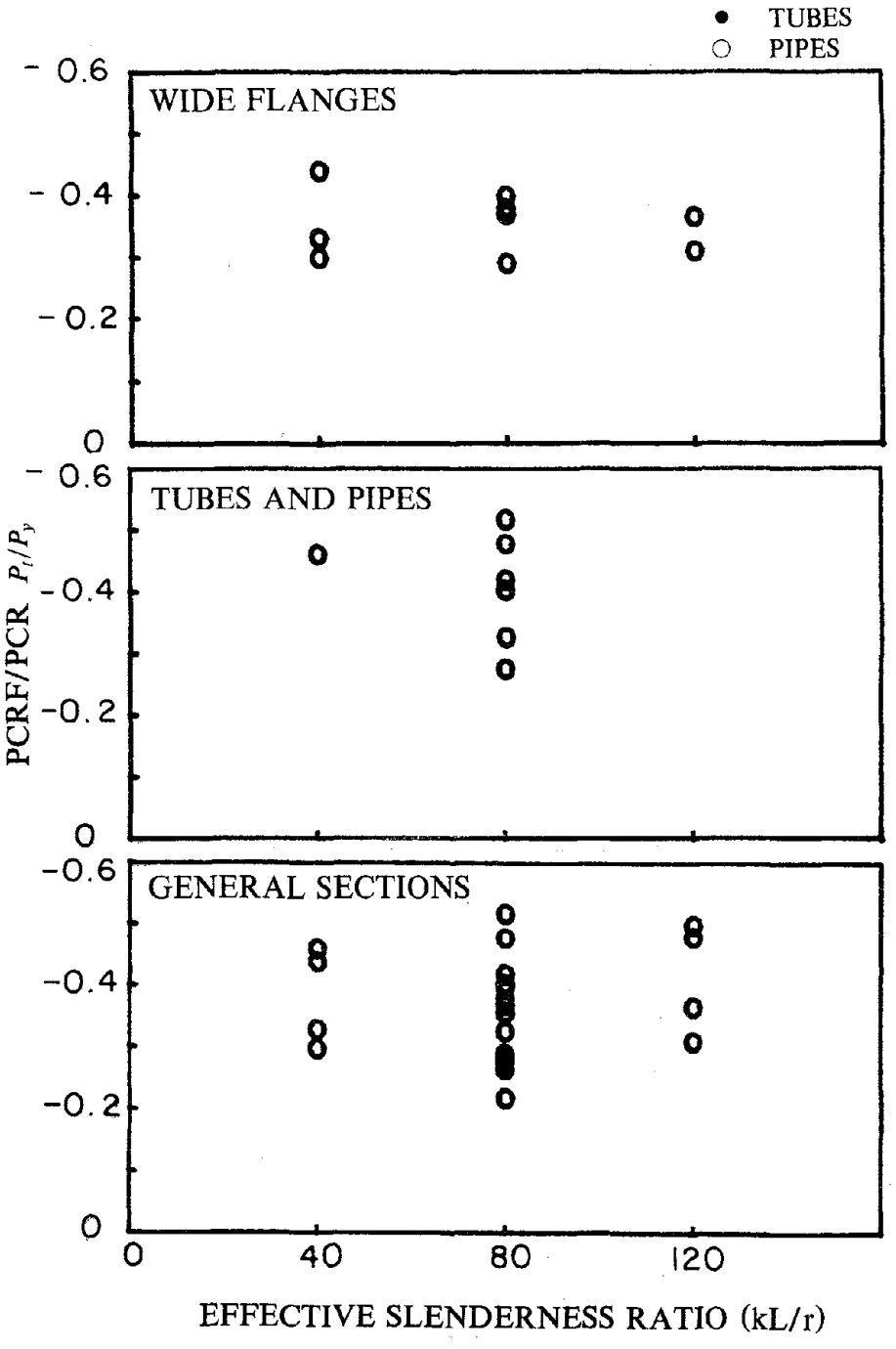

Fig. 6.4 PCRF versus Effective Slenderness Ratio Relationships

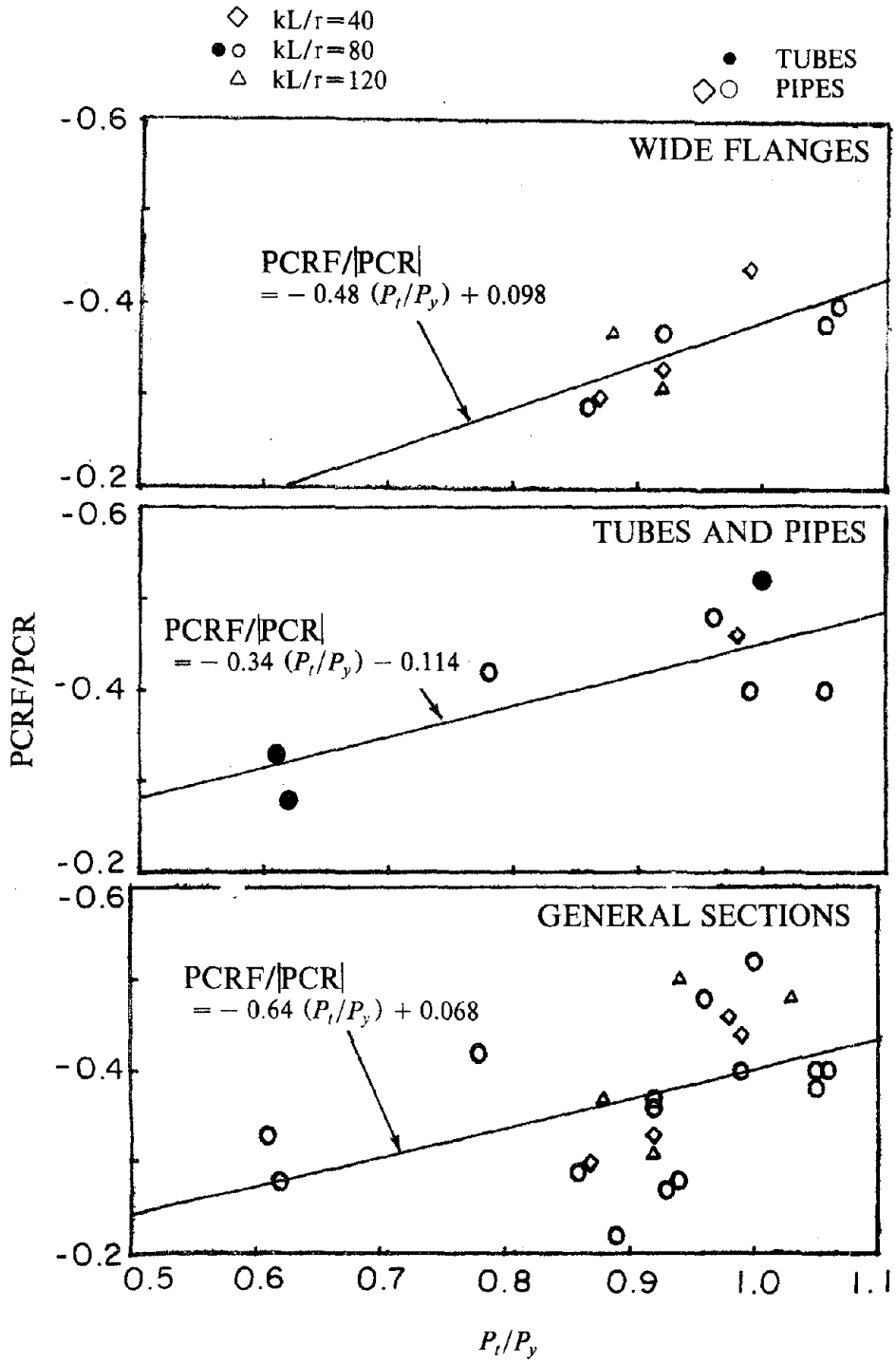

Fig. 6.5 PCRF versus P_t Relationships

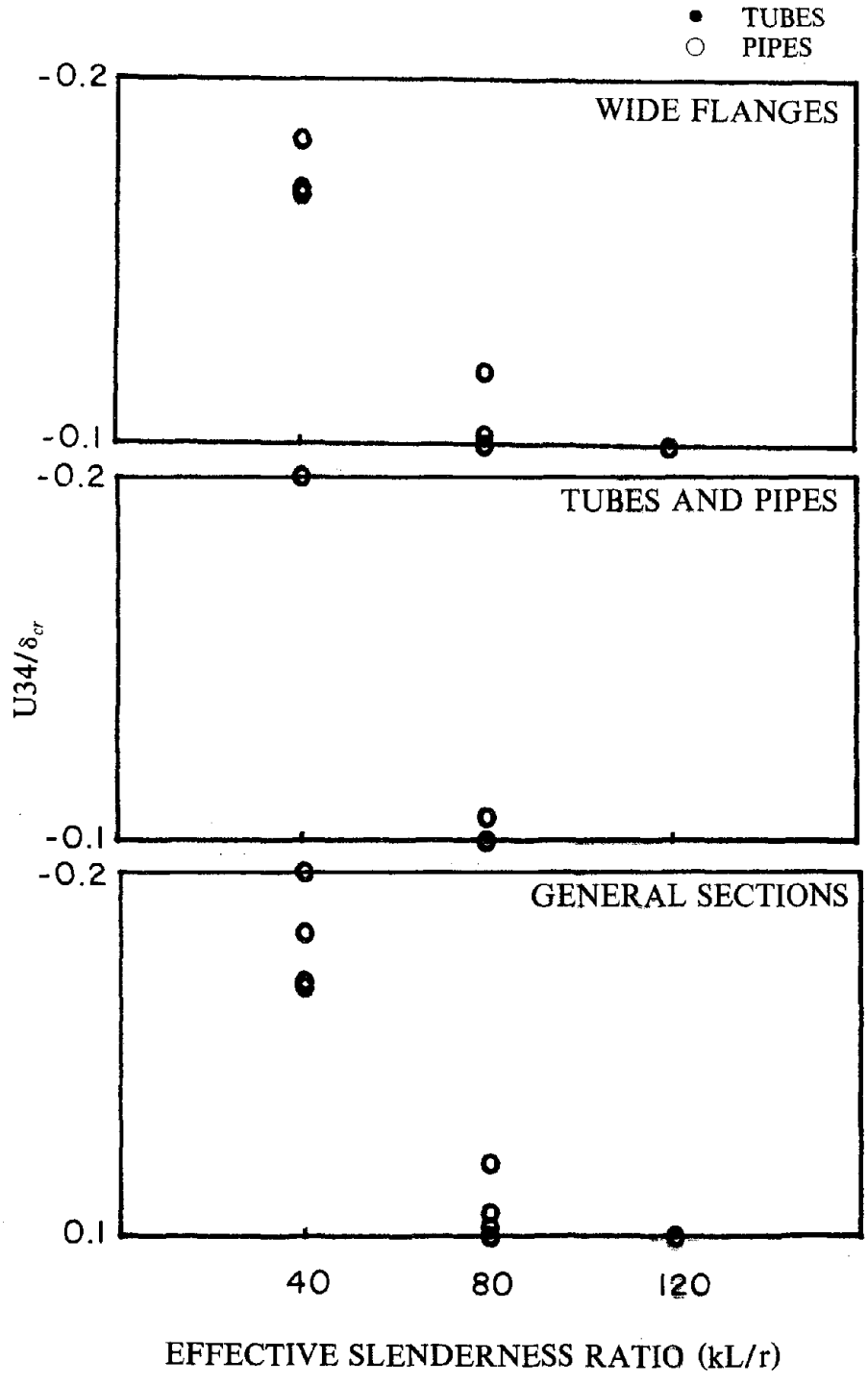

Fig. 6.6 U34 versus Effective Slenderness Ratio Relationships

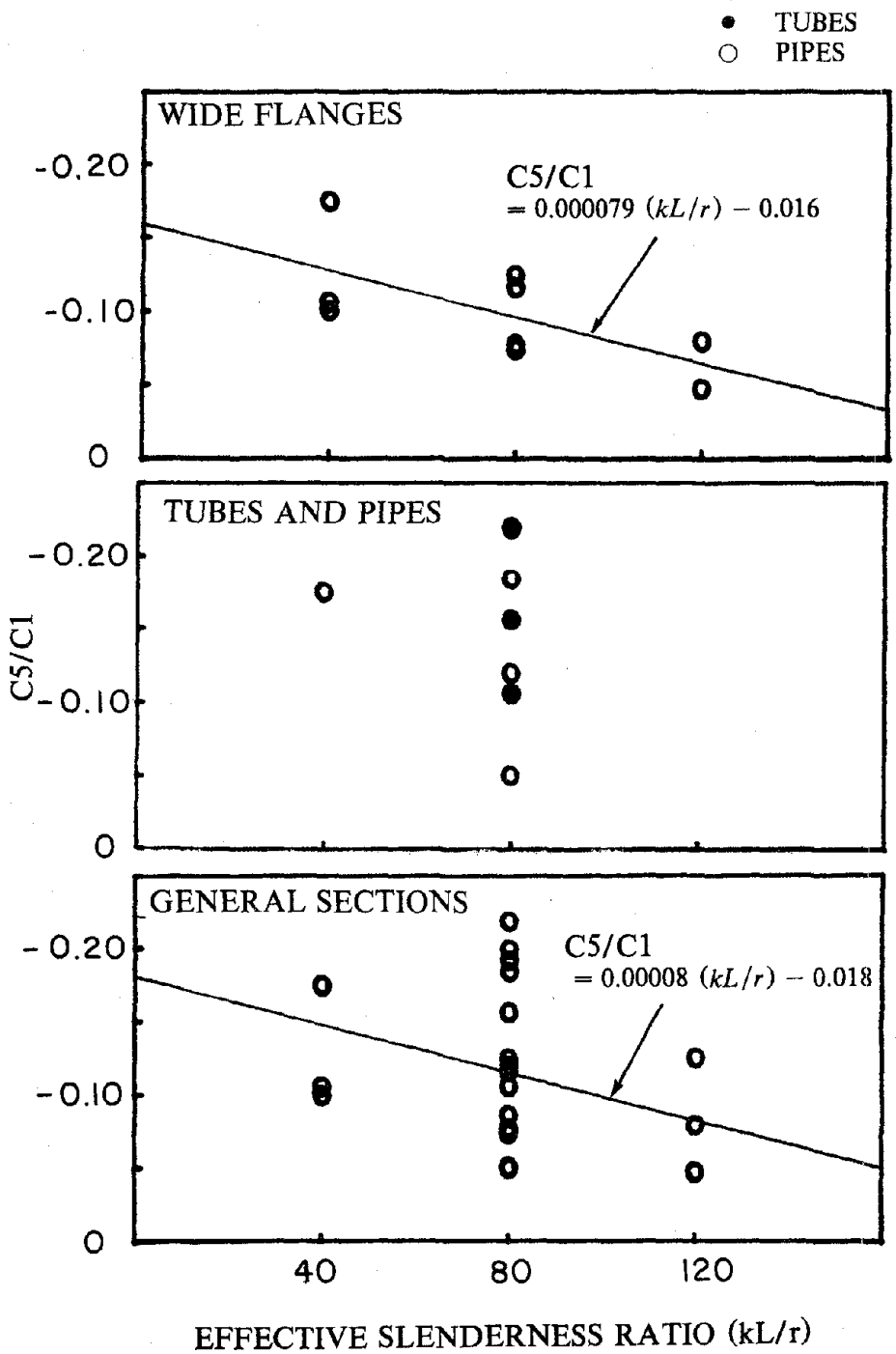

Fig. 6.7 C5 versus Effective Slenderness Ratio Relationships

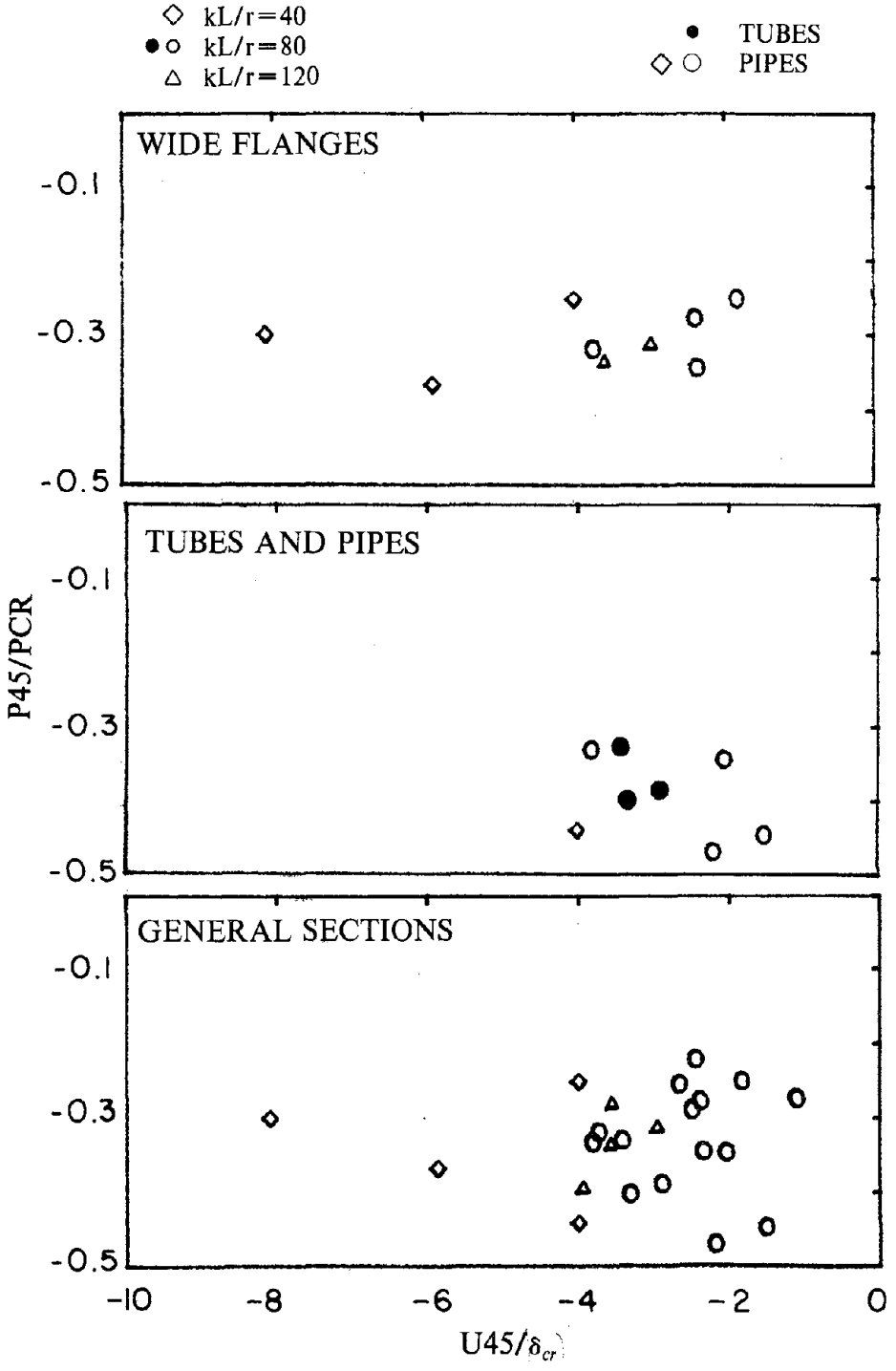

Fig. 6.8 Plots of Points (U45,P45)

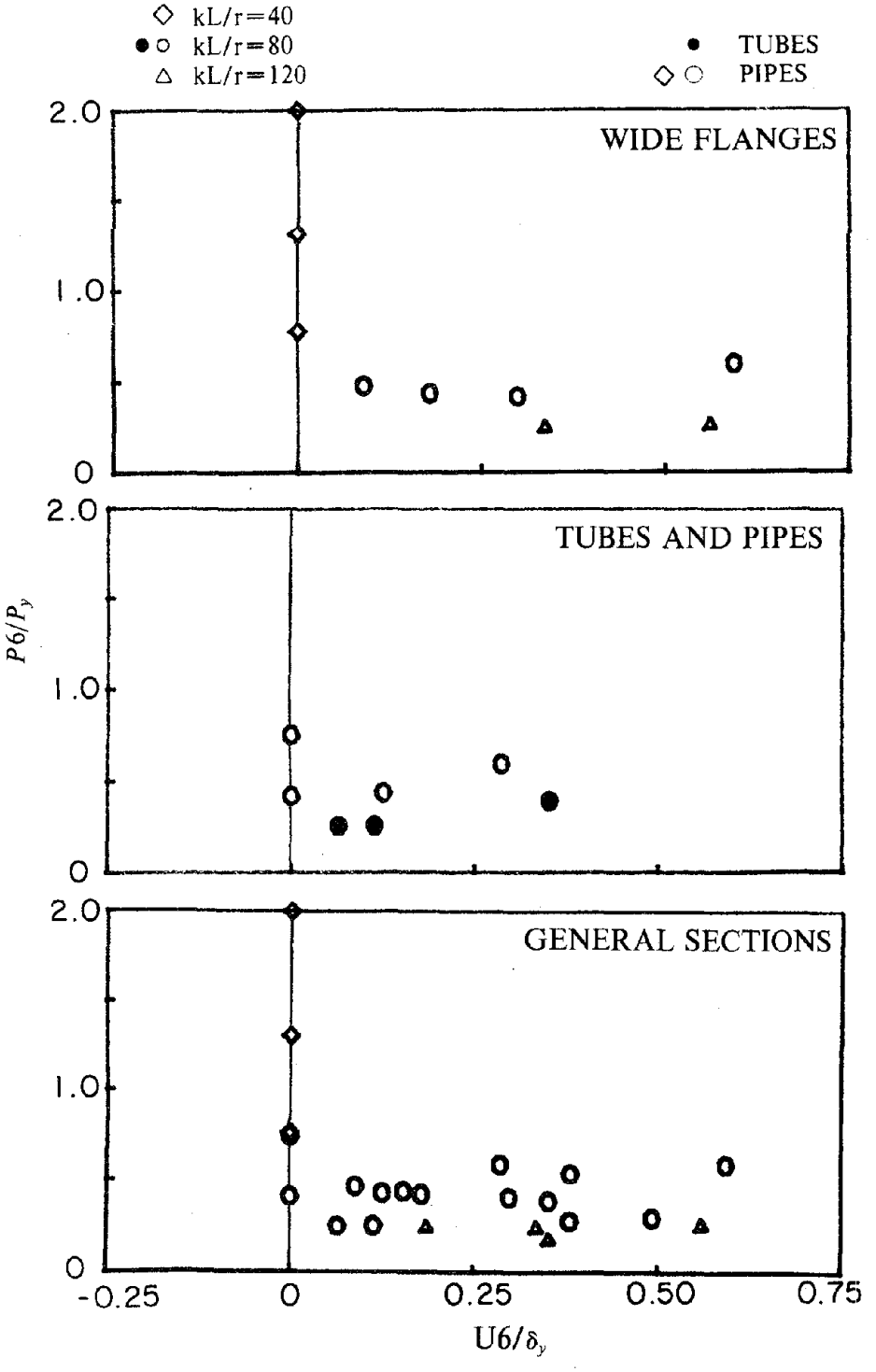

Fig. 6.9 Plots of Points (U6,P6)

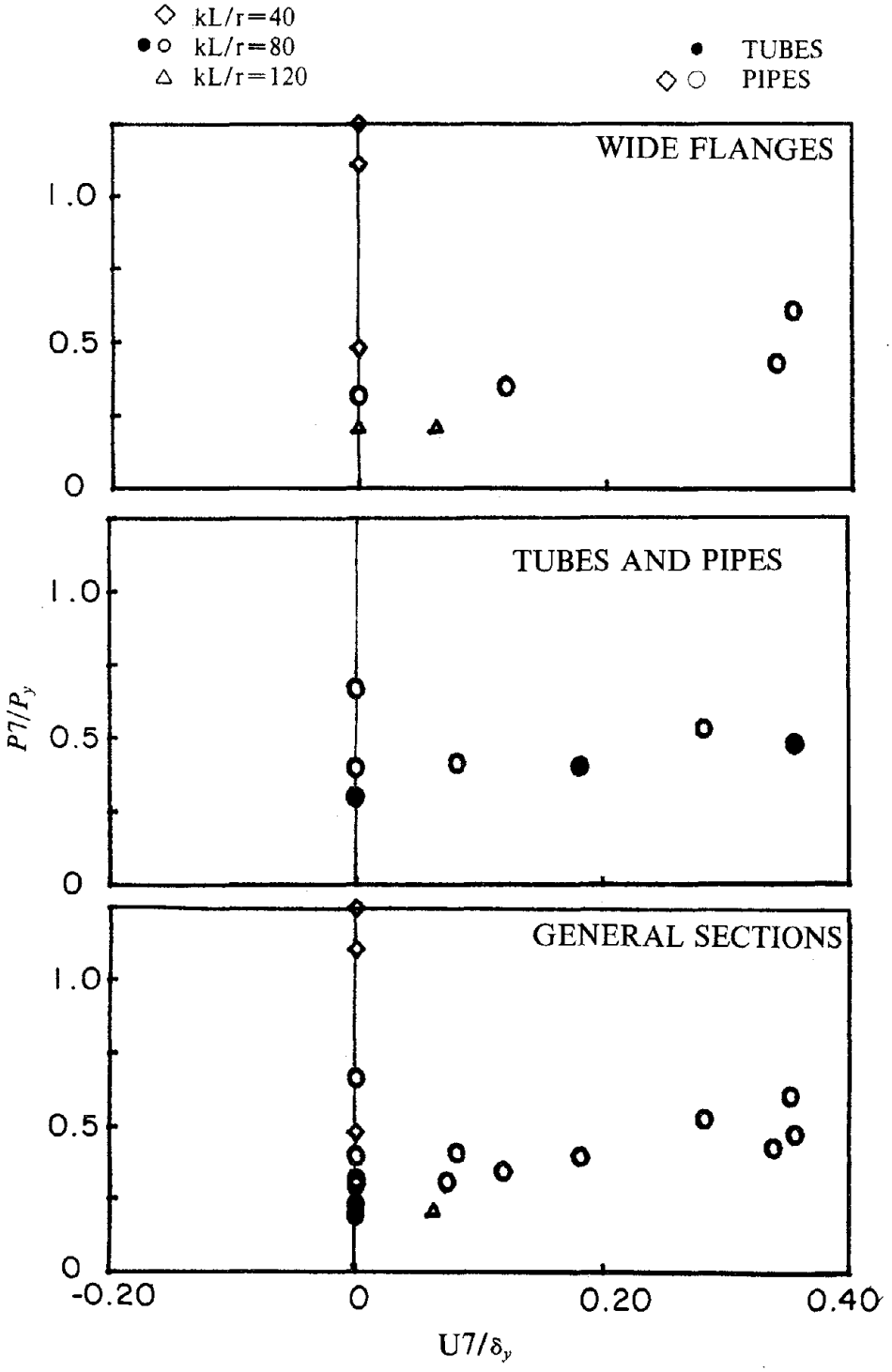

Fig. 6.10 Plots of Points (U7,P7)

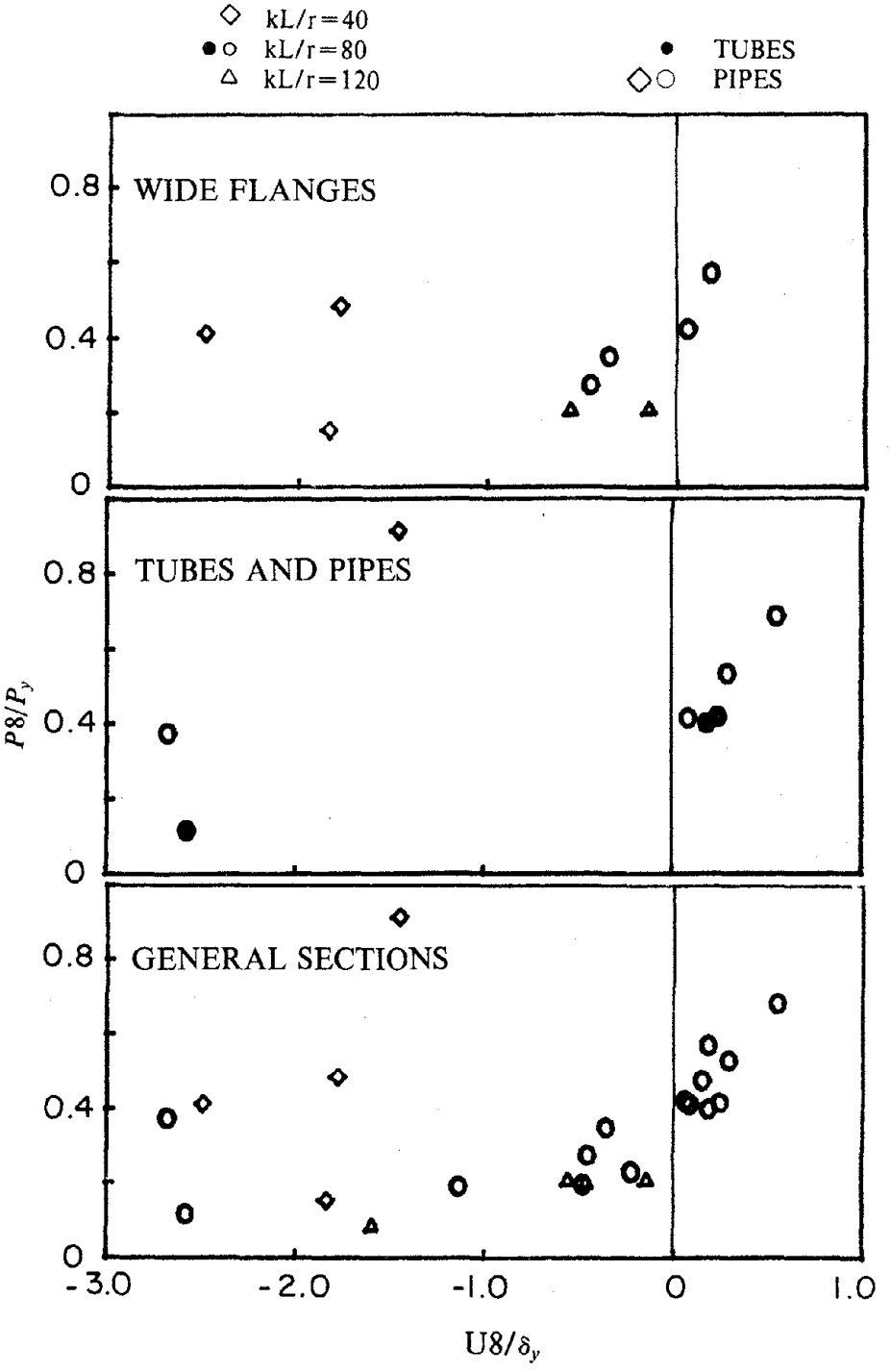

Fig. 6.11 Plots of Points (U8,P8)

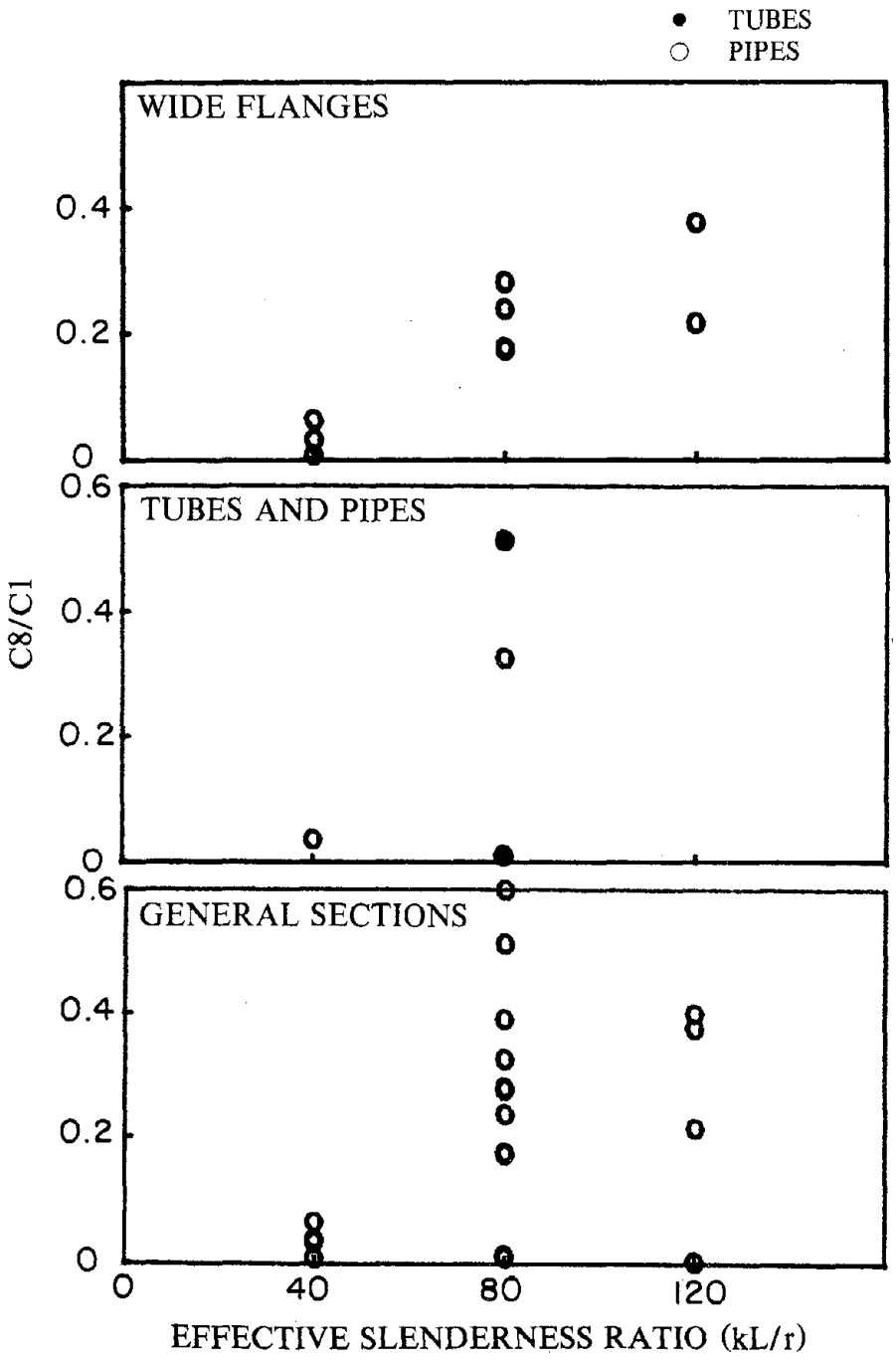

Fig. 6.12 C8 versus Effective Slenderness Ratio Relationships

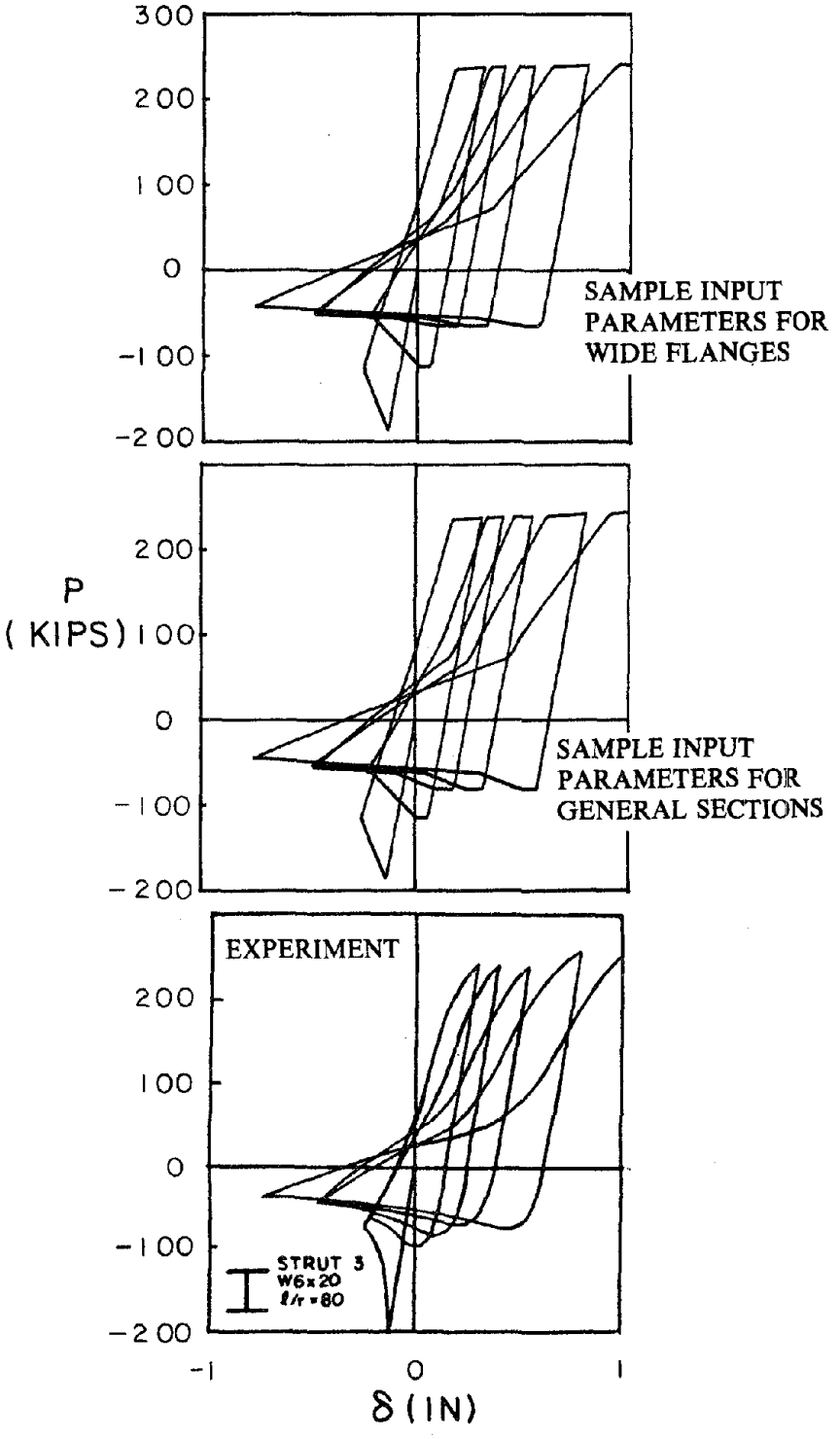

Fig. 6.13 Analytical Hysteresis Loops Obtained Using Generalized Input Parameters for Individual Sections (Strut 3, kL/r = 80) (1 kip = 4.45 kN; 1 in. = 25.4 mm)

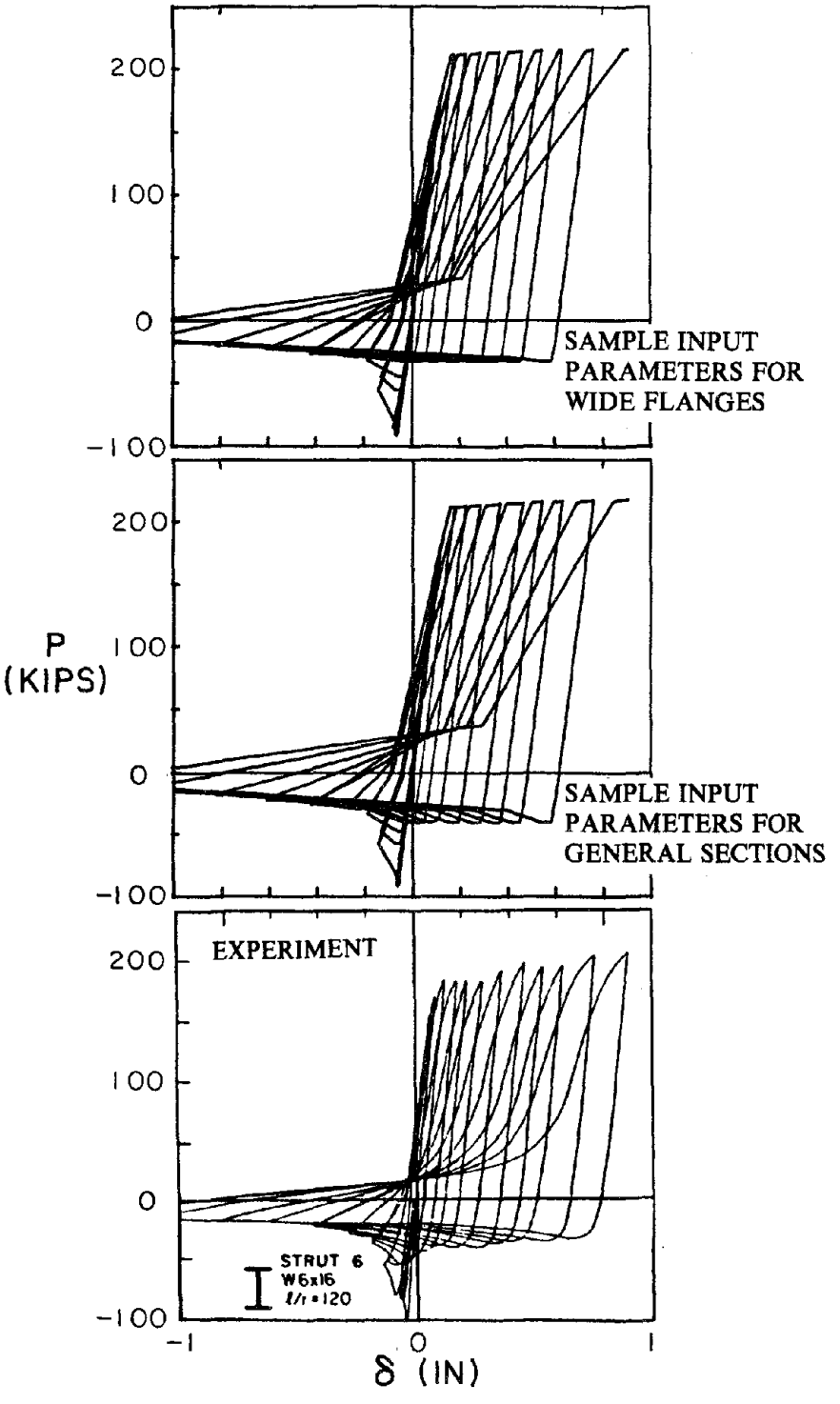

Fig. 6.14 Analytical Hysteresis Loops Obtained Using Sample Input Parameters for Individual Sections (Strut 6, kL/r = 120) (1 kip = 4.45 kN; 1 in. = 25.4 mm)

APPENDIX A

COMPARISON OF ANALYSIS AND EXPERIMENT

Experimental data from Reference 1 and analytical results obtained using the refined phenomenological model are compared for the 24 individual struts. In these analyses, the generalized input parameters presented in Tables 5.1 through 5.4 were used. Figures 5.1 and 5.2 have already presented the comparison for four of these struts. This Appendix presents the comparison for the remaining struts. This comparison is used for the evaluation of the validity of the generalized input parameters as well as of the capabilities of the element.

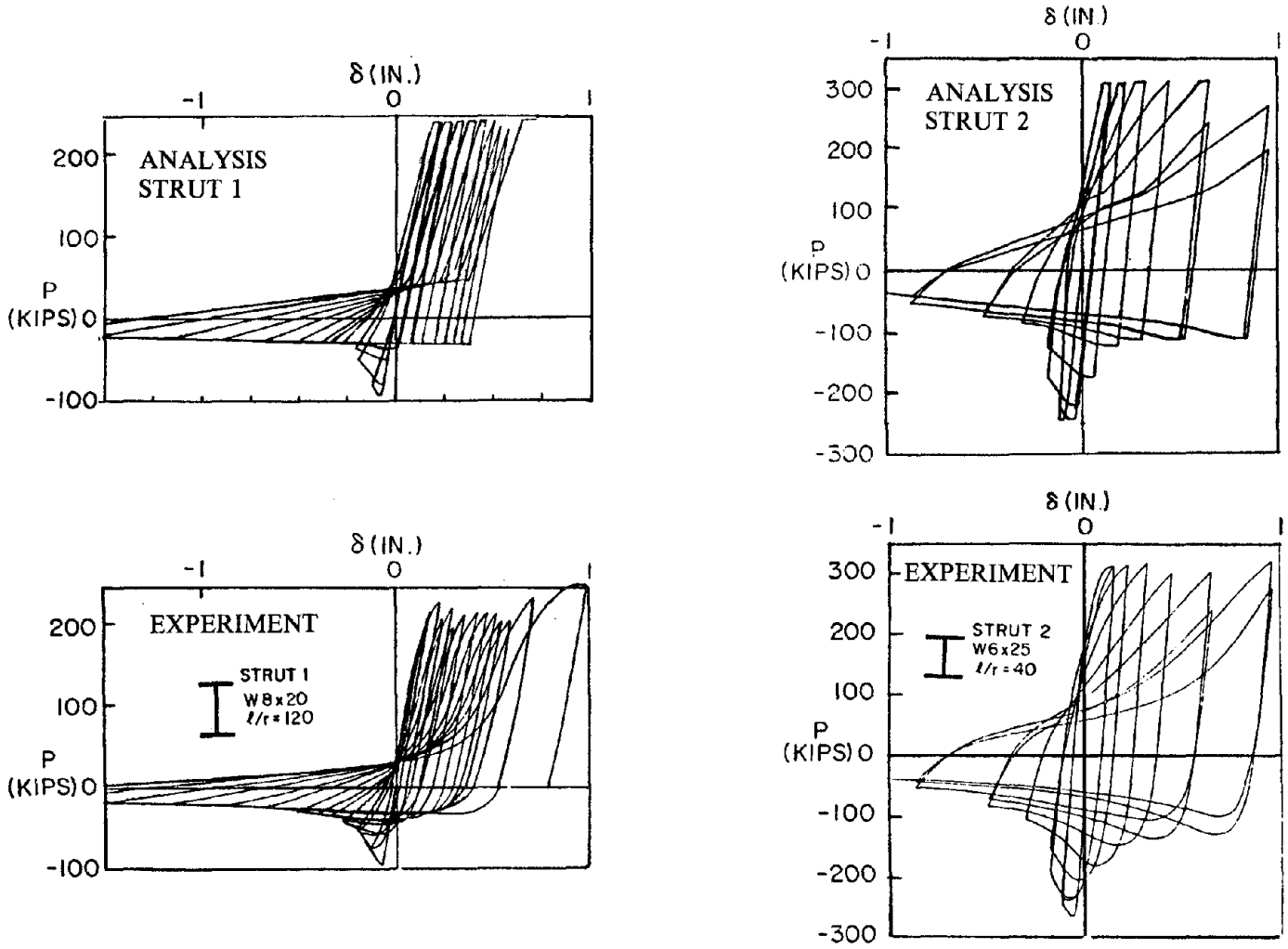

Fig. A1 Comparison of Analytical and Experimental Hysteresis Loops for Struts 1 and 2 (1 kip = 4.45 kN; 1 in. = 25.4 mm)

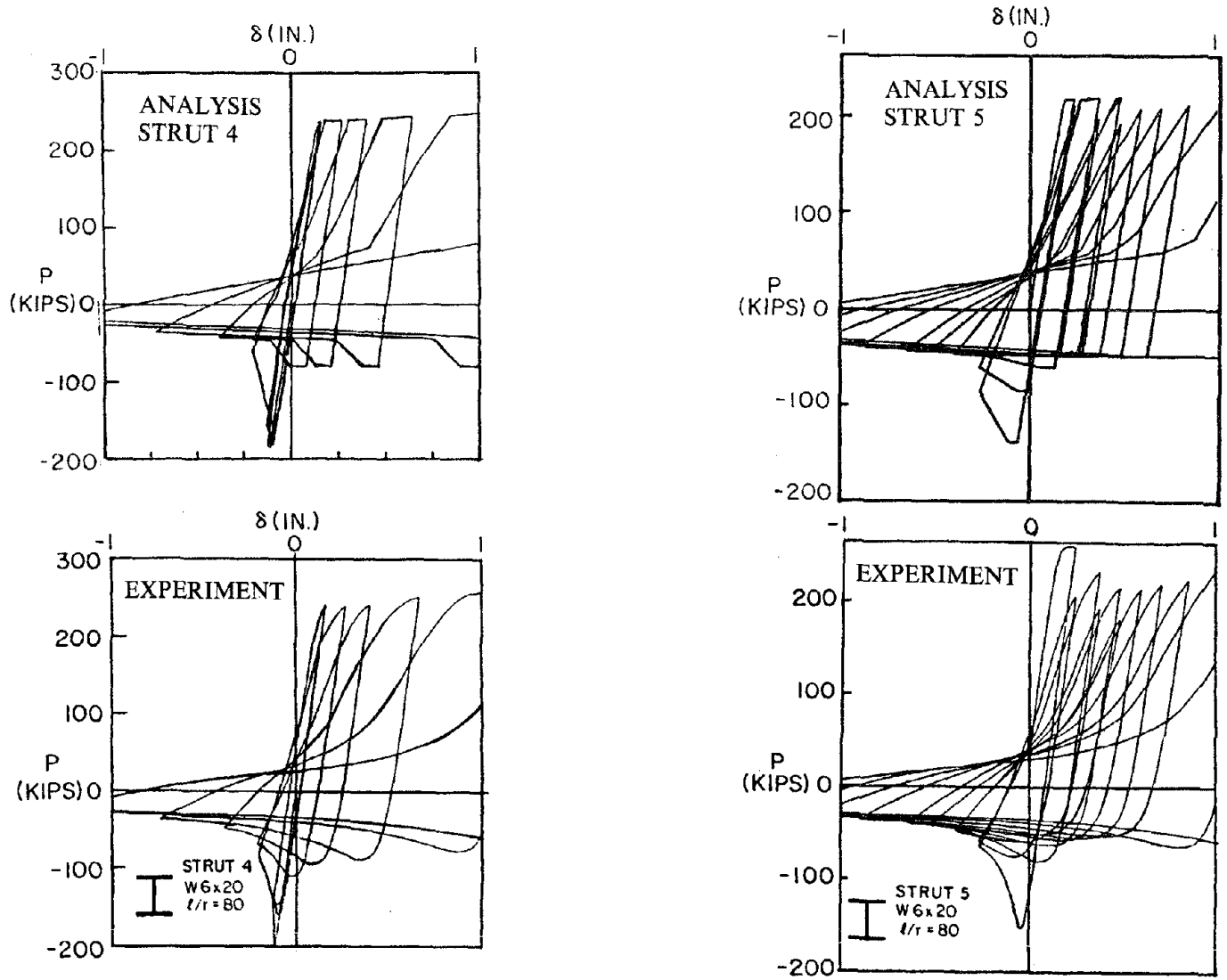

Fig. A2 Comparison of Analytical and Experimental Hysteresis Loops for Struts 4 and 5 (1 kip = 4.45 kN; 1 in. = 25.4 mm)

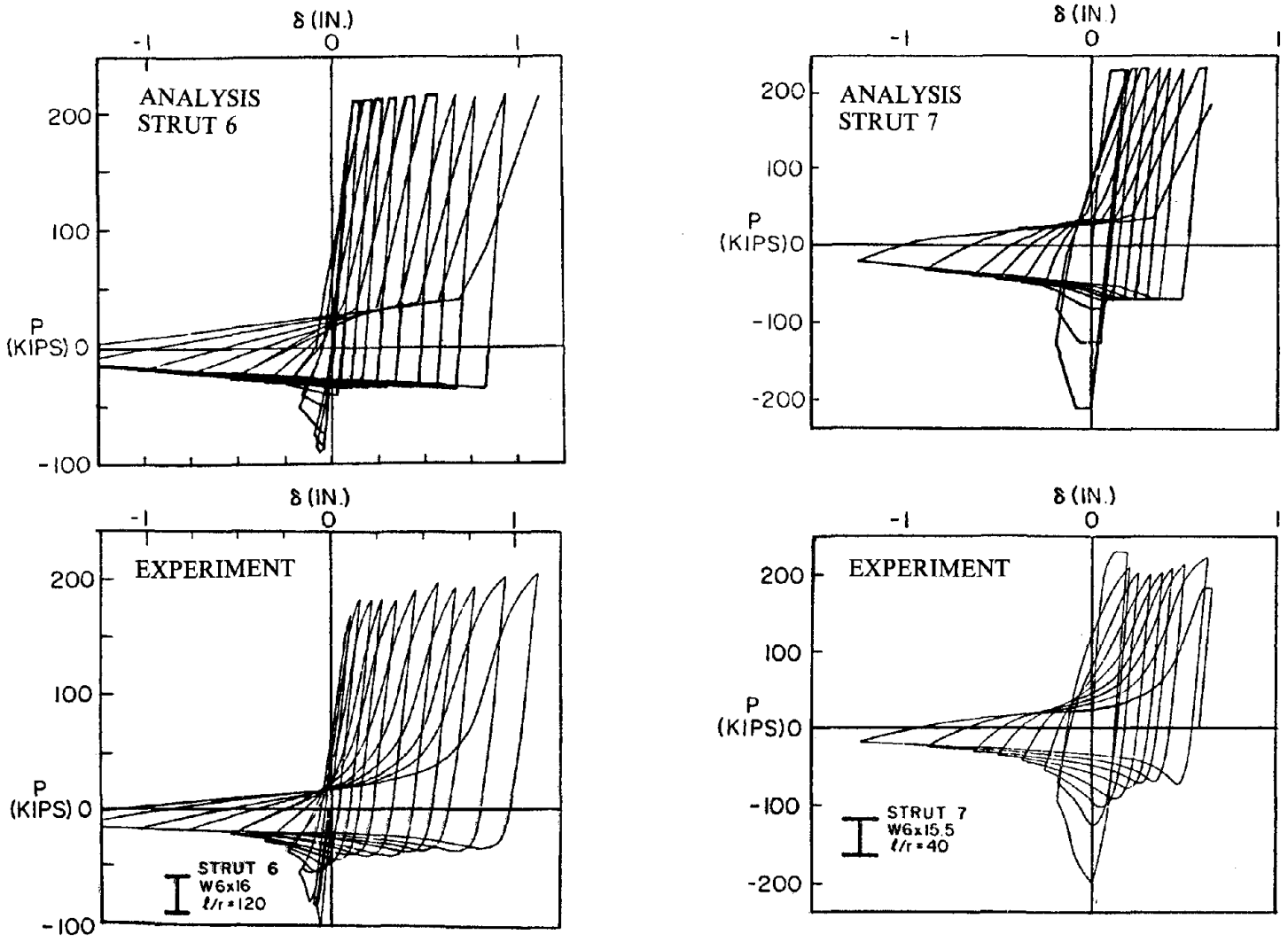

Fig. A3 Comparison of Analytical and Experimental Hysteresis Loops for Struts 6 and 7 (1 kip = 4.45 kN; 1 in. = 25.4 mm)

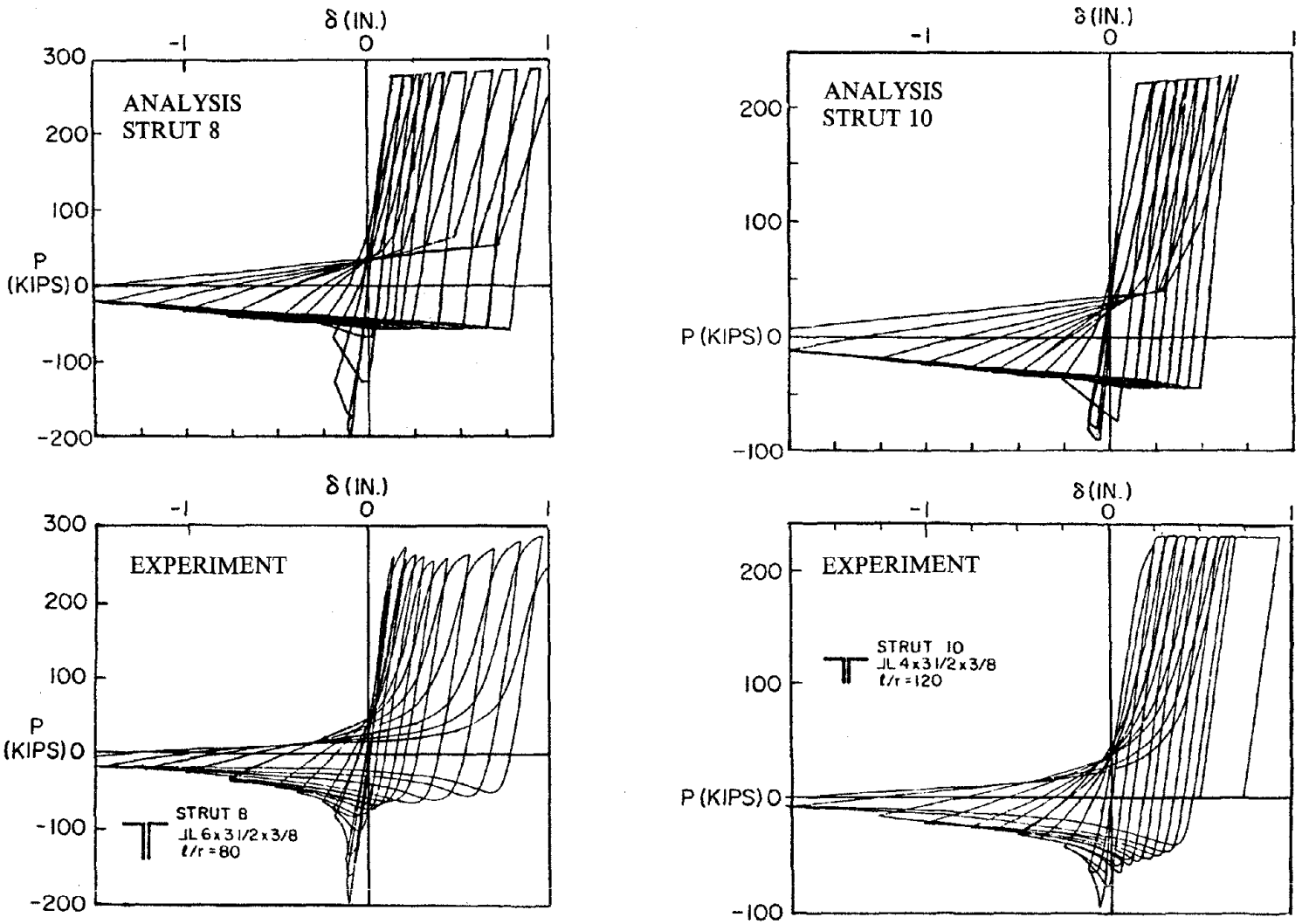

Fig. A4 Comparison of Analytical and Experimental Hysteresis Loops for Struts 8 and 10 (1 kip = 4.45 kN; 1 in. = 25.4 mm)

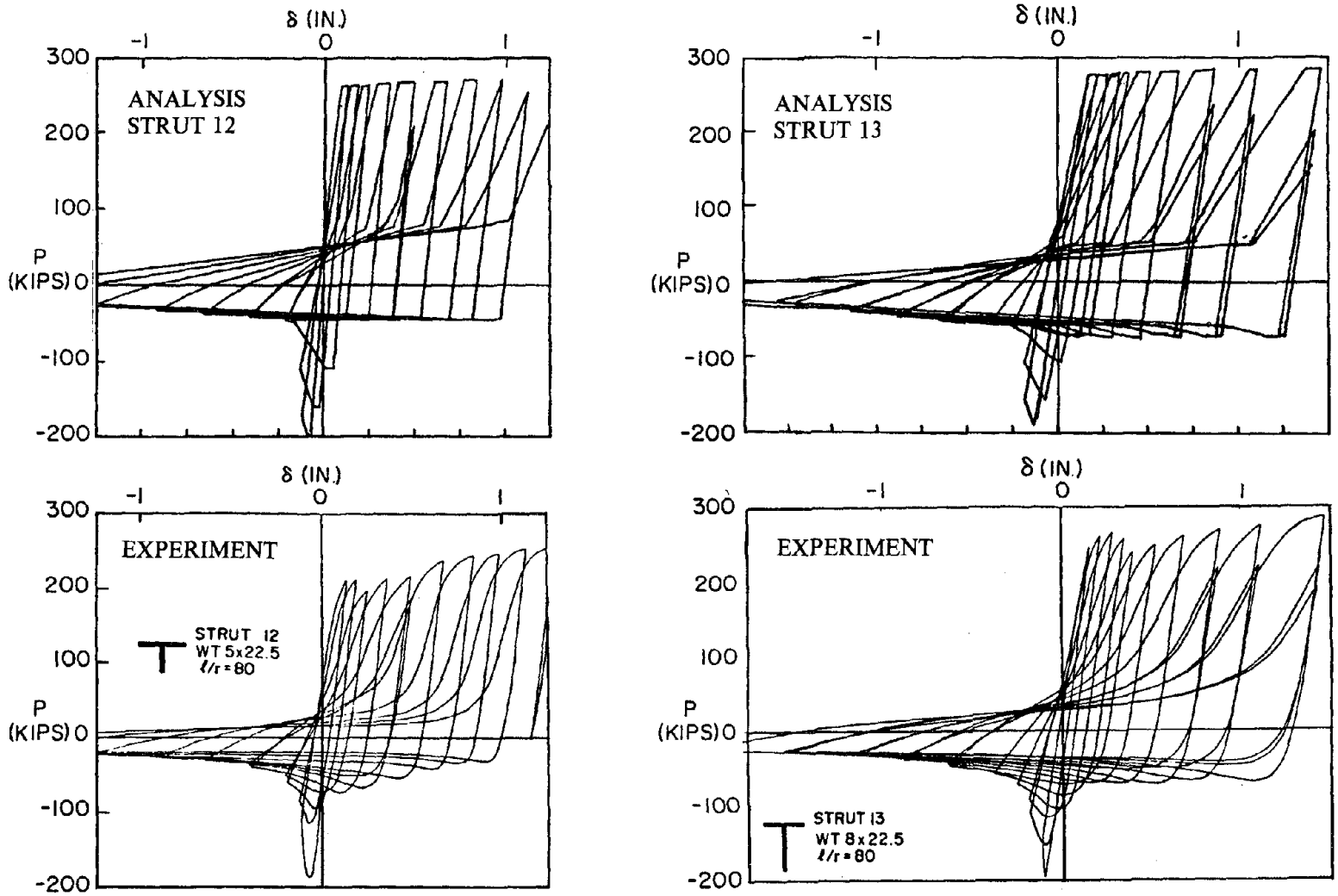

Fig. A5 Comparison of Analytical and Experimental Hysteresis Loops for Struts 12 and 13 (1 kip = 4.45 kN; 1 in. = 25.4 mm)

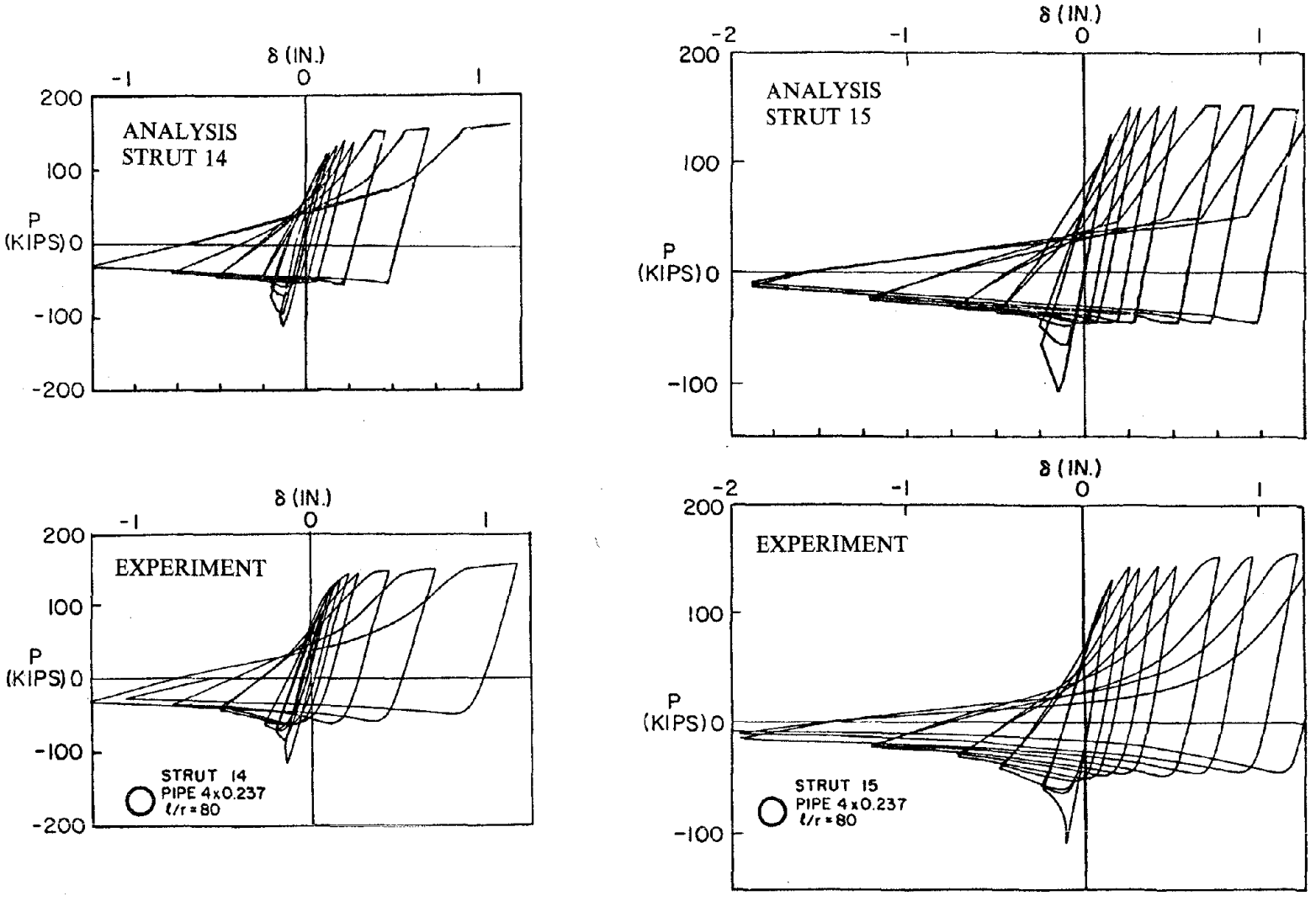

Fig. A6 Comparison of Analytical and Experimental Hysteresis Loops for Struts 14 and 15 (1 kip = 4.45 kN; 1 in. = 25.4 mm)

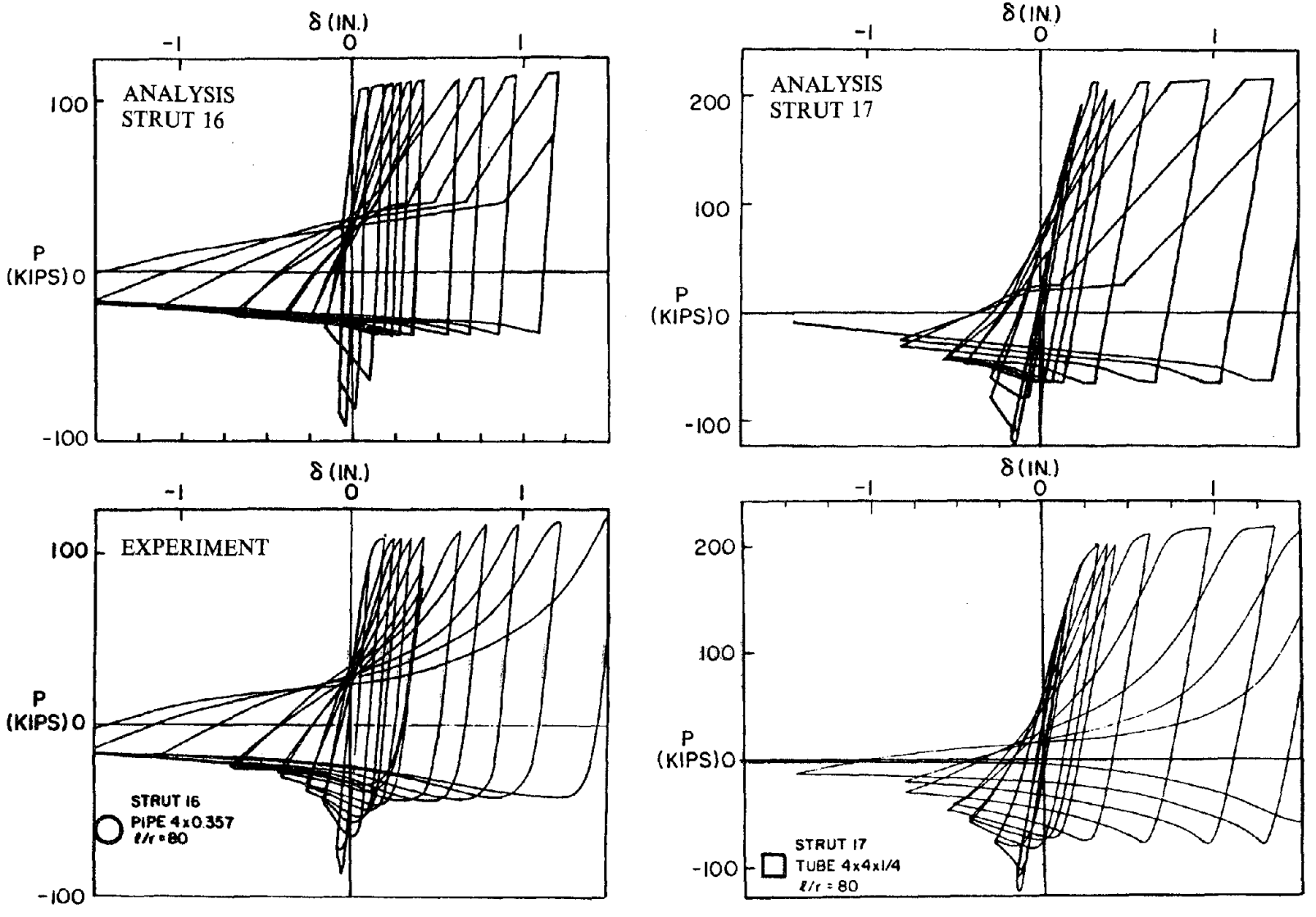

Fig. A7 Comparison of Analytical and Experimental Hysteresis Loops for Struts 16 and 17 (1 kip = 4.45 kN; 1 in. = 25.4 mm)

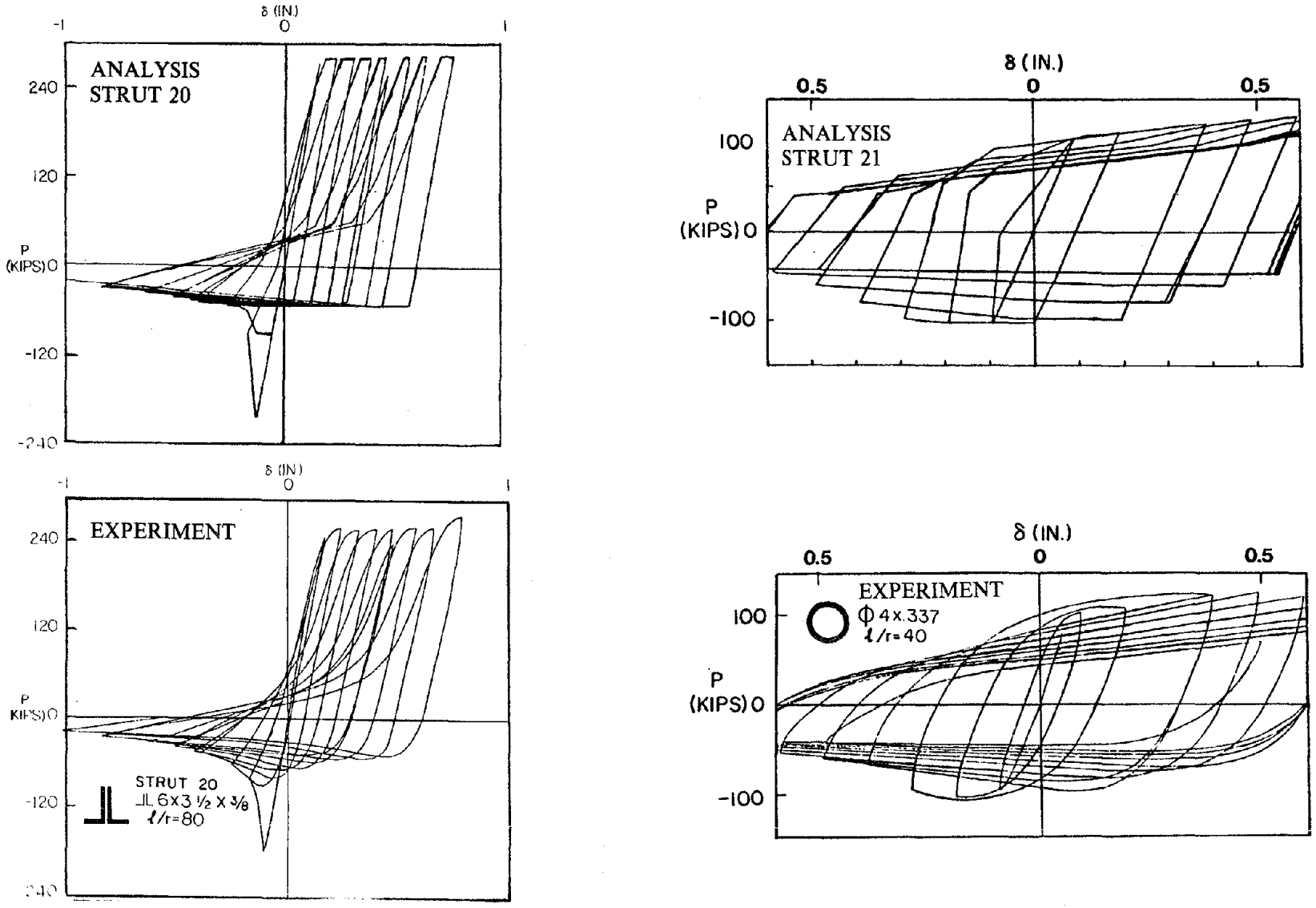

Comparison of Analytical and Experimental Hysteresis Loops for Struts 20 and 21 (1 kip = 4.45 kN; 1 in. = 25.4 mm)

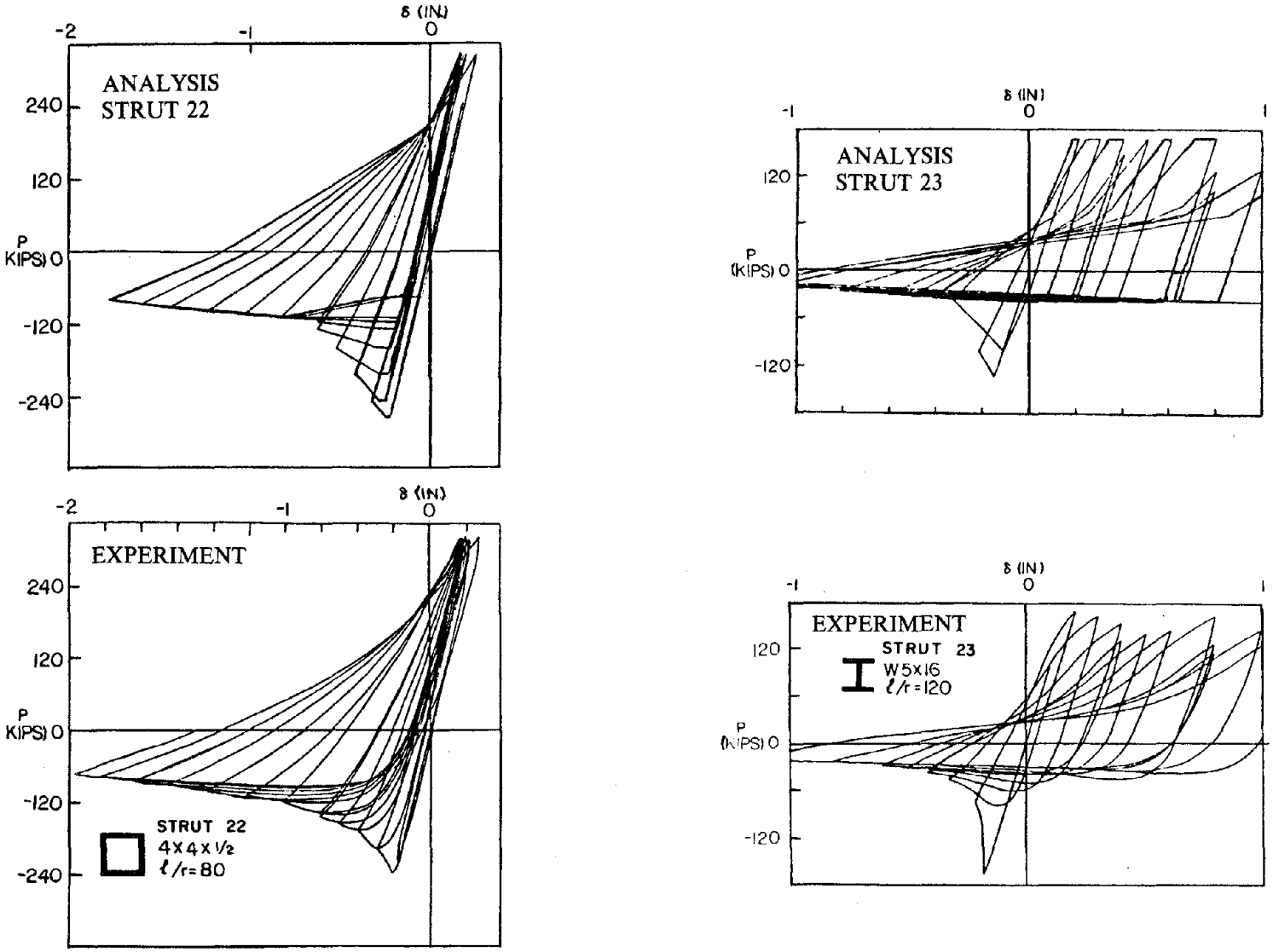

Fig. A9 Comparison of Analytical and Experimental Hysteresis Loops for Struts 22 and 23 (1 kip = 4.45 kN; 1 in. = 25.4 mm)

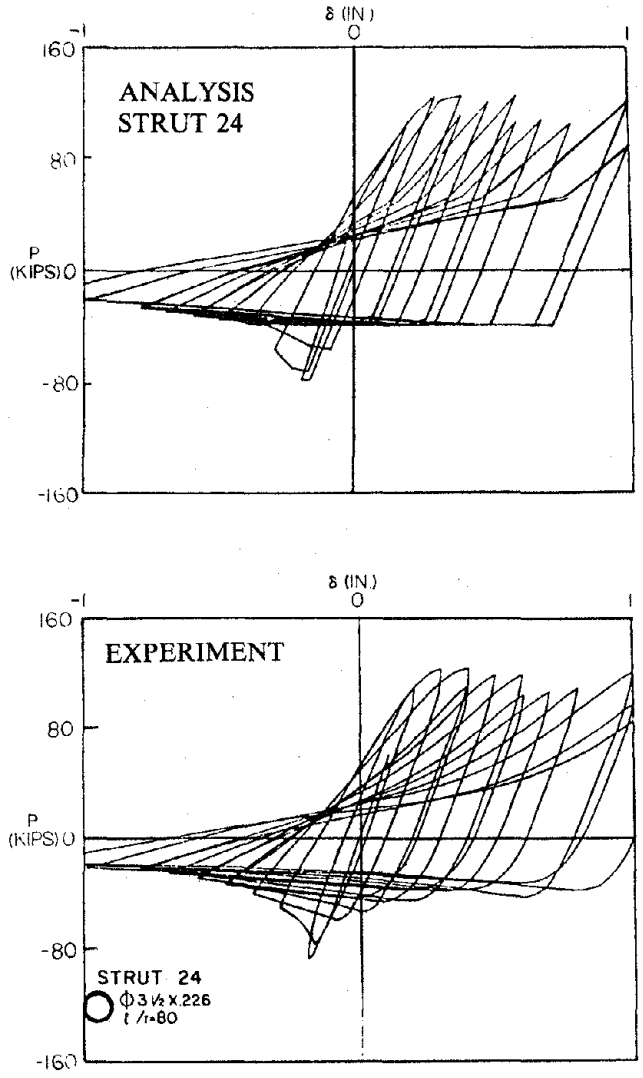

Fig. A10 Comparison of Analytical and Experimental Hysteresis Loops for Strut 24 (1 kip = 4.45 kN; 1 in. = 25.4 mm)

APPENDIX B

USER'S GUIDE FOR DRAIN-2D2 ELEMENT TYPE 4

B.1 General Characteristics

The post-buckling truss element is assumed to lie arbitrarily in the two-dimensional plane defined by the DRAIN-2D2 program. However, the element has only one local degree of freedom, δ, i.e., the axial deformation of the line between its end nodes (see Fig. B1).

The element is assumed pin-ended, thus providing no flexural resistance at its ends. The behavior of the member is governed by the inelastic axial force - axial deformation relation which is specified by the user. No geometric stiffness effects are included in the element's response and no initial forces can be specified.

B.2 Element Stiffnesses and Deformations

The hysteretic behavior of the post-buckling truss element is developed in ten distinct zones of axial force - axial deformation relationship (Fig. B2). One complete cycle of loading does not necessarily include all the zones. Throughout each zone, the element maintains a constant stiffness. The stiffness value changes as soon as the element enters a new zone. The characteristics of all the zones will be described in full detail in Section B.3.

When the element deforms in tension beyond the yield point, a permanent deformation (equal to the plastic deformation after the yield point) occurs and all displacement control points shift by this amount.

In addition, after loading cycle involving inelastic compressive zones, the tensile yield point is translated by a factor times the inelastic shortening during the current cycle (Fig. B3). This factor is specified by the user (the growth factor).

Every time the element exits Zone 4, the peak compressive load capacity of the brace (PCR) is reduced to the lowest value reached in Zone 4. This shall not, however, be less than the user specified final buckling load (PCRF) (see Fig. B3).

Based on the capabilities of the DRAIN-2D2 program, the exact axial force - deformation relationship of the element can be followed using the event-to-event strategy, as described in Chapter 3. The user can also use the step-by-step method utilizing the unbalanced force correction procedure.

B.3 Description of Zones

The graphical representation of the ten zones used in the new element are illustrated in Figs. B4 through B13. The following symbols are used in these figures.

Zone location;

Allowable current path;

Possible previous path;

Illustration of adjacent zones;


Entry point to zone;


Exit point from zone;


Possible next point at end of analysis time step.

The behavioral characteristics of the zones are described in detail in the following tables.

ZONE 1

Characteristics :	Elastic region for both tensile and compressive action. Bounded by the U29 yield displacement (in tension), and by the U13 buckling displacement (in compression).
Stiffness :	Program variable C1. Determined by the elastic stiffness of the element, $\frac{EA}{L}$.
Entry from Zones :	9,2.
Exit to Zones :	3,4,5,10 (C) (C denotes the compression) 9,2 (T) (T denotes the tension)

ZONE 2

Characteristics :	Tensile yield region. In this zone, the element has a tensile extension bigger than or equal to the U29 yield limit.
Stiffness :	Program variable C2. Determined as a proportion of the elastic stiffness C1.
Entry from Zones :	1,3,4,5,6,7,8,9,10
Exit to Zones :	1,3,4,5,10 (C) 1 (T)

ZONE 3

Characteristics :	Inelastic buckling region; the first zone the element enters after buckling occurs. Bounded by the U13 and U34 displacement control points.
Stiffness :	Set to zero.
Entry from Zones :	1,2,6,7,8,9
Exit to Zones :	1,2,7,8,9 (T) 1,4,5,6,10 (C)

ZONE 4

Characteristics :	Inelastic post-buckling compressive region with negative stiffness.
Stiffness :	Program variable C4. Determined by the slope between the intersecting points of Zones 3 and 4 and of Zones 4 and 5: $C4=\frac{(PCR-P45)}{(U13-U45)}$
Entry from Zones :	1,2,3,6,7,8,9
Exit to Zones :	5,6,10 (C) 1,2,7,8,9 (T)

ZONE 5

Characteristics :	Inelastic post-buckling compressive region with negative stiffness. Usually, a more "flat" region than Zone 4.
Stiffness :	Program variable C5. User specified value; must be negative.
Entry from Zones :	1,2,3,4,6,7,8,9
Exit to Zones :	6,10 (C) 2,7,8,9 (T)

ZONE 6

Characteristics :	Elastic post-buckling zone in compression. The element enters this zone when unloading from a post buckling state (Zones 3,4 and 5).
Stiffness :	Program variable C6. Determined by the intersection point (UPO,0) of the force - deformation curve and the displacement axis, and the user specified point (U7,P7).
Entry from Zones :	3,4,5,7,8
Exit to Zones :	1,2,7,8,9 (T) 1,3,4,5,10 (C)

ZONE 7

Characteristics :	Elastic post-buckling zone in tension. The element enters this zone when the element is in tension in a post-buckling stage.
Stiffness :	Program variable C7. Determined by the points (UPO,0) and (U7,P7).
Entry from Zones :	3,4,5,6,8,10
Exit to Zones :	3,4,5,6,10 (C) 8,9,10 (T)

ZONE 8

Characteristics :	Inelastic post-buckling tensile region.
Stiffness :	Program variable C8. User specified value; must be positive.
Entry from Zones :	3,4,5,6,7,10
Exit to Zones :	7,9,2 (T) 3,4,5,6,10 (C)
Remarks :	1. If the intersecting point of Zones 7 and 8 is below the displacement axis, Zone 7 is bypassed and the element enters Zone 8. At the same time, a new slope for Zone 8 is defined by the (U8,P8) control point and the intersection of the force-deformation curve and the displacement axis (Fig. B11 (g)). 2. The user is recommended to specify a nearly "flat" slope for Zone 8.

ZONE 9

Characteristics :	Inelastic post-buckling tensile region after buckling occurred in the same hysteretic loop.
Stiffness :	Program variable C9. Determined by the point at which the element enters Zone 9 and the yield point (U29,P_y).
Entry from Zones :	1,3,4,5,6,7,8,10
Exit to Zones :	1,2 (T) 1,3,4,5,10 (C)

ZONE 10

Characteristics :	This zone is included to account for an asymptotic behavior of Zone 5. If the slope of Zone 5 is very steep and the element undergoes shortening to a large extent, it will reach the predicted displacement without having to cross over the displacement axis. At the intersection of Zone 5 and the displacement axis, the element enters Zone 10 and it develops the remaining shortening providing zero resistance.
Stiffness :	Set to zero.
Entry from Zones :	1,2,3,4,5,7,8,9
Exit to Zones :	2,7,8,9 (T)

B.4 Input Data for the Refined Phenomenological Element

This section presents the input data for the refined model, developed as an element for the DRAIN-2D2 program. See Reference 21 for remainder of input data required and see Fig. B14 for an illustration of the input parameters.

B.4.1 CONTROL INFORMATION (2 Cards)

1.1 First Card (3I5,F10.0)

Notes	*Columns*	*Variable*	*Data*
	1-5(I)		Punch 4 (to indicate the group type number).
	6-10(I)	NMEM	Number of elements in group.
	11-15(I)	KREP	Event calculation code : 1 if it applies. 0 or blank if the event-to-event strategy is not desired.

1.2 Second Card (I5)

Notes	*Columns*	*Variable*	*Data*
	1-5(I)	NSTF	Number of different stiffness types.

B.4.2 STIFFNESS TYPES (3 Cards per stiffness type)

The stiffness information can be given in either of two ways :

(a) The user can directly provide the actual values for all the parameters.

(b) The user can input the stiffness parameters by providing normalized coefficients with respect to the yield displacement (δy) and the yield force (Py). The only actual values which must be specified are those of δy and Py. The program internally converts all the normalized coefficients to dimensioned values of displacement, force and stiffness.

2.1 First Card (I4,I1,5X,7F10.0)

Notes	*Columns*	*Variable*	*Data*
	1-4(I)		Stiffness type number. Must be in increasing numerical sequence beginning with 1.
	5(I)		Punch: 0 if input is not normalized, or, 1 if input is normalized.
	6-10		Leave blank.
(1)	11-20(R)		Cross-sectional area of element. (positive number)
(1)	21-30(R)		Young's modulus of elasticity. (positive number)
(2)	31-40(R)	U29	Yield displacement (positive number). Leave blank *if input is not normalized.*
	41-50(R)	PYP	Tension yield force. (positive number)
	51-60(R)	PCR	Initial buckling force. (negative number)
	61-70(R)	PCRF	Final buckling force after inelastic cycling. (negative number) PCR$\leqslant$PCRF$\leqslant$P45
	71-80(R)		Strain hardening ratio of Zone 2 stiffness to Zone 1 stiffness. (positive number)

2.2 Second Card (7F10.0)

Notes	*Columns*	*Variable*	*Data*
	1-10(R)	FACTOR	Growth factor. (positive number)
	11-20(R)	GROF	Column growth limit (positive number) The total accumulated amount of inelastic column growth that may occur in the element.
(3)	21-30(R)	U34	Displacement coordinate of intersection of Zone 3 and Zone 4. (negative number)
(4)	31-40(R)	U45	Displacement coordinate of intersection of Zone 4 and Zone 5. (negative number)
	41-50(R)	P45	Force coordinate of intersection of Zone 4 and Zone 5. (negative number)
	51-60(R)	C5	Slope of Zone 5. (negative number)
(5)	61-70(R)	U6	Displacement coordinate for control point of Zone 6. (positive number)
(5)	71-80(R)	P6	Force coordinate for control point of Zone 6. (positive number)

2.3 Third Card (5F10.0)

Notes	*Columns*	*Variable*	*Data*
(5)	1-10(R)	U7	Displacement coordinate for control point of Zone 7 (positive number)
(5)	11-20(R)	P7	Force coordinate for control point of Zone 7. (positive number)
	21-30(R)	U8	Displacement coordinate of intersection of Zones 8 and 9. (negative number)
	31-40(R)	P8	Force coordinate of intersection of Zones 8 and 9. (positive number)
	41-50(R)	C8	Slope of Zone 8. (positive number)

3. ELEMENT GENERATION (1 Card per element)

Notes	*Columns*	*Variable*	*Data*
	1-5(I)	IMEM	Element number
	6-10(I)	NODI	Node number at element end I
	11-15(I)	NODJ	Node number at element end J
	15-20(I)	ISTIF	Stiffness type number
(6)	21-25(I)	IPRINT	Time history output code: 0 : no print 1 : print only 2 : print and save 3 : save only 4 : save and print reorganized time history

NOTES

(1) The actual values of the cross-sectional area and the modulus of elasticity must be provided, regardless of whether the stiffness input is normalized or not.

(2) A positive value of the yield displacement must be provided in the case of normalized input. If the input is not normalized, the yield displacement is computed by the program internally and this space in the input should be left blank. In such a case, the echo of the yield displacement in the output must be ignored.

(3) U34<U13

(4) U45<U34

(5) It is desirable to select the control points (U6,P6) and (U7,P7) to be in the shaded area in Fig. B15 in order to avoid unreasonable analytical results.

(6) The user has the option of saving the time history results of any element in the file named "TAPE8" and/or printing a "reorganized" time history for any element at the end of the output listing.

B.5 Results Output

B.5.1 Time History

The following items are printed at the specified time history output intervals for the elements for which results are requested.

1. Element number
2. Node numbers for ends I and J
3. Zone number of current state of the element
4. Current axial force
5. Current axial deformation
6. Accumulated column growth
7. Accumulated plastic extension
8. Current axial stiffness

B.5.2 Results Envelopes

The following items are printed at the specified envelope output intervals for the elements for which results are requested.

1. Element number
2. Maximum displacements

    2.1.1 Maximum tensile deformation

    2.1.2 Ratio of the maximum tensile deformation to the initial yield point displacement.

    2.1.3 Time of occurrence of maximum tensile deformation.

    2.2.1 Maximum compressive shortening

    2.2.2 Ratio of the maximum compressive shortening to the initial buckling point deformation.

2.2.3 Time of occurrence of maximum compressive shortening.

3. Maximum axial forces

3.1.1 Maximum tensile force

3.1.2 Ratio of the maximum tensile force to the initial yield force.

3.1.3 Time of occurrence of maximum tensile force.

3.2.1 Maximum compressive force

3.2.2 Ratio of the maximum compressive force to the initial buckling force.

3.2.3 Time of occurrence of the maximum compressive force.

4. Inelastic Displacement Data

4.1.1 Maximum inelastic tensile deformation which the element undergoes through one cycle of loading. During the same loading cycle, the inelastic tensile deformation is the deformation developed in Zones 8,9 and 2.

4.1.2 Ratio of the maximum inelastic tensile deformation to the initial yield displacement.

4.1.3 Accumulated inelastic tensile deformation for all loading cycles.

4.2.1 Maximum inelastic shortening which the element undergoes through one cycle of loading. During the same loading cycle, the inelastic shortening is the deformation developed in Zones 3,4,5 and 10.

5. Events

5.1 Number of times the element enters Zones 3,4,5 and 10 *from the elastic state* (Zone 1).

Note: A temporary reversal of loading to Zones 6,7 and 8 does not trigger the counting of additional entries upon re-entering Zones 3,4,5 and 10.

5.2 Number of times the element enters Zones 8,9 and 2 after it has buckled in compression.

Note: A temporary reversal of loading to Zones 1,6, and 7 does not trigger the counting of additional entries upon re-entering Zones 8,9 and 2.

6. Plastic Extension

Accumulated inelastic deformation occurring only in Zone 2 for all cycles.

7. Column Growth

Accumulated column growth for all cycles.

8. Current buckling load

9. Final buckling load

10. Total energy absorbed by the element.

The energy absorbed by the element in one time step is defined as the area of the trapezoid between the old and the new values of the axial force and the axial deformation of the member (Fig. B16).

B.6 **Example Analysis**

A single story steel braced frame, as shown in Figure B17, was modeled and subjected to the El Centro 1940 NS horizontal ground motion. The accelerogram was scaled to have a peak acceleration of 0.5g. This analysis was performed in order to demonstrate an application of the post-buckling brace element when used together with the DRAIN-2D2 program.

The horizontal beam element BC2 is modeled to be axially rigid. Column elements BC1 and BC3 are modeled to have fixed connections with the ground. An x-axis translational mass of 40.8 kips is carried by the first story of the frame. Table B1 summarizes the input parameters of all the members used in the frame.

The analysis was performed with a constant time step of 0.01 sec. and without the event-to-event strategy. No energy calculation was included. Figures B18 and B19 illustrate the force-displacement relation and the displacement time history of the response of Braces 1 and 2, respectively. A listing of the echo of the input data is shown in Table B2, while Table B3 illustrates the envelope output for all the braces.

An attention must be exercised in using the post-buckling truss element to model concentric K-brace frames (Fig. B20). Large unbalanced forces may be generated at node m due to the buckling and/or yielding of the members around it, which, in turn, may cause the node to develop unrealistically high vertical displacements. This phenomenon can greatly be cured by assigning a small vertical translational mass to node m. The user is recommended to assign vertical translational masses equal in magnitude to the dead load of the "tributary area" of the affected nodes.

BEAM-COLUMN ELEMENTS BC1-BC2-BC3	
ELEMENT TYPE 2 (IN DRAIN-2D2)	
Modulus of elasticity (E)	29,000 *ksi*
Cross-sectional area (A)	4.61 in^2
Moment of inertia (I)	35.22 in^4
Yield moment (M_y)	422.6 $k \cdot in$
Hardening ratio	0.05

POST-BUCKLING TRUSS ELEMENTS BRACE 1-BRACE 2			
ELEMENT TYPE 4 (IN DRAIN-2D2)			
E = 25,000 *ksi* A = 0.377 in^2 Hardening ratio = 0.05			
Displ. control points (in)		Force control points (kips)	
U13	-0.12	PYP	10.5
U34	-0.26	PCR	-10.6
U45	-0.32	PCRF	-4.0
U6	1.0	P45	-3.93
U7	0.8	P6	32.0
U8	-0.14	P7	10.0
		P8	2.8
C5 = -0.01 k/in C8 = 0.01 k/in			

Table B1 Input Data Used in the X-Braced Frame Analysis
(1 kips = 4.45kN; 1 in. = 25.4 mm)

POST BUCKLING TRUSS ELEMENTS (TYPE 4)

NO. OF ELEMENTS = 2
NO. OF STIFFNESS TYPES = 1
EVENT FACTOR CALCULATION CODE = 0 IF = 1 . IT APPLIES
INITIAL STIFFNESS DAMPING FACTOR = 0.

STIFFNESS TYPES

TYPE NO.	INPUT NORMALIZED	SECTION AREA	YOUNG'S MODULUS	YIELD DISPL.	YIELD FORCE	BUCKLING LOAD PCR	BUCKLING LOAD PCRF	HARDENING RATIO
1	NO	0.377	25000.000	-0.000	10.500	-10.600	-4.000	0.050

GROWTH FACTOR	GROWTH LIMIT	ZONE 3-4 DISPL.	ZONE 4-5 DISPL.	ZONE 4-5 FORCE	ZONE 5 SLOPE	POINT 6 DISPL.	POINT 6 FORCE
0.040	5.000	-0.260	-0.320	-3.930	-0.010	1.000	32.000

POINT 7 DISPL.	POINT 7 FORCE	POINT 8 DISPL.	POINT 8 FORCE	ZONE 8 SLOPE
0.800	10.000	-0.140	2.800	0.010

ELEMENT SPECIFICATION

ELEMENT NUMBER	NODE I	NODE J	STIFFNESS TYPE	PRINT RESPONSE
1	1	3	1	S-R
2	2	4	1	S-R

Table B2 Echo of Input Data

RESULTS ENVELOPES, ELEMENT GROUP 2 TIMES = 3.000

POST BUCKLING TRUSS ELEMENTS

ELEM NO.	--MAXIMUM DISPL.-- VALUE	RATIO	TIME	--MAXIMUM FORCES-- VALUE	RATIO	TIME	INELASTIC DISPL DATA VALUE	RATIO	ACCUM	--EVENTS-- Z8/Z3	Z9/Z4	Z2/Z5	Z10	PL.EXT./ COL.GR.	PCR/ PCRF	ENERGY ABSD.
1 TENS	0.222	1.88	2.410	10.92	1.04	2.410	0.208	1.76	0.44	0	3	2		0.095	4.00	-4.1
COMP	-0.335	2.81	2.530	-10.60	1.00	1.710	-0.345	2.89	-0.79	5	2	1	0	0.032	-4.0	
2 TENS	0.333	2.82	2.530	11.39	1.09	2.530	0.356	3.02	0.64	0	3	3		0.201	-4.00	-1.6
COMP	-0.274	1.88	2.410	-10.60	1.00	1.990	-0.222	1.86	-0.68	4	1	1	0	0.027	-4.0	

Table B3 Envelope Output

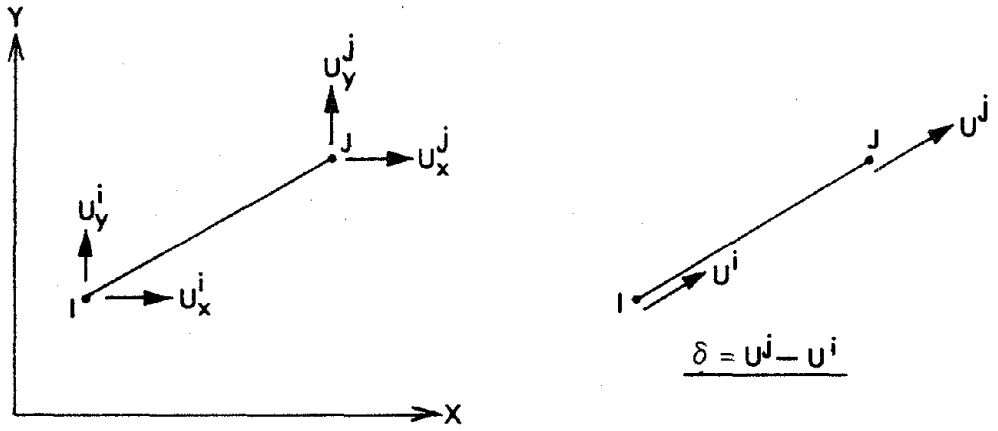

Fig. B1 Post-Buckling Truss Element
(Refined Phenomenological Model)

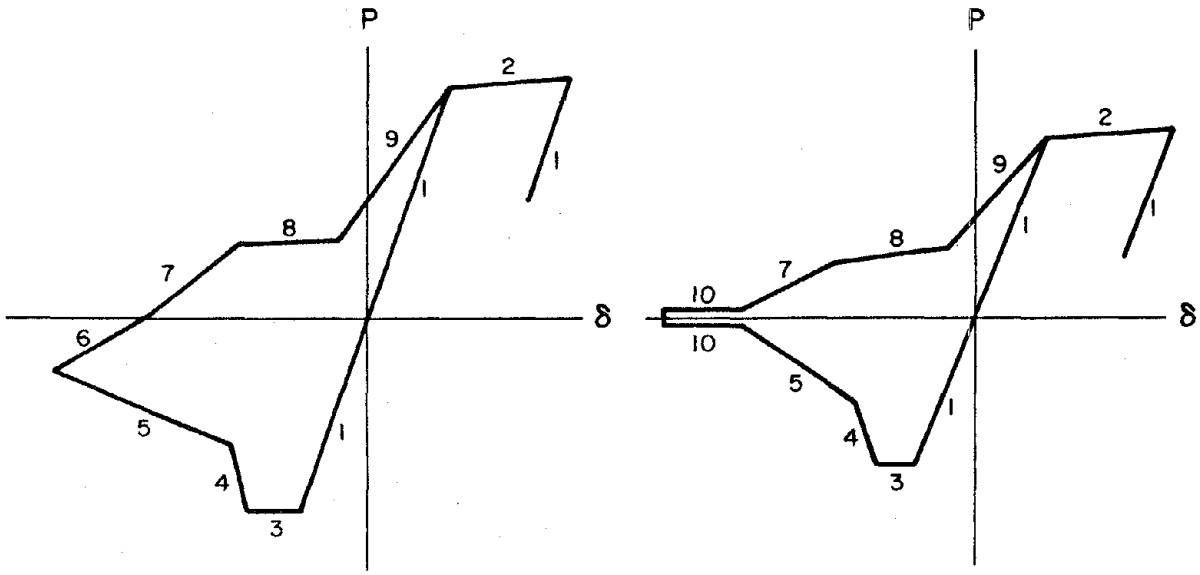

Fig. B2 Zones Used in the Refined Phenomenological Model

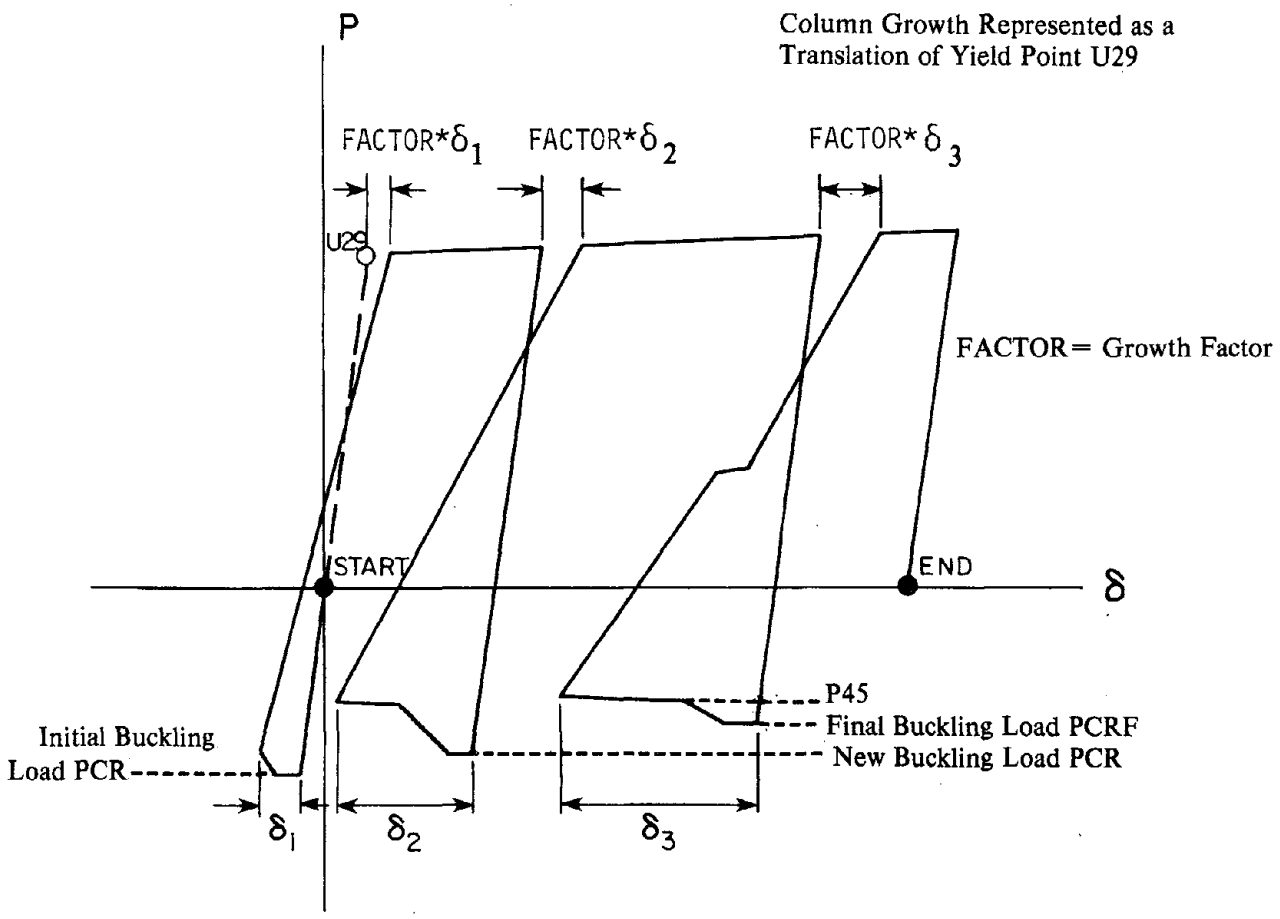

Fig. B3 Inelastic Elongation of a Strut During Cycles

ZONE 1

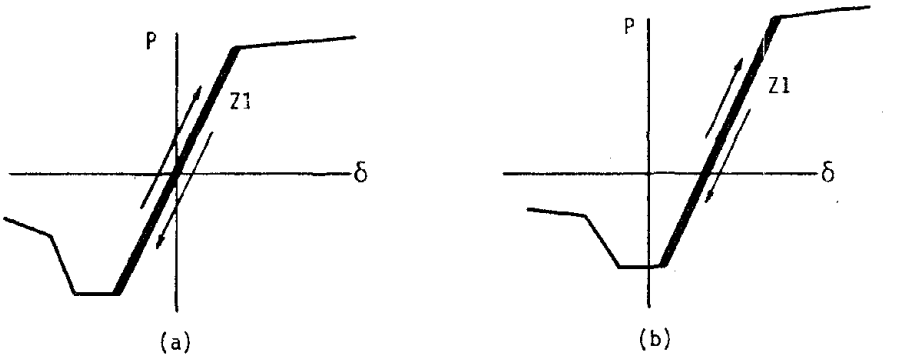

ENTRY FROM OTHER ZONES

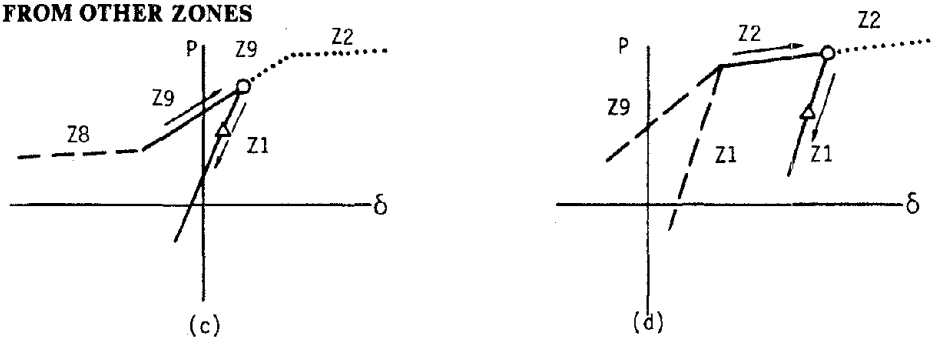

EXIT TO OTHER ZONES

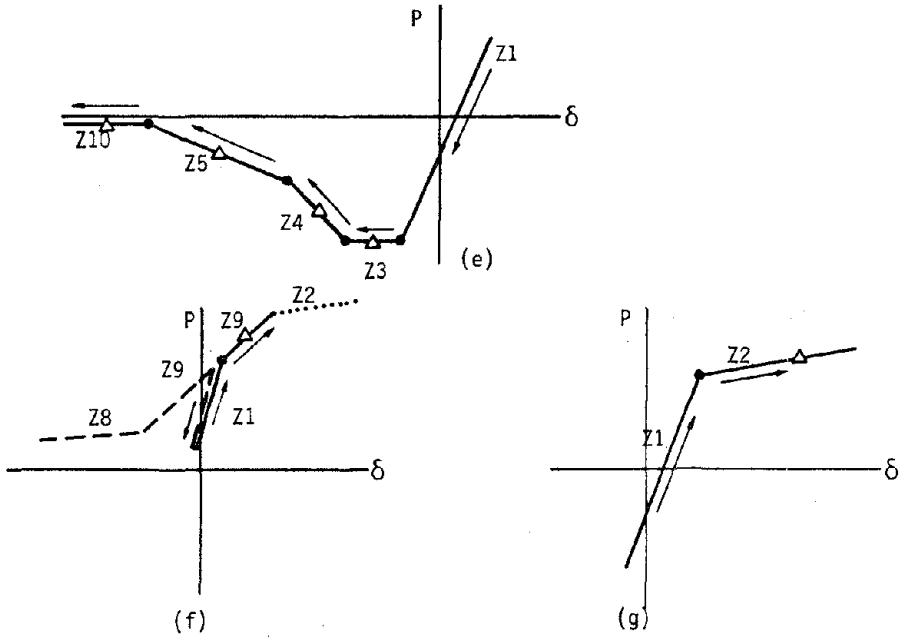

Fig. B4 Zone 1 Behavior

ZONE 2

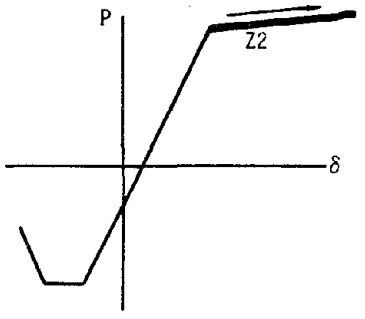

(a)

ENTRY FROM OTHER ZONES

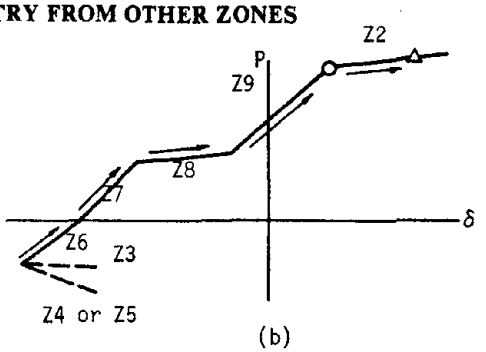

(b)

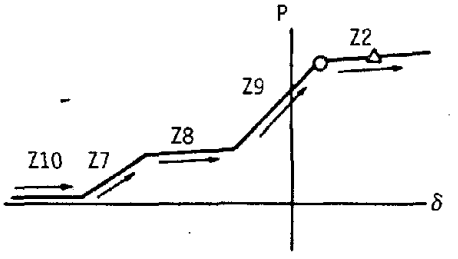

(c)

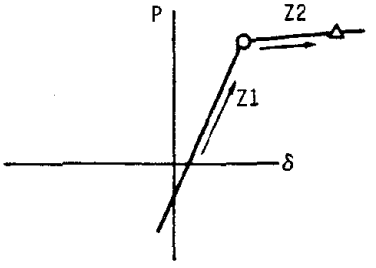

(d)

EXIT TO OTHER ZONES

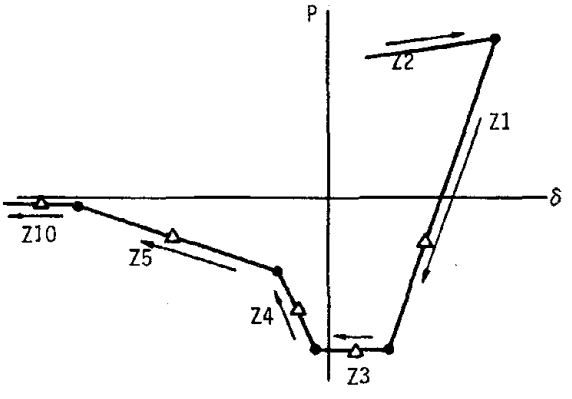

(e)

Fig. B5 Zone 2 Behavior

ZONE 3

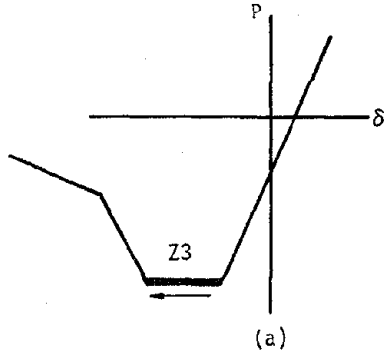

(a)

ENTRY FROM OTHER ZONES

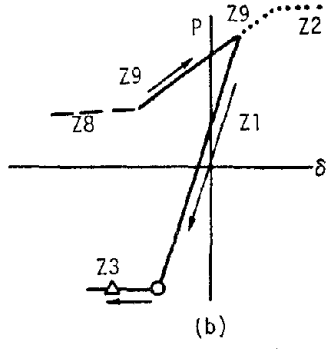

(b)

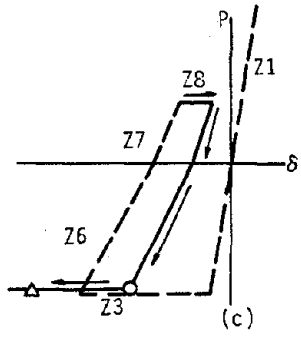

(c)

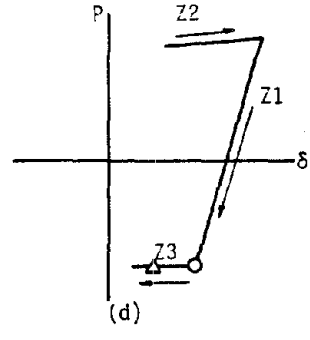

(d)

EXIT TO OTHER ZONES

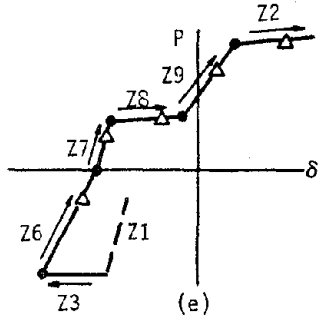

(e)

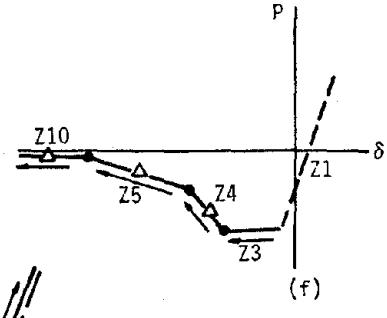

(f)

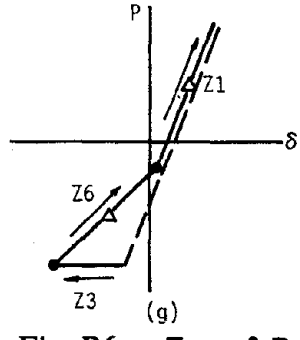

(g)

Fig. B6 Zone 3 Behavior

ZONE 4

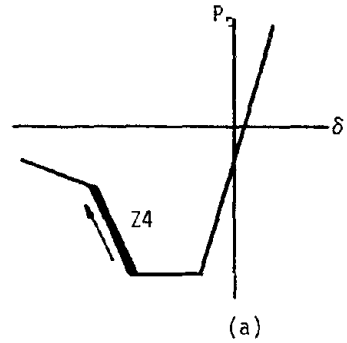

(a)

ENTRY FROM OTHER ZONES

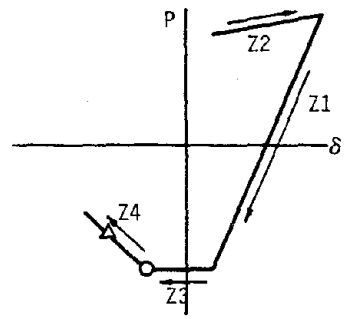

(b)

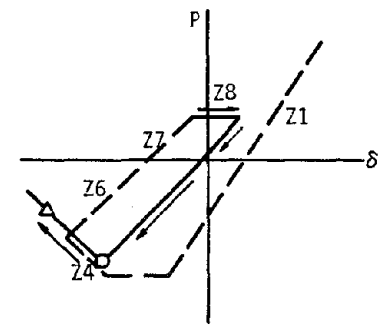

(c)

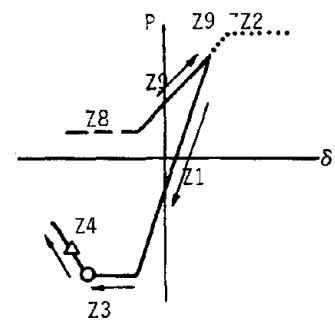

(d)

EXIT TO OTHER ZONES

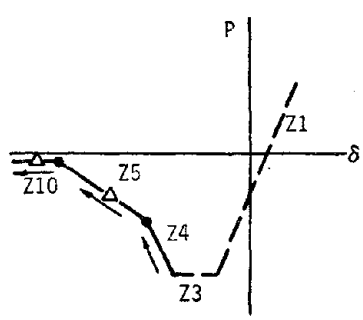

(e)

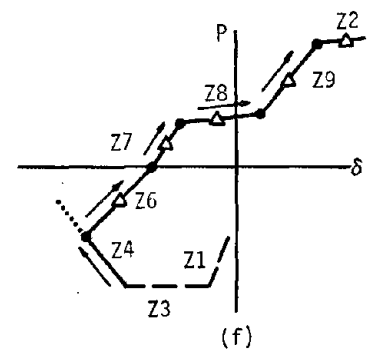

(f)

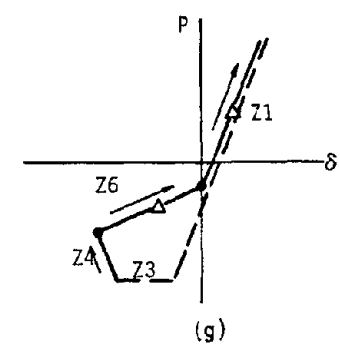

(g)

Fig. B7 Zone 4 Behavior

ZONE 5

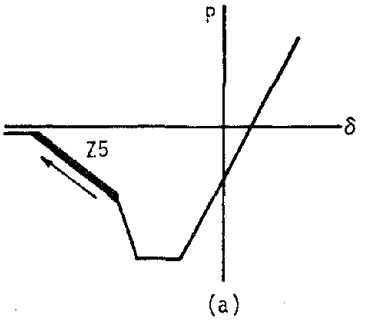

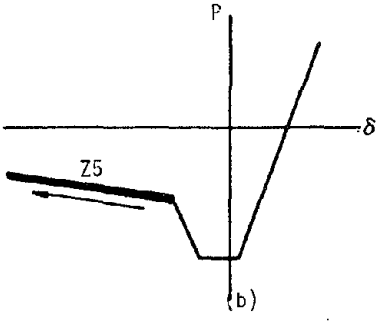

ENTRY FROM OTHER ZONES

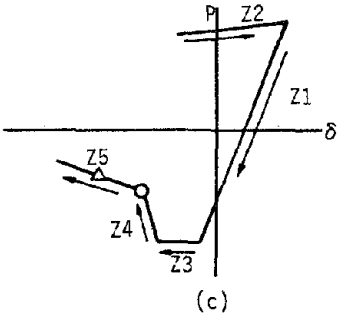

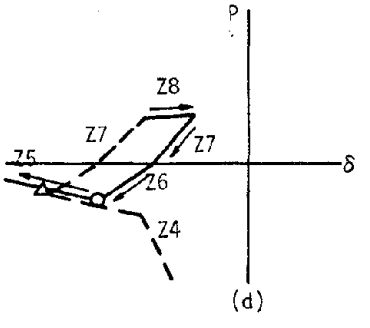

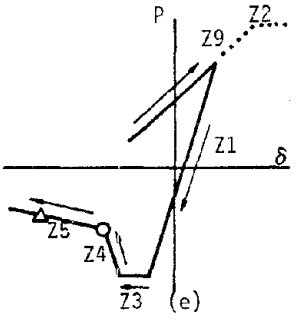

EXIT TO OTHER ZONES

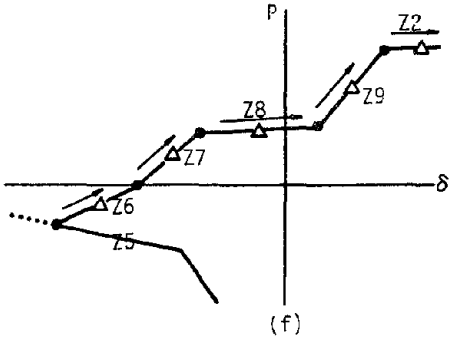

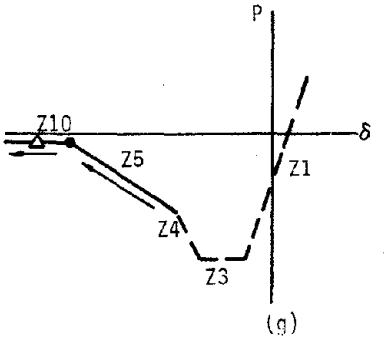

Fig. B8 Zone 5 Behavior

ZONE 6

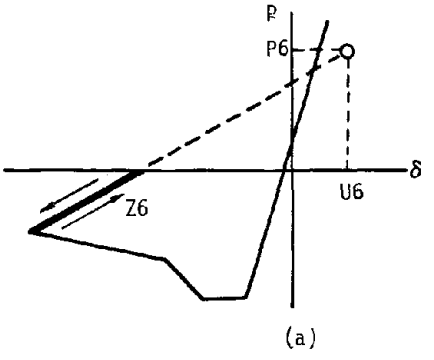

ENTRY FROM OTHER ZONES

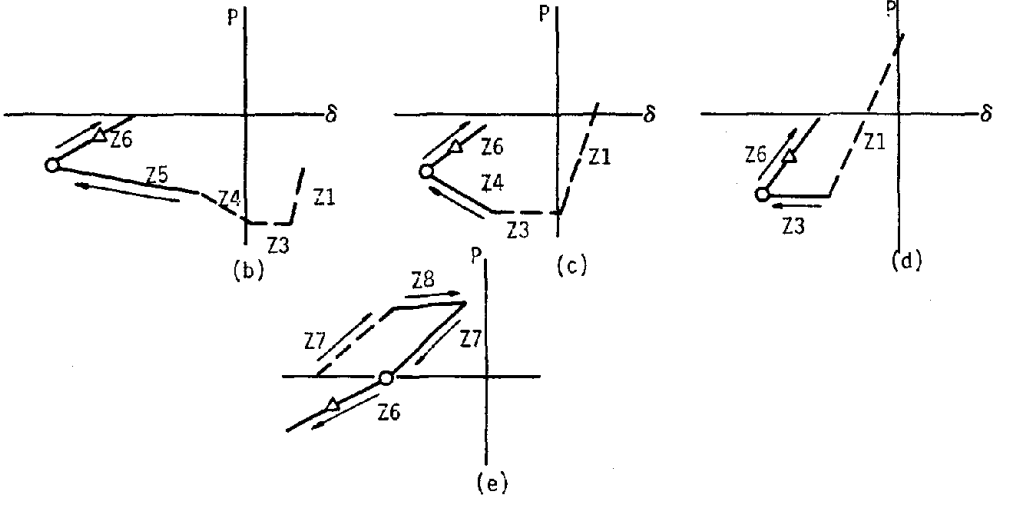

EXIT TO OTHER ZONES

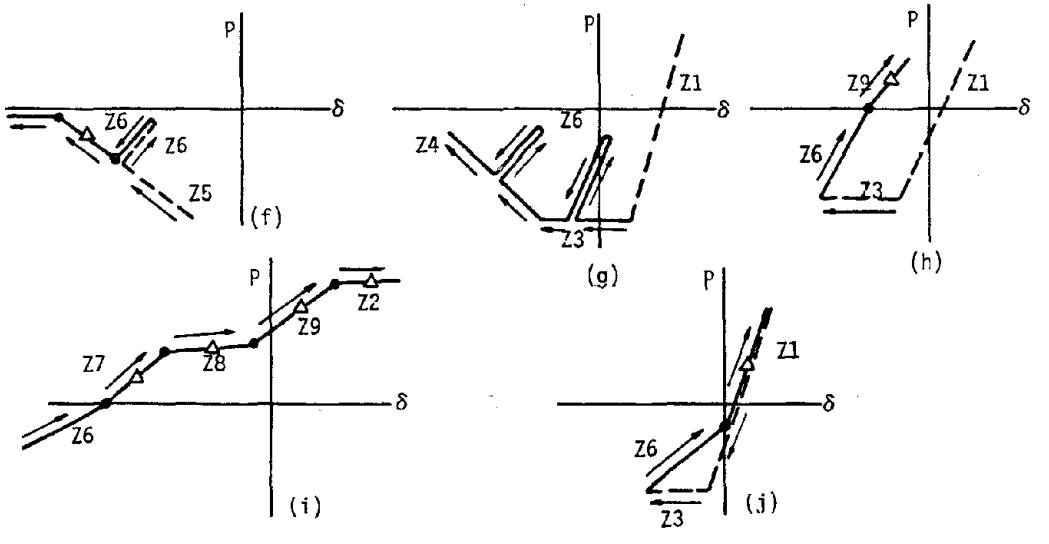

Fig. B9 Zone 6 Behavior

ZONE 7

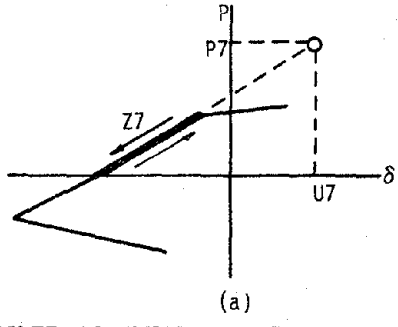

(a)

ENTRY FROM OTHER ZONES

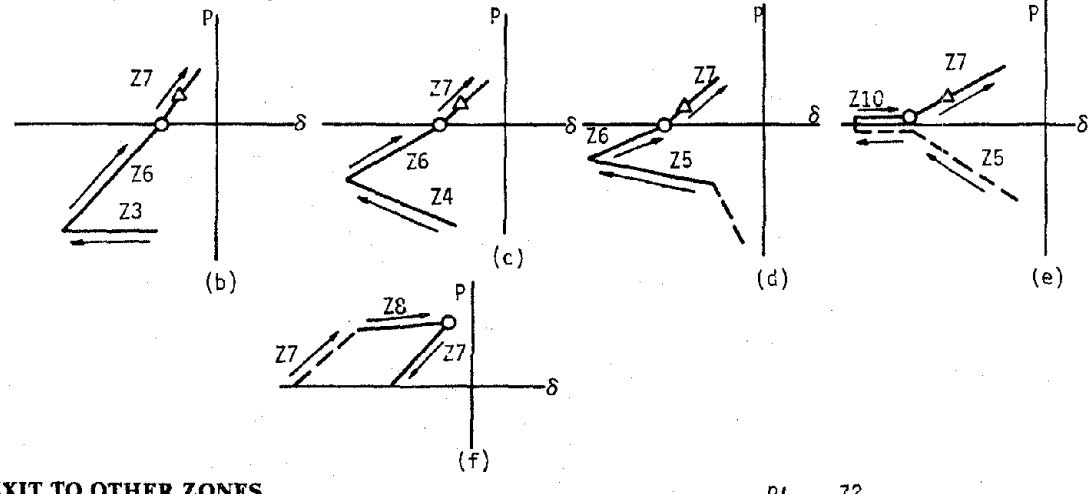

(b) (c) (d) (e) (f)

EXIT TO OTHER ZONES

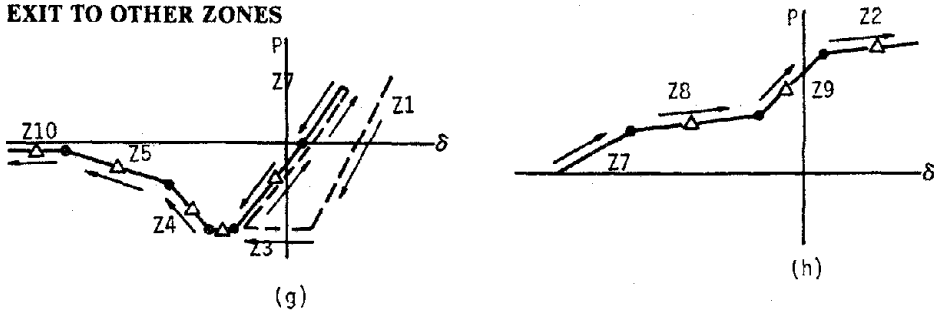

(g) (h)

Fig. B10 Zone 7 Behavior

ZONE 8

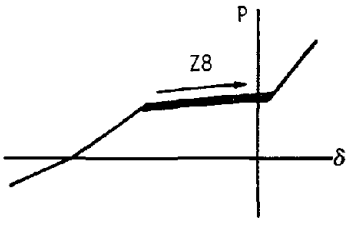

(a)

ENTRY FROM OTHER ZONES

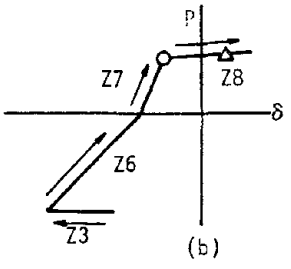

(b)

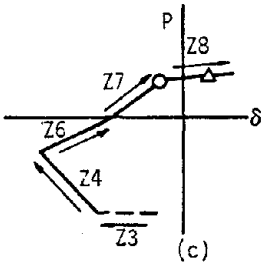

(c)

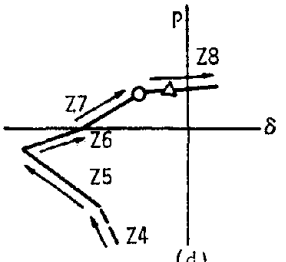

(d)

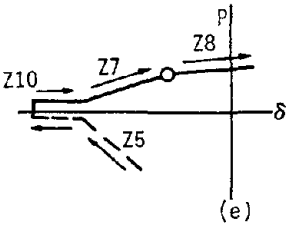

(e)

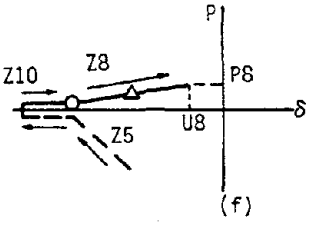

(f)

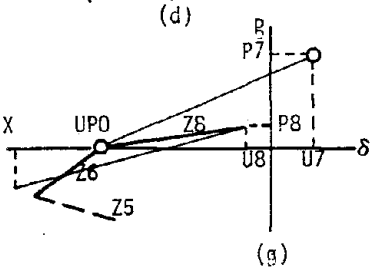

(g)

EXIT TO OTHER ZONES

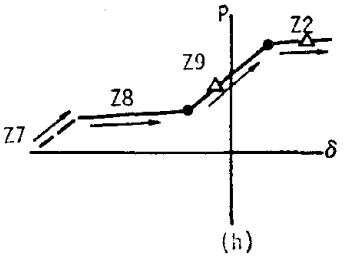

(h)

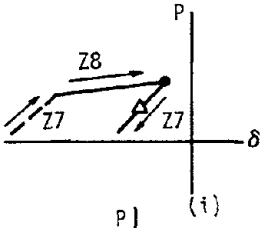

(i)

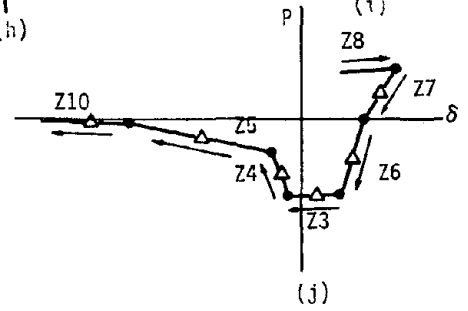

(j)

Fig. B11 Zone 8 Behavior

ZONE 9

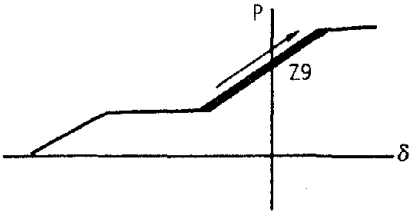

ENTRY FROM OTHER ZONES

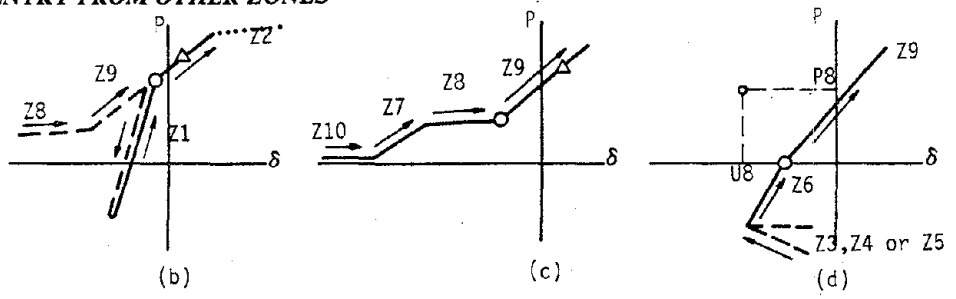

EXIT TO OTHER ZONES

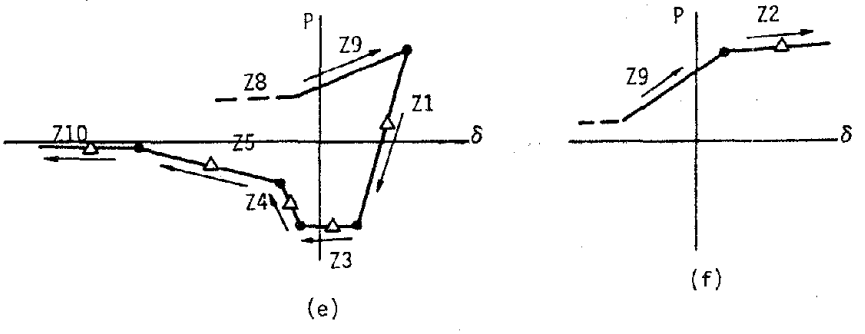

Fig. B12 Zone 9 Behavior

ZONE 10

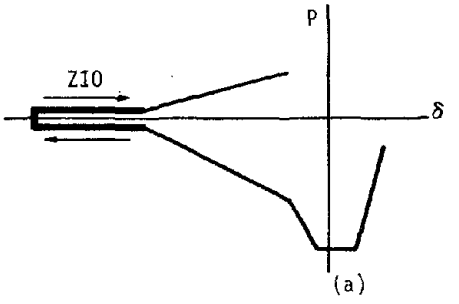

ENTRY FROM OTHER ZONES

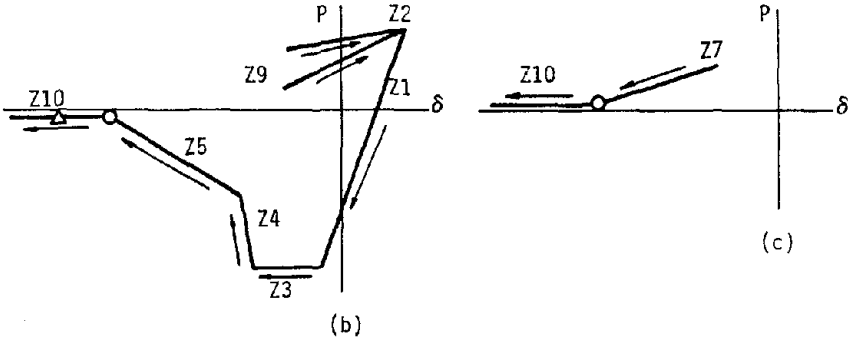

EXIT TO OTHER ZONES

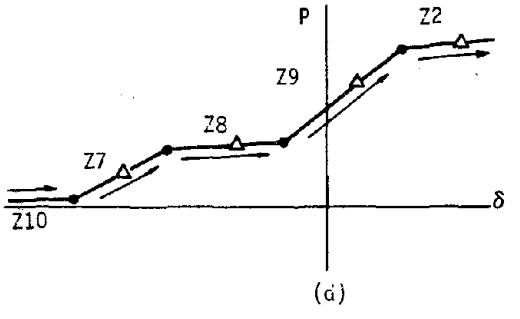

Fig. B13 Zone 10 Behavior

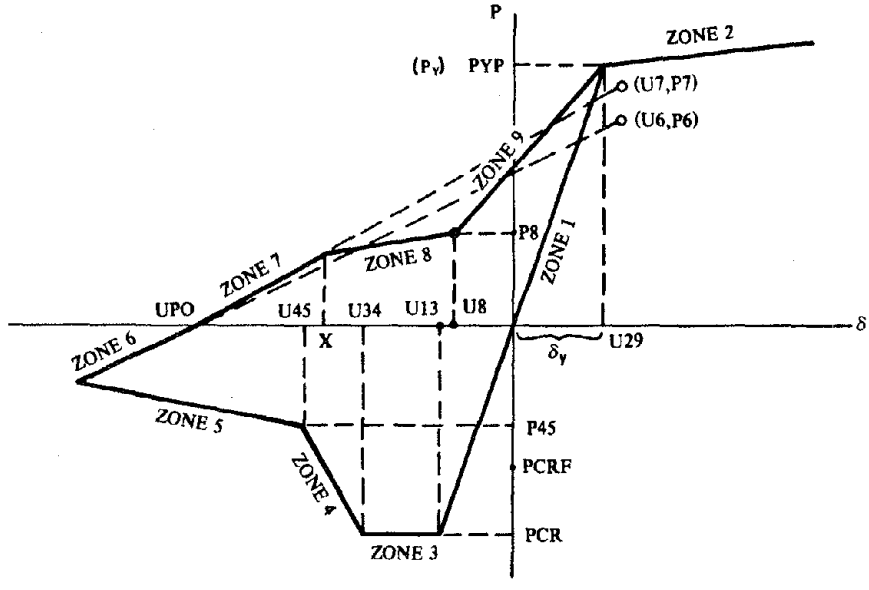

Fig. B14 Input Parameters

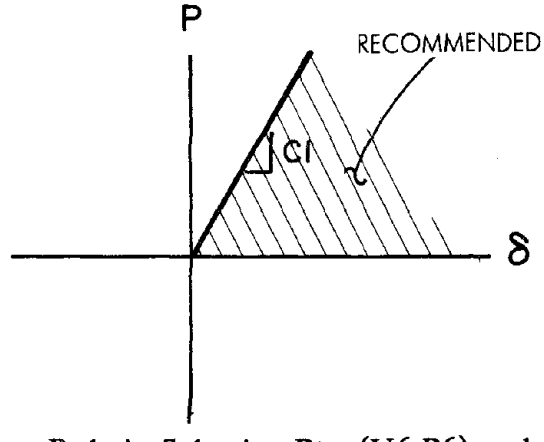

Fig. B15 Rule in Selecting Pts. (U6,P6) and (U7,P7)

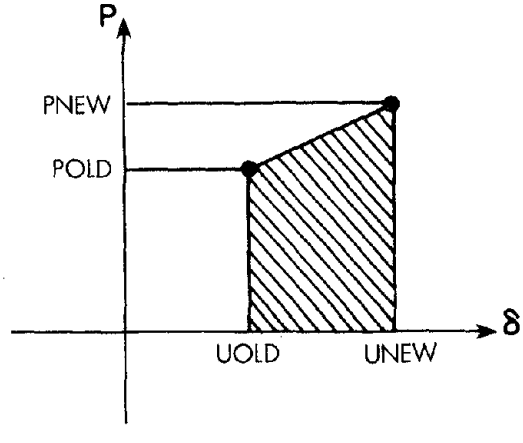

Fig. B16 Energy Absorbed in the Element during a Time Step

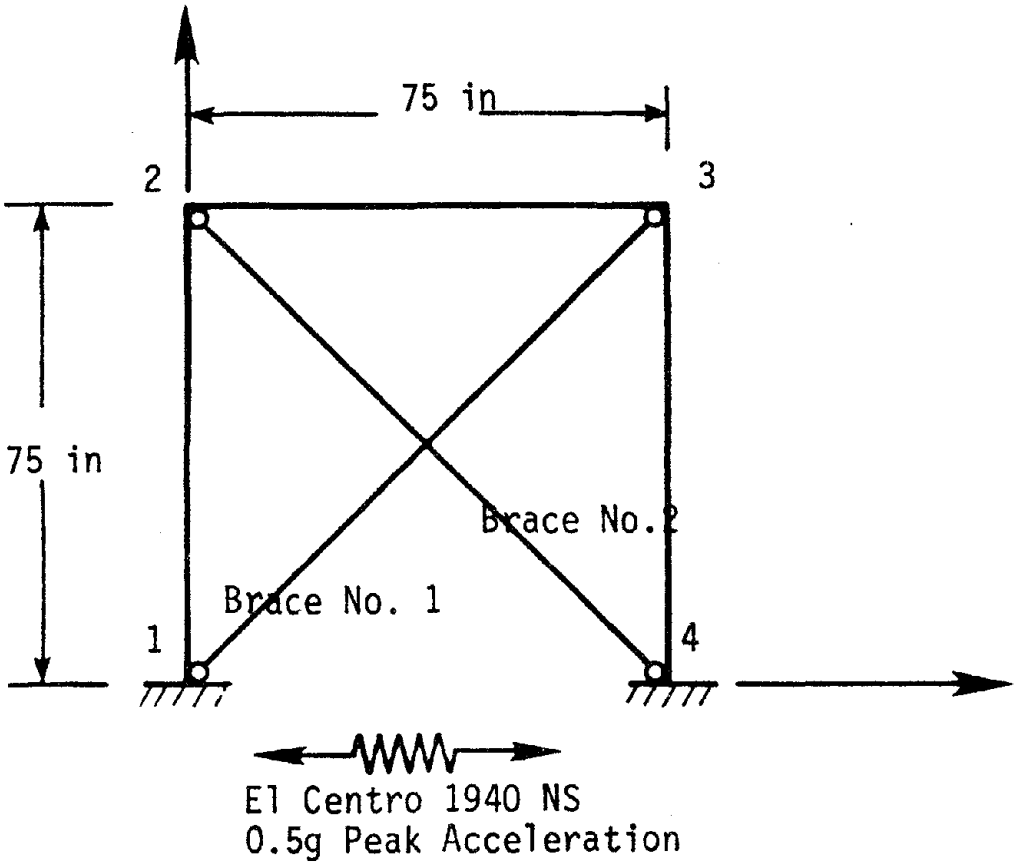

Fig. B17 X-Braced Frame

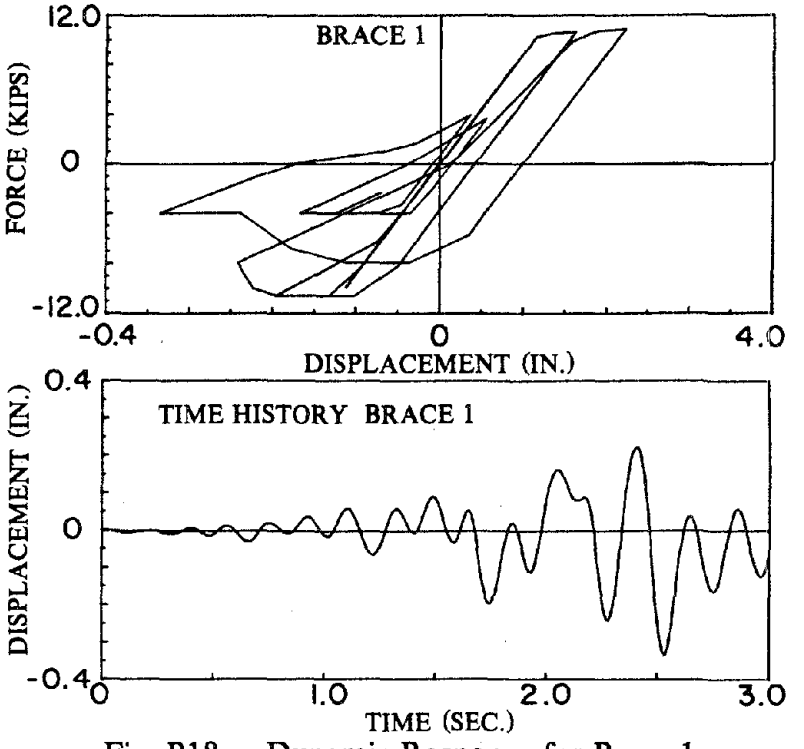

Fig. B18 Dynamic Response for Brace 1

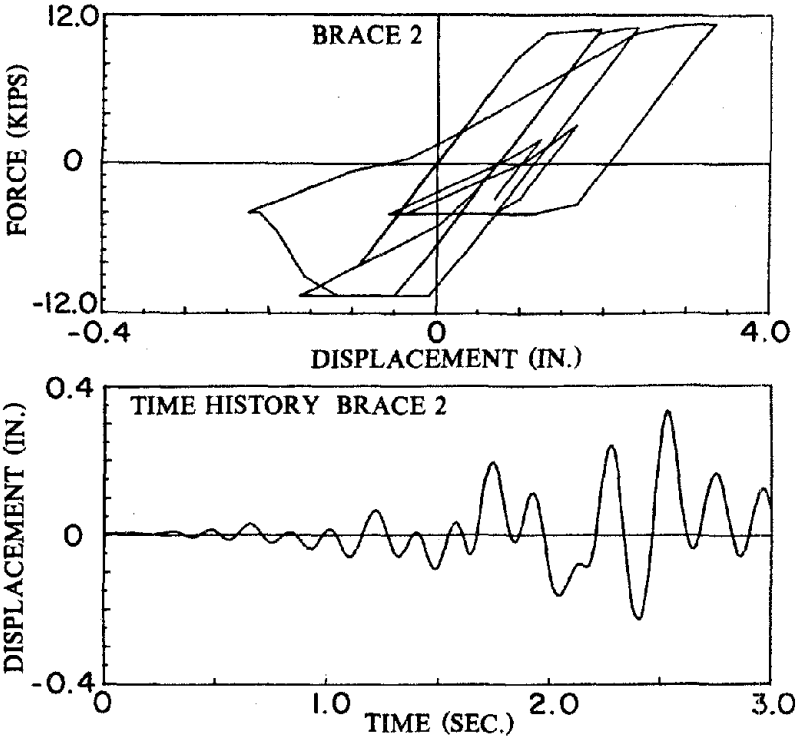

Fig. B19 Dynamic Response for Brace 2

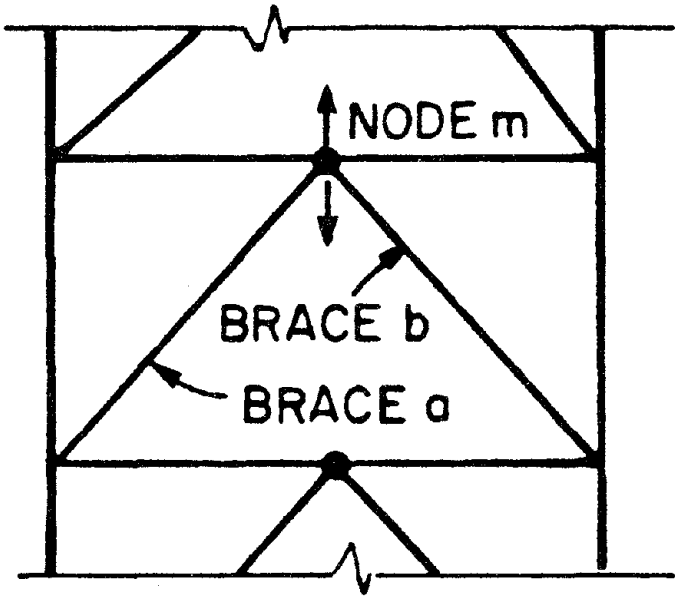

Fig. B20 Concentric K-Braced Frame

EARTHQUAKE ENGINEERING RESEARCH CENTER REPORTS

NOTE: Numbers in parentheses are Accession Numbers assigned by the National Technical Information Service; these are followed by a price code. Copies of the reports may be ordered from the National Technical Information Service, 5285 Port Royal Road, Springfield, Virginia, 22161. Accession Numbers should be quoted on orders for reports (PB --- ---) and remittance must accompany each order. Reports without this information were not available at time of printing. The complete list of EERC reports (from EERC 67-1) is available upon request from the Earthquake Engineering Research Center, University of California, Berkeley, 47th Street and Hoffman Boulevard, Richmond, California 94804.

UCB/EERC-79/01 "Hysteretic Behavior of Lightweight Reinforced Concrete Beam-Column Subassemblages," by B. Forzani, E.P. Popov and V.V. Bertero - April 1979(PB 298 267)A06

UCB/EERC-79/02 "The Development of a Mathematical Model to Predict the Flexural Response of Reinforced Concrete Beams to Cyclic Loads, Using System Identification," by J. Stanton & H. McNiven - Jan. 1979(PB 295 875)A10

UCB/EERC-79/03 "Linear and Nonlinear Earthquake Response of Simple Torsionally Coupled Systems," by C.L. Kan and A.K. Chopra - Feb. 1979(PB 298 262)A06

UCB/EERC-79/04 "A Mathematical Model of Masonry for Predicting its Linear Seismic Response Characteristics," by Y. Mengi and H.D. McNiven - Feb. 1979(PB 298 266)A06

UCB/EERC-79/05 "Mechanical Behavior of Lightweight Concrete Confined by Different Types of Lateral Reinforcement," by M.A. Manrique, V.V. Bertero and E.P. Popov - May 1979(PB 301 114)A06

UCB/EERC-79/06 "Static Tilt Tests of a Tall Cylindrical Liquid Storage Tank," by R.W. Clough and A. Niwa - Feb. 1979 (PB 301 167)A06

UCB/EERC-79/07 "The Design of Steel Energy Absorbing Restrainers and Their Incorporation into Nuclear Power Plants for Enhanced Safety: Volume 1 - Summary Report," by P.N. Spencer, V.F. Zackay, and E.R. Parker - Feb. 1979(UCB/EERC-79/07)A09

UCB/EERC-79/08 "The Design of Steel Energy Absorbing Restrainers and Their Incorporation into Nuclear Power Plants for Enhanced Safety: Volume 2 - The Development of Analyses for Reactor System Piping,""Simple Systems" by M.C. Lee, J. Penzien, A.K. Chopra and K, Suzuki "Complex Systems" by G.H. Powell, E.L. Wilson, R.W. Clough and D.G. Row - Feb. 1979(UCB/EERC-79/08)A10

UCB/EERC-79/09 "The Design of Steel Energy Absorbing Restrainers and Their Incorporation into Nuclear Power Plants for Enhanced Safety: Volume 3 - Evaluation of Commercial Steels," by W.S. Owen, R.M.N. Pelloux, R.O. Ritchie, M. Faral, T. Ohhashi, J. Toplosky, S.J. Hartman, V.F. Zackay and E.R. Parker - Feb. 1979(UCB/EERC-79/09)A04

UCB/EERC-79/10 "The Design of Steel Energy Absorbing Restrainers and Their Incorporation into Nuclear Power Plants for Enhanced Safety: Volume 4 - A Review of Energy-Absorbing Devices," by J.M. Kelly and M.S. Skinner - Feb. 1979(UCB/EERC-79/10)A04

UCB/EERC-79/11 "Conservatism In Summation Rules for Closely Spaced Modes," by J.M. Kelly and J.L. Sackman - May 1979(PB 301 328)A03

UCB/EERC-79/12 "Cyclic Loading Tests of Masonry Single Piers; Volume 3 - Height to Width Ratio of 0.5," by P.A. Hidalgo, R.L. Mayes, H.D. McNiven and R.W. Clough - May 1979(PB 301 321)A08

UCB/EERC-79/13 "Cyclic Behavior of Dense Course-Grained Materials in Relation to the Seismic Stability of Dams," by N.G. Banerjee, H.B. Seed and C.K. Chan - June 1979(PB 301 373)A13

UCB/EERC-79/14 "Seismic Behavior of Reinforced Concrete Interior Beam-Column Subassemblages," by S. Viwathanatepa, E.P. Popov and V.V. Bertero - June 1979(PB 301 326)A10

UCB/EERC-79/15 "Optimal Design of Localized Nonlinear Systems with Dual Performance Criteria Under Earthquake Excitations," by M.A. Bhatti - July 1979(PB 80 167 109)A06

UCB/EERC-79/16 "OPTDYN - A General Purpose Optimization Program for Problems with or without Dynamic Constraints," by M.A. Bhatti, E. Polak and K.S. Pister - July 1979(PB 80 167 091)A05

UCB/EERC-79/17 "ANSR-II, Analysis of Nonlinear Structural Response, Users Manual," by D.P. Mondkar and G.H. Powell July 1979(PB 80 113 301)A05

UCB/EERC-79/18 "Soil Structure Interaction in Different Seismic Environments," A. Gomez-Masso, J. Lysmer, J.-C. Chen and H.B. Seed - August 1979(PB 80 101 520)A04

UCB/EERC-79/19 "ARMA Models for Earthquake Ground Motions," by M.K. Chang, J.W. Kwiatkowski, R.F. Nau, R.M. Oliver and K.S. Pister - July 1979(PB 301 166)A05

UCB/EERC-79/20 "Hysteretic Behavior of Reinforced Concrete Structural Walls," by J.M. Vallenas, V.V. Bertero and E.P. Popov - August 1979(PB 80 165 905)A12

UCB/EERC-79/21 "Studies on High-Frequency Vibrations of Buildings - 1: The Column Effect," by J. Lubliner - August 1979 (PB 80 158 553)A03

UCB/EERC-79/22 "Effects of Generalized Loadings on Bond Reinforcing Bars Embedded in Confined Concrete Blocks," by S. Viwathanatepa, E.P. Popov and V.V. Bertero - August 1979(PB 81 124 018)A14

UCB/EERC-79/23 "Shaking Table Study of Single-Story Masonry Houses, Volume 1: Test Structures 1 and 2," by P. Gülkan, R.L. Mayes and R.W. Clough - Sept. 1979 (HUD-000 1763)A12

UCB/EERC-79/24 "Shaking Table Study of Single-Story Masonry Houses, Volume 2: Test Structures 3 and 4," by P. Gülkan, R.L. Mayes and R.W. Clough - Sept. 1979 (HUD-000 1836)A12

UCB/EERC-79/25 "Shaking Table Study of Single-Story Masonry Houses, Volume 3: Summary, Conclusions and Recommendations," by R.W. Clough, R.L. Mayes and P. Gülkan - Sept. 1979 (HUD-000 1837)A06

UCB/EERC-79/26 "Recommendations for a U.S.-Japan Cooperative Research Program Utilizing Large-Scale Testing Facilities," by U.S.-Japan Planning Group - Sept. 1979(PB 301 407)A06

UCB/EERC-79/27 "Earthquake-Induced Liquefaction Near Lake Amatitlan, Guatemala," by H.B. Seed, I. Arango, C.K. Chan, A. Gomez-Masso and R. Grant de Ascoli - Sept. 1979(NUREG-CR1341)A03

UCB/EERC-79/28 "Infill Panels: Their Influence on Seismic Response of Buildings," by J.W. Axley and V.V. Bertero Sept. 1979(PB 80 163 371)A10

UCB/EERC-79/29 "3D Truss Bar Element (Type 1) for the ANSR-II Program," by D.P. Mondkar and G.H. Powell - Nov. 1979 (PB 80 169 709)A02

UCB/EERC-79/30 "2D Beam-Column Element (Type 5 - Parallel Element Theory) for the ANSR-II Program," by D.G. Row, G.H. Powell and D.P. Mondkar - Dec. 1979(PB 80 167 224)A03

UCB/EERC-79/31 "3D Beam-Column Element (Type 2 - Parallel Element Theory) for the ANSR-II Program," by A. Riahi, G.H. Powell and D.P. Mondkar - Dec. 1979(PB 80 167 216)A03

UCB/EERC-79/32 "On Response of Structures to Stationary Excitation," by A. Der Kiureghian - Dec. 1979(PB 80166 929)A03

UCB/EERC-79/33 "Undisturbed Sampling and Cyclic Load Testing of Sands," by S. Singh, H.B. Seed and C.K. Chan Dec. 1979(ADA 087 298)A07

UCB/EERC-79/34 "Interaction Effects of Simultaneous Torsional and Compressional Cyclic Loading of Sand," by P.M. Griffin and W.N. Houston - Dec. 1979(ADA 092 352)A15

UCB/EERC-80/01 "Earthquake Response of Concrete Gravity Dams Including Hydrodynamic and Foundation Interaction Effects," by A.K. Chopra, P. Chakrabarti and S. Gupta - Jan. 1980(AD-A087297)A10

UCB/EERC-80/02 "Rocking Response of Rigid Blocks to Earthquakes," by C.S. Yim, A.K. Chopra and J. Penzien - Jan. 1980 (PB80 166 002)A04

UCB/EERC-80/03 "Optimum Inelastic Design of Seismic-Resistant Reinforced Concrete Frame Structures," by S.W. Zagajeski and V.V. Bertero - Jan. 1980(PB80 164 635)A06

UCB/EERC-80/04 "Effects of Amount and Arrangement of Wall-Panel Reinforcement on Hysteretic Behavior of Reinforced Concrete Walls," by R. Iliya and V.V. Bertero - Feb. 1980(PB81 122 525)A09

UCB/EERC-80/05 "Shaking Table Research on Concrete Dam Models," by A. Niwa and R.W. Clough - Sept. 1980(PB81 122 368)A06

UCB/EERC-80/06 "The Design of Steel Energy-Absorbing Restrainers and their Incorporation into Nuclear Power Plants for Enhanced Safety (Vol 1A): Piping with Energy Absorbing Restrainers: Parameter Study on Small Systems," by G.H. Powell, C. Oughourlian and J. Simons - June 1980

UCB/EERC-80/07 "Inelastic Torsional Response of Structures Subjected to Earthquake Ground Motions," by Y. Yamazaki April 1980(PB81 122 327)A08

UCB/EERC-80/08 "Study of X-Braced Steel Frame Structures Under Earthquake Simulation," by Y. Ghanaat - April 1980 (PB81 122 335)A11

UCB/EERC-80/09 "Hybrid Modelling of Soil-Structure Interaction," by S. Gupta, T.W. Lin, J. Penzien and C.S. Yeh May 1980(PB81 122 319)A07

UCB/EERC-80/10 "General Applicability of a Nonlinear Model of a One Story Steel Frame," by B.I. Sveinsson and H.D. McNiven - May 1980(PB81 124 877)A06

UCB/EERC-80/11 "A Green-Function Method for Wave Interaction with a Submerged Body," by W. Kioka - April 1980 (PB81 122 269)A07

UCB/EERC-80/12 "Hydrodynamic Pressure and Added Mass for Axisymmetric Bodies," by F. Nilrat - May 1980(PB81 122 343)A08

UCB/EERC-80/13 "Treatment of Non-Linear Drag Forces Acting on Offshore Platforms," by B.V. Dao and J. Penzien May 1980(PB81 153 413)A07

UCB/EERC-80/14 "2D Plane/Axisymmetric Solid Element (Type 3 - Elastic or Elastic-Perfectly Plastic) for the ANSR-II Program," by D.P. Mondkar and G.H. Powell - July 1980(PB81 122 350)A03

UCB/EERC-80/15 "A Response Spectrum Method for Random Vibrations," by A. Der Kiureghian - June 1980(PB81 122 301)A03

UCB/EERC-80/16 "Cyclic Inelastic Buckling of Tubular Steel Braces," by V.A. Zayas, E.P. Popov and S.A. Mahin June 1980(PB81 124 885)A10

UCB/EERC-80/17 "Dynamic Response of Simple Arch Dams Including Hydrodynamic Interaction," by C.S. Porter and A.K. Chopra - July 1980(PB81 124 000)A13

UCB/EERC-80/18 "Experimental Testing of a Friction Damped Aseismic Base Isolation System with Fail-Safe Characteristics," by J.M. Kelly, K.E. Beucke and M.S. Skinner - July 1980(PB81 148 595)A04

UCB/EERC-80/19 "The Design of Steel Energy-Absorbing Restrainers and their Incorporation into Nuclear Power Plants for Enhanced Safety (Vol 1B): Stochastic Seismic Analyses of Nuclear Power Plant Structures and Piping Systems Subjected to Multiple Support Excitations," by M.C. Lee and J. Penzien - June 1980

UCB/EERC-80/20 "The Design of Steel Energy-Absorbing Restrainers and their Incorporation into Nuclear Power Plants for Enhanced Safety (Vol 1C): Numerical Method for Dynamic Substructure Analysis," by J.M. Dickens and E.L. Wilson - June 1980

UCB/EERC-80/21 "The Design of Steel Energy-Absorbing Restrainers and their Incorporation into Nuclear Power Plants for Enhanced Safety (Vol 2): Development and Testing of Restraints for Nuclear Piping Systems," by J.M. Kelly and M.S. Skinner - June 1980

UCB/EERC-80/22 "3D Solid Element (Type 4-Elastic or Elastic-Perfectly-Plastic) for the ANSR-II Program," by D.P. Mondkar and G.H. Powell - July 1980(PB81 123 242)A03

UCB/EERC-80/23 "Gap-Friction Element (Type 5) for the ANSR-II Program," by D.P. Mondkar and G.H. Powell - July 1980 (PB81 122 285)A03

UCB/EERC-80/24 "U-Bar Restraint Element (Type 11) for the ANSR-II Program," by C. Oughourlian and G.H. Powell July 1980(PB81 122 293)A03

UCB/EERC-80/25 "Testing of a Natural Rubber Base Isolation System by an Explosively Simulated Earthquake," by J.M. Kelly - August 1980(PB81 201 360)A04

UCB/EERC-80/26 "Input Identification from Structural Vibrational Response," by Y. Hu - August 1980(PB81 152 308)A05

UCB/EERC-80/27 "Cyclic Inelastic Behavior of Steel Offshore Structures," by V.A. Zayas, S.A. Mahin and E.P. Popov August 1980(PB81 196 180)A15

UCB/EERC-80/28 "Shaking Table Testing of a Reinforced Concrete Frame with Biaxial Response," by M.G. Oliva October 1980(PB81 154 304)A10

UCB/EERC-80/29 "Dynamic Properties of a Twelve-Story Prefabricated Panel Building," by J.G. Bouwkamp, J.P. Kollegger and R.M. Stephen - October 1980(PB82 117 128)A06

UCB/EERC-80/30 "Dynamic Properties of an Eight-Story Prefabricated Panel Building," by J.G. Bouwkamp, J.P. Kollegger and R.M. Stephen - October 1980(PB81 200 313)A05

UCB/EERC-80/31 "Predictive Dynamic Response of Panel Type Structures Under Earthquakes," by J.P. Kollegger and J.G. Bouwkamp - October 1980(PB81 152 316)A04

UCB/EERC-80/32 "The Design of Steel Energy-Absorbing Restrainers and their Incorporation into Nuclear Power Plants for Enhanced Safety (Vol 3): Testing of Commercial Steels in Low-Cycle Torsional Fatigue," by P. Spencer, E.R. Parker, E. Jongewaard and M. Drory

UCB/EERC-80/33 "The Design of Steel Energy-Absorbing Restrainers and their Incorporation into Nuclear Power Plants for Enhanced Safety (Vol 4): Shaking Table Tests of Piping Systems with Energy-Absorbing Restrainers," by S.F. Stiemer and W.G. Godden - Sept. 1980

UCB/EERC-80/34 "The Design of Steel Energy-Absorbing Restrainers and their Incorporation into Nuclear Power Plants for Enhanced Safety (Vol 5): Summary Report," by P. Spencer

UCB/EERC-80/35 "Experimental Testing of an Energy-Absorbing Base Isolation System," by J.M. Kelly, M.S. Skinner and K.E. Beucke - October 1980(PB81 154 072)A04

UCB/EERC-80/36 "Simulating and Analyzing Artificial Non-Stationary Earthquake Ground Motions," by R.F. Nau, R.M. Oliver and K.S. Pister - October 1980(PB81 153 397)A04

UCB/EERC-80/37 "Earthquake Engineering at Berkeley - 1980," - Sept. 1980(PB81 205 874)A09

UCB/EERC-80/38 "Inelastic Seismic Analysis of Large Panel Buildings," by V. Schricker and G.H. Powell - Sept. 1980 (PB81 154 338)A13

UCB/EERC-80/39 "Dynamic Response of Embankment, Concrete-Gravity and Arch Dams Including Hydrodynamic Interaction," by J.F. Hall and A.K. Chopra - October 1980(PB81 152 324)A11

UCB/EERC-80/40 "Inelastic Buckling of Steel Struts Under Cyclic Load Reversal," by R.G. Black, W.A. Wenger and E.P. Popov - October 1980(PB81 154 312)A08

UCB/EERC-80/41 "Influence of Site Characteristics on Building Damage During the October 3, 1974 Lima Earthquake," by P. Repetto, I. Arango and H.B. Seed - Sept. 1980(PB81 161 739)A05

UCB/EERC-80/42 "Evaluation of a Shaking Table Test Program on Response Behavior of a Two Story Reinforced Concrete Frame," by J.M. Blondet, R.W. Clough and S.A. Mahin

UCB/EERC-80/43 "Modelling of Soil-Structure Interaction by Finite and Infinite Elements," by F. Medina - December 1980(PB81 229 270)A04

UCB/EERC-81/01 "Control of Seismic Response of Piping Systems and Other Structures by Base Isolation," edited by J.M. Kelly - January 1981 (PB81 200 735)A05

UCB/EERC-81/02 "OPTNSR - An Interactive Software System for Optimal Design of Statically and Dynamically Loaded Structures with Nonlinear Response," by M.A. Bhatti, V. Ciampi and K.S. Pister - January 1981 (PB81 218 851)A09

UCB/EERC-81/03 "Analysis of Local Variations in Free Field Seismic Ground Motions," by J.-C. Chen, J. Lysmer and H.B. Seed - January 1981 (AD-A099508)A13

UCB/EERC-81/04 "Inelastic Structural Modeling of Braced Offshore Platforms for Seismic Loading," by V.A. Zayas, P.-S.B. Shing, S.A. Mahin and E.P. Popov - January 1981(PB82 138 777)A07

UCB/EERC-81/05 "Dynamic Response of Light Equipment in Structures," by A. Der Kiureghian, J.L. Sackman and B. Nour-Omid - April 1981 (PB81 218 497)A04

UCB/EERC-81/06 "Preliminary Experimental Investigation of a Broad Base Liquid Storage Tank," by J.G. Bouwkamp, J.P. Kollegger and R.M. Stephen - May 1981(PB82 140 385)A03

UCB/EERC-81/07 "The Seismic Resistant Design of Reinforced Concrete Coupled Structural Walls," by A.E. Aktan and V.V. Bertero - June 1981(PB82 113 358)A11

UCB/EERC-81/08 "The Undrained Shearing Resistance of Cohesive Soils at Large Deformations," by M.R. Pyles and H.B. Seed - August 1981

UCB/EERC-81/09 "Experimental Behavior of a Spatial Piping System with Steel Energy Absorbers Subjected to a Simulated Differential Seismic Input," by S.F. Stiemer, W.G. Godden and J.M. Kelly - July 1981

UCB/EERC-81/10 "Evaluation of Seismic Design Provisions for Masonry in the United States," by B.I. Sveinsson, R.L. Mayes and H.D. McNiven - August 1981 (PB82 166 075)A08

UCB/EERC-81/11 "Two-Dimensional Hybrid Modelling of Soil-Structure Interaction," by T.-J. Tzong, S. Gupta and J. Penzien - August 1981(PB82 142 118)A04

UCB/EERC-81/12 "Studies on Effects of Infills in Seismic Resistant R/C Construction," by S. Brokken and V.V. Bertero - September 1981 (PB82 166 190)A09

UCB/EERC-81/13 "Linear Models to Predict the Nonlinear Seismic Behavior of a One-Story Steel Frame," by H. Valdimarsson, A.H. Shah and H.D. McNiven - September 1981(PB82 138 793)A07

UCB/EERC-81/14 "TLUSH: A Computer Program for the Three-Dimensional Dynamic Analysis of Earth Dams," by T. Kagawa, L.H. Mejia, H.B. Seed and J. Lysmer - September 1981(PB82 139 940)A06

UCB/EERC-81/15 "Three Dimensional Dynamic Response Analysis of Earth Dams," by L.H. Mejia and H.B. Seed - September 1981 (PB82 137 274)A12

UCB/EERC-81/16 "Experimental Study of Lead and Elastomeric Dampers for Base Isolation Systems," by J.M. Kelly and S.B. Hodder - October 1981 (PB82 166 182)A05

UCB/EERC-81/17 "The Influence of Base Isolation on the Seismic Response of Light Secondary Equipment," by J.M. Kelly - April 1981 (PB82 255 266)A04

UCB/EERC-81/18 "Studies on Evaluation of Shaking Table Response Analysis Procedures," by J. Marcial Blondet - November 1981 (PB82 197 278)A10

UCB/EERC-81/19 "DELIGHT.STRUCT: A Computer-Aided Design Environment for Structural Engineering," by R.J. Balling, K.S. Pister and E. Polak - December 1981 (PB82 218 496)A07

UCB/EERC-81/20 "Optimal Design of Seismic-Resistant Planar Steel Frames," by R.J. Balling, V. Ciampi, K.S. Pister and E. Polak - December 1981 (PB82 220 179)A07

UCB/EERC-82/01 "Dynamic Behavior of Ground for Seismic Analysis of Lifeline Systems," by T. Sato and A. Der Kiureghian - January 1982 (PB82 218 926)A05

UCB/EERC-82/02 "Shaking Table Tests of a Tubular Steel Frame Model," by Y. Ghanaat and R. W. Clough - January 1982 (PB82 220 161)A07

UCB/EERC-82/03 "Behavior of a Piping System under Seismic Excitation: Experimental Investigations of a Spatial Piping System supported by Mechanical Shock Arrestors and Steel Energy Absorbing Devices under Seismic Excitation," by S. Schneider, H.-M. Lee and W. G. Godden - May 1982 (PB83 172 544)A09

UCB/EERC-82/04 "New Approaches for the Dynamic Analysis of Large Structural Systems," by E. L. Wilson - June 1982 (PB83 148 080)A05

UCB/EERC-82/05 "Model Study of Effects of Damage on the Vibration Properties of Steel Offshore Platforms," by F. Shahrivar and J. G. Bouwkamp - June 1982 (PB83 148 742)A10

UCB/EERC-82/06 "States of the Art and Practice in the Optimum Seismic Design and Analytical Response Prediction of R/C Frame-Wall Structures," by A. E. Aktan and V. V. Bertero - July 1982 (PB83 147 736)A05

UCB/EERC-82/07 "Further Study of the Earthquake Response of a Broad Cylindrical Liquid-Storage Tank Model," by G. C. Manos and R. W. Clough - July 1982 (PB83 147 744)A11

UCB/EERC-82/08 "An Evaluation of the Design and Analytical Seismic Response of a Seven Story Reinforced Concrete Frame - Wall Structure," by F. A. Charney and V. V. Bertero - July 1982(PB83 157 628)A09

UCB/EERC-82/09 "Fluid-Structure Interactions: Added Mass Computations for Incompressible Fluid," by J. S.-H. Kuo - August 1982 (PB83 156 281)A07

UCB/EERC-82/10 "Joint-Opening Nonlinear Mechanism: Interface Smeared Crack Model," by J. S.-H. Kuo - August 1982 (PB83 149 195)A05

UCB/EERC-82/11 "Dynamic Response Analysis of Techi Dam," by R. W. Clough, R. M. Stephen and J. S.-H. Kuo - August 1982 (PB83 147 496)A06

UCB/EERC-82/12 "Prediction of the Seismic Responses of R/C Frame-Coupled Wall Structures," by A. E. Aktan, V. V. Bertero and M. Piazza - August 1982 (PB83 149 203)A09

UCB/EERC-82/13 "Preliminary Report on the SMART 1 Strong Motion Array in Taiwan," by B. A. Bolt, C. H. Loh, J. Penzien, Y. B. Tsai and Y. T. Yeh - August 1982 (PB83 159 400)A10

UCB/EERC-82/14 "Shaking-Table Studies of an Eccentrically X-Braced Steel Structure," by M. S. Yang - September 1982 (PB83 260 778)A12

UCB/EERC-82/15 "The Performance of Stairways in Earthquakes," by C. Roha, J. W. Axley and V. V. Bertero - September 1982 (PB83 157 693)A07

UCB/EERC-82/16 "The Behavior of Submerged Multiple Bodies in Earthquakes," by W.-G. Liao - Sept. 1982 (PB83 158 709)A07

UCB/EERC-82/17 "Effects of Concrete Types and Loading Conditions on Local Bond-Slip Relationships," by A. D. Cowell, E. P. Popov and V. V. Bertero - September 1982 (PB83 153 577)A04

UCB/EERC-82/18 "Mechanical Behavior of Shear Wall Vertical Boundary Members: An Experimental Investigation," by M. T. Wagner and V. V. Bertero - October 1982 (PB83 159 764)A05

UCB/EERC-82/19 "Experimental Studies of Multi-support Seismic Loading on Piping Systems," by J. M. Kelly and A. D. Cowell - November 1982

UCB/EERC-82/20 "Generalized Plastic Hinge Concepts for 3D Beam-Column Elements," by P. F.-S. Chen and G. H. Powell - November 1982 (PB83 247 981)A13

UCB/EERC-82/21 "ANSR-III: General Purpose Computer Program for Nonlinear Structural Analysis," by C. V. Oughourlian and G. H. Powell - November 1982 (PB83 251 330)A12

UCB/EERC-82/22 "Solution Strategies for Statically Loaded Nonlinear Structures," by J. W. Simons and G. H. Powell - November 1982 (PB83 197 970)A06

UCB/EERC-82/23 "Analytical Model of Deformed Bar Anchorages under Generalized Excitations," by V. Ciampi, R. Eligehausen, V. V. Bertero and E. P. Popov - November 1982 (PB83 169 532)A06

UCB/EERC-82/24 "A Mathematical Model for the Response of Masonry Walls to Dynamic Excitations," by H. Sucuoğlu, Y. Mengi and H. D. McNiven - November 1982 (PB83 169 011)A07

UCB/EERC-82/25 "Earthquake Response Considerations of Broad Liquid Storage Tanks," by F. J. Cambra - November 1982 (PB83 251 215)A09

UCB/EERC-82/26 "Computational Models for Cyclic Plasticity, Rate Dependence and Creep," by B. Mosaddad and G. H. Powell - November 1982 (PB83 245 829)A08

UCB/EERC-82/27 "Inelastic Analysis of Piping and Tubular Structures," by M. Mahasuverachai and G. H. Powell - November 1982 (PB83 249 987)A07

UCB/EERC-83/01 "The Economic Feasibility of Seismic Rehabilitation of Buildings by Base Isolation," by J. M. Kelly - January 1983 (PB83 197 988)A05

UCB/EERC-83/02 "Seismic Moment Connections for Moment-Resisting Steel Frames," by E. P. Popov - January 1983 (PB83 195 412)A04

UCB/EERC-83/03 "Design of Links and Beam-to-Column Connections for Eccentrically Braced Steel Frames," by E. P. Popov and J. O. Malley - January 1983 (PB83 194 811)A04

UCB/EERC-83/04 "Numerical Techniques for the Evaluation of Soil-Structure Interaction Effects in the Time Domain," by E. Bayo and E. L. Wilson - February 1983 (PB83 245 605)A09

UCB/EERC-83/05 "A Transducer for Measuring the Internal Forces in the Columns of a Frame-Wall Reinforced Concrete Structure," by R. Sause and V. V. Bertero - May 1983 (PB84 119 494)A06

UCB/EERC-83/06 "Dynamic Interactions between Floating Ice and Offshore Structures," by P. Croteau - May 1983 (PB84 119 486)A16

UCB/EERC-83/07 "Dynamic Analysis of Multiply Tuned and Arbitrarily Supported Secondary Systems," by T. Igusa and A. Der Kiureghian - June 1983 (PB84 118 272)A11

UCB/EERC-83/08 "A Laboratory Study of Submerged Multi-body Systems in Earthquakes," by G. R. Ansari - June 1983 (PB83 261 842)A17

UCB/EERC-83/09 "Effects of Transient Foundation Uplift on Earthquake Response of Structures," by C.-S. Yim and A. K. Chopra - June 1983 (PB83 261 396)A07

UCB/EERC-83/10 "Optimal Design of Friction-Braced Frames under Seismic Loading," by M. A. Austin and K. S. Pister - June 1983 (PB84 119 288)A06

UCB/EERC-83/11 "Shaking Table Study of Single-Story Masonry Houses: Dynamic Performance under Three Component Seismic Input and Recommendations," by G. C. Manos, R. W. Clough and R. L. Mayes - June 1983

UCB/EERC-83/12 "Experimental Error Propagation in Pseudodynamic Testing," by P. B. Shing and S. A. Mahin - June 1983 (PB84 119 270)A09

UCB/EERC-83/13 "Experimental and Analytical Predictions of the Mechanical Characteristics of a 1/5-scale Model of a 7-story R/C Frame-Wall Building Structure," by A. E. Aktan, V. V. Bertero, A. A. Chowdhury and T. Nagashima - August 1983 (PB84 119 213)A07

UCB/EERC-83/14 "Shaking Table Tests of Large-Panel Precast Concrete Building System Assemblages," by M. G. Oliva and R. W. Clough - August 1983

UCB/EERC-83/15 "Seismic Behavior of Active Beam Links in Eccentrically Braced Frames," by K. D. Hjelmstad and E. P. Popov - July 1983 (PB84 119 676)A09

UCB/EERC-83/16 "System Identification of Structures with Joint Rotation," by J. S. Dimsdale and H. D. McNiven - July 1983

UCB/EERC-83/17 "Construction of Inelastic Response Spectra for Single-Degree-of-Freedom Systems," by S. Mahin and J. Lin - July 1983

UCB/EERC-83/18 "Interactive Computer Analysis Methods for Predicting the Inelastic Cyclic Behaviour of Structural Sections," by S. Kaba and S. Mahin - July 1983 (PB84 192 012) A06

UCB/EERC-83/19 "Effects of Bond Deterioration on Hysteretic Behavior of Reinforced Concrete Joints," by F.C. Filippou, E.P. Popov and V.V. Bertero - August 1983 (PB84 192 020) A10

UCB/EERC-83/20 "Analytical and Experimental Correlation of Large-Panel Precast Building System Performance," by M.G. Oliva, R.W. Clough, M. Velkov, P. Gavrilovic and J. Petrovski - November 1983

UCB/EERC-83/21 "Mechanical Characteristics of Materials Used in a 1/5 Scale Model of a 7-Story Reinforced Concrete Test Structure," by V.V. Bertero, A.E. Aktan, H.G. Harris and A.A. Chowdhury - September 1983 (PB84 193 697) A05

UCB/EERC-83/22 "Hybrid Modelling of Soil-Structure Interaction in Layered Media," by T.-J. Tzong and J. Penzien - October 1983 (PB84 192 178) A08

UCB/EERC-83/23 "Local Bond Stress-Slip Relationships of Deformed Bars under Generalized Excitations," by R. Eligehausen, E.P. Popov and V.V. Bertero - October 1983 (PB84 192 848) A09

UCB/EERC-83/24 "Design Considerations for Shear Links in Eccentrically Braced Frames," by J.O. Malley and E.P. Popov - November 1983 (PB84 192 186) A07

UCB/EERC-84/01 "Pseudodynamic Test Method for Seismic Performance Evaluation: Theory and Implementation," by P.-S. B. Shing and S. A. Mahin - January 1984 (PB84 190 644) A08

UCB/EERC-84/02 "Dynamic Response Behavior of Xiang Hong Dian Dam," by R.W. Clough, K.-T. Chang, H.-Q. Chen, R.M. Stephen, G.-L. Wang, and Y. Ghanaat - April 1984

UCB/EERC-84/03 "Refined Modelling of Reinforced Concrete Columns for Seismic Analysis," by S.A. Kaba and S.A. Mahin - April, 1984

UCB/EERC-84/04 "A New Floor Response Spectrum Method for Seismic Analysis of Multiply Supported Secondary Systems," by A. Asfura and A. Der Kiureghian - June 1984

UCB/EERC-84/05 "Earthquake Simulation Tests and Associated Studies of a 1/5th-scale Model of a 7-Story R/C Frame-Wall Test Structure," by V.V. Bertero, A.E. Aktan, F.A. Charney and R. Sause - June 1984

UCB/EERC-84/06 "R/C Structural Walls: Seismic Design for Shear," by A.E. Aktan and V.V. Bertero

UCB/EERC-84/07 "Behavior of Interior and Exterior Flat-Plate Connections subjected to Inelastic Load Reversals," by H.L. Zee and J.P. Moehle

UCB/EERC-84/08 "Experimental Study of the Seismic Behavior of a two-story Flat-Plate Structure," by J.W. Diebold and J.P. Moehle

UCB/EERC-84/09 "Phenomenological Modeling of Steel Braces under Cyclic Loading," by K. Ikeda, S.A. Mahin and S.N. Dermitzakis - May 1984